The reaction $e^+e^- \to \gamma\pi^0 \to \gamma\nu\bar{\nu}$ as a probe of neutrino mass

R. V. Konoplich[a)]

Dipartimento di Fisica ''E. Amaldi'' Università di Roma, I - 00146 Rome, Italy; INFN Sezione di Roma 1 c/o Dipartimento di Fisica Università degli Studi ''La Sapienza,'' 00185 Rome, Italy; Cosmion Center for Cosmoparticle Physics, 125047 Moscow, Russia; Moscow Engineering Physics Institute, 115409 Moscow, Russia

R. Mignani[b)]

Dipartimento di Fisica ''E. Amaldi'' Università di Roma, I - 00146 Rome, Italy; INFN Sezione di Roma 1 c/o Dipartimento di Fisica Università degli Studi ''La Sapienza,'' 00185 Rome, Italy

(Submitted 30 June 1997)
Pis'ma Zh. Éksp. Teor. Fiz. **66**, No. 3, 129–133 (10 August 1997)

The reaction $e^+e^- \to \gamma\pi^0 \to \gamma\nu\bar{\nu}$ is considered. It is shown that this reaction possesses a clear signature, producing in the resonance region practically monochromatic photons, which can easily be distinguished from background bremsstrahlung photons. Since the cross section of the reaction is proportional to the square of the neutrino mass, such a reaction can be used as a probe for neutrino mass. © *1997 American Institute of Physics.* [S0021-3640(97)00115-1]

PACS numbers: 13.10.+q, 14.60.Pq, 13.65.+i

The question of neutrino mass is one of the most important problems facing both particle physics and cosmology. In particle physics the neutrino mass provides a clue to understanding the origin of the mass of all particles. In the so-called grand unified theories, based on the standard electroweak theory, nonzero neutrino masses are expected on general grounds, since in these theories the strong, electromagnetic, and weak interactions are unified at a high energy scale, and neutrinos acquire masses which are inversely proportional to this scale. There are many intriguing hypotheses as to the role of massive neutrinos in cosmology and astrophysics. The big bang theory predicts the existence in the universe of a relic neutrino background similar to the cosmic microwave background radiation. If neutrinos have masses in the range of several to several tens of electron volts, then they could give a significant contribution to the dark matter in the universe. In the case of much smaller masses, neutrino oscillations could deplete the flux of solar electron neutrinos by converting some of them into other neutrino species, thus permitting solution of the solar neutrino puzzle.

However, until now there is no experimental evidence from direct searches for nonzero neutrino mass. They set only upper limits on the respective neutrino masses. The analysis of the endpoint in nuclear β decay gives the formal upper limit[1]

$$m(\nu_e) < 5.1 \text{ eV}. \tag{1}$$

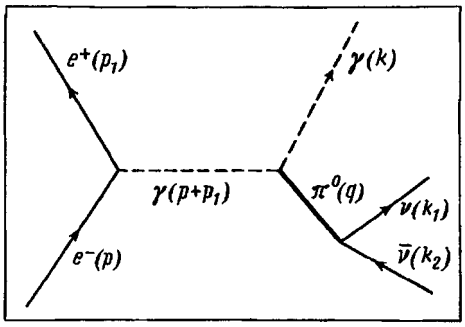

FIG. 1. The Feynman diagram for the process (3).

Particle physics limits for the masses of the muon neutrino and tau neutrino come respectively from the measurement of the muon momentum in $\pi \to \mu \nu_\mu$ decay and from the kinematical analysis of tau-lepton decay modes:

$$m(\nu_\mu) < 0.27 \text{ MeV (Ref. 1)}, \quad m(\nu_\tau) < 24 \text{ MeV (Ref. 2)}. \tag{2}$$

In this article we consider the possibility of improving the upper limit on the neutrino mass from an experimental investigation of the process

$$e^+ e^- \to \gamma \pi^0 \to \gamma \nu \overline{\nu}. \tag{3}$$

In the π^0 decay into neutrino and antineutrino, momentum and angular-momentum conservation implies that the helicities of the two final particles must be the same. Because the probability of a change in helicity is proportional to the neutrino mass, the π^0 decay will occur only in the case of massive neutrinos (or/and if lepton number is not conserved), with an amplitude proportional to the neutrino mass (see, for example, Refs. 3 and 4). In the following, we shall consider the standard electroweak model minimally extended to include a nonzero neutrino mass.

Let us calculate the cross section for the reaction (3) assuming a nonvanishing neutrino mass. The Feynman diagram corresponding to the process (3) is shown in Fig. 1. The amplitude of this process is

$$M = \overline{\nu_e} i e \gamma_\alpha u_e \frac{g^{\alpha\sigma}}{(p+p_1)^2} \frac{ie^2}{4\pi f_\pi} \epsilon_{\gamma\delta\sigma\xi} \epsilon^{*\gamma} (p+p_1)^\xi k^\delta D_\pi f_\pi \frac{G}{\sqrt{2}} q_\beta \overline{u}_\nu \gamma^\beta (1+\gamma_5) \nu_\nu, \tag{4}$$

where $\epsilon^{*\gamma}$ is the polarization vector of the outgoing photon, G is the Fermi constant, α is the fine-structure constant, f_π is the pion decay constant, D_π is the π-meson propagator. All other notations are indicated in Fig. 1. Standard straightforward calculations give us the differential cross section

$$\frac{d\sigma}{d\omega \cdot dz} = \frac{G^2 \alpha^3 m^2}{16\pi^2 S} \frac{\omega^3 q^2 \sqrt{1-4m^2/q^2}}{[(q^2-m_\pi^2)^2+\Gamma^2 m_\pi^2]} (1+z^2), \tag{5}$$

where ω is the photon energy, $z=\cos\theta$, θ is the angle between the electron momentum and the photon momentum, m and m_π are the neutrino and pion mass respectively, $\sqrt{S}$ is the total energy in the center of mass of the reaction (3), Γ is the total pion width, $q^2=S-2\sqrt{S}\omega$. As is seen from Eq. (5), the process (3) exhibits resonance behavior: the cross section (5) increases significantly in the resonance region at $q^2\approx m_\pi^2$, leading to the production of practically monochromatic photons with energy

$$\omega_0=\sqrt{\frac{S}{2}}\,(1-m_\pi^2/S), \quad \Delta\omega\approx\Gamma\approx 7.7 \text{ eV}. \tag{6}$$

In this case the resonance region gives the dominant contribution to the total cross section. Carrying out the integration over this region and a trivial integration over z ($|z|\leqslant z_0$, where z_0 is the experimental cutoff), we obtain

$$\sigma\approx 2.4\times 10^{-46} z_0\left(1+\frac{z_0^2}{3}\right)\left(\frac{m}{m_e}\right)^2\left(1-\frac{m_\pi^2}{S}\right)^3 \text{ cm}^2, \tag{7}$$

where m_e is the electron mass. We note that in deriving Eq. (7) it was assumed that $S>m_\pi^2$ in order to be in the resonance region. Therefore, in the special but reasonable case $\theta_0=30^\circ$ and $S=10m_\pi^2$, we find the following value of the cross section:

$$\sigma\approx 2\times 10^{-46}(m/m_e)^2 \text{ cm}^2. \tag{8}$$

Of course for ν_e the cross section (8) is completely negligible, but this is not the case for ν_μ and especially for ν_τ. In the near future a luminosity of about 10^{34} cm$^{-2}\cdot$sec^{-1} will be achieved at accelerators. There are also discussions about the construction of accelerators with a luminosity of 10^{36} cm$^{-2}\cdot$sec^{-1}. For such accelerators we could expect about 15 events per year due to the reaction (3) in the case of a tau neutrino mass near the present experimental limit.[2] Moreover, although the cross section (7) is very small, the signature of the process (3) is very clear. Photons are produced in reaction (3) essentially at the fixed energy (6), and can be therefore easily distinguished from the $1/\omega$ behavior of the background bremsstrahlung spectrum. Let us compare the result (7) with the prediction for the neutrino counting experiment with a bremsstrahlung photon in the final state:

$$e^+e^-\to\gamma Z\to\gamma\nu\overline{\nu}. \tag{9}$$

The cross section for this process, far from the Z pole, is given by[5,6]

$$\frac{d\sigma}{d\omega\cdot dz}=\frac{\alpha}{3\pi^2}\frac{[(x^2z^2/4)+(1-x/2)^2]}{x(1-z^2)})(1-x)G^2\sqrt{S}[N(g_V^2+g_A^2)+2(g_V+g_A)+2], \tag{10}$$

where $x=2\omega/\sqrt{S}$, $g_V=2\sin^2\theta_W-1/2$, $g_A=-1/2$, $N=3$ is the number of light neutrino species. Carrying out the integration in Eq. (10) over $|z|<\sqrt{3}/2$ and $\omega_0-\Gamma<\omega<\omega_0+\Gamma$, we find that the reaction (3) can be seen over the background reaction (9) in the case of a neutrino mass $m>10$ keV. Even if we choose the wide region of photon energies $\Delta\omega/\omega\leqslant 0.01$, the process (3) dominates over the process (9) for $m>15$ MeV. Let us note that it follows from Eqs. (7) and (10) that the cross section (7) of the reaction (3) depends weakly on the total energy, while the cross section (10) grows as $\sqrt{S}$, so that the signal/background ratio decreases with increasing total energy. Therefore the investigation of

process (3) could be carried out at accelerators at low energies $\sqrt{S}<1$ GeV, where the background conditions are more favorable and where also the number of secondary particles in the final state is small.

The background processes like $e^+e^-\to\gamma\gamma$, $\gamma\gamma\gamma$ and $e^+e^-\to\pi^0\to\gamma\gamma$, in spite of their large cross sections, are not very dangerous because they produce photons with a completely different signature, and in some of them there are additional photons which can be detected. The resonance process $e^+e^-\to\pi^0\to\gamma\nu\overline{\nu}$ produces photons with completely different kinematical characteristics. The resonance process $e^+e^-\to\gamma\pi^0\to\gamma\gamma\gamma$ seems more important, but in this case we have three detectable photons with fixed energies.

In conclusion, in this article we have considered the application of the resonance reaction (3) to the determination of the neutrino mass. This process possesses three important features: 1) the cross section is proportional to the square of the neutrino mass; 2) the cross section has a resonant behavior; 3) the photons in reaction (3) are produced practically monochromatically. Of course there are problems with the luminosity (due to the small value of the cross section) and with the need to have highly monochromatic electron and positron beams, but these are technical problems which could possibly be solved in the future.

We should also note that even the search for a neutrino mass in the region 1–50 MeV is useful, first, because it can give an independent confirmation of the upper limit on the neutrino mass (there are indeed some problems with upper bounds from kinematical methods; see, e.g., Ref. 1). Second, even setting the upper bound on the neutrino mass at 1 MeV is important, because it would allow one to rule out or confirm some popular models (for example, an unstable tau neutrino with lifetime 0.1–100 sec and mass in the range 1–10 MeV can play an important role within the cold dark matter scenario, permitting agreement between the spectrum of density perturbations and the observed one).

In the past, the search for the decays $\pi^0\to\nu\overline{\nu}$ (Refs. 8 and 9) and $\pi^0\to\gamma\nu\overline{\nu}$ (Ref. 10) have been proposed to probe the neutrino properties. However, the process (3), in comparison with these decays, offers a clear signature and could be experimentally easier to study in spite of its small cross section.

This work was conducted within the framework of the international project AstroDAMUS and was supported in part by the Cosmion Scientific and Educational Center within the framework of the project ''Cosmoparticle Physics.'' R. V. K. is grateful to the Rome University ''Roma Tre'' for warm hospitality and financial support and to the Rome University ''La Sapienza'' for warm hospitality. We thank Prof. D. Fargion for many helpful discussions.

[a)]e-mail: konoplic@etp.mepi.msk.su
[b)]e-mail: mignani@romal.infn.it

[1]Particle Data Group, Phys. Rev. D **52**, 1173 (1994).
[2]D. Buskulic *et al.*, Phys. Lett. B **349**, 585 (1995).
[3]B. Kayser, G. T. Garvey, E. Fishbach, and S. P. Rosen, Phys. Lett. B **52**, 385 (1974).
[4]M. A. Beg, W. J. Marciano, and M. Ruderman, Phys. Rev. D **17**, 1395 (1978).

[5] E. Ma and J. Ovada, Phys. Rev. Lett. **41**, 287 (1978).
[6] K. J. F. Gaemers, R. Gastmans, and F. M. Renard, Phys. Rev. D **19**, 1605 (1979).
[7] S. Dodelson, G. Gyuk, and M. S. Turner, Phys. Rev. Lett. **72**, 3754 (1994).
[8] P. Herezeg and C. M. Hoffman, Phys. Lett. B **100**, 347 (1981).
[9] C. M. Hoffman, Phys. Lett. B **208**, 149 (1988).
[10] D. Grasso and M. Lusignoli, Phys. Lett. B **279**, 161 (1992).

Published in English in the original Russian journal. Edited by Steve Torstveit.

The BFKL–Regge phenomenology of deep inelastic scattering

N. N. Nikolaev
Institut für Kernphysik, Forschungszentrum Jülich, D-52425 Jülich, Germany; Landau Institute of Theoretical Physics, 117334 Moscow, Russia

B. G. Zakharov
Landau Institute of Theoretical Physics, 117334 Moscow, Russia

V. R. Zoller
Institute of Theoretical and Experimental Physics, 117218 Moscow, Russia

(Submitted 3 July 1997)
Pis'ma Zh. Éksp. Teor. Fiz. **66**, No. 3, 134–138 (10 August 1997)

We calculate the Regge trajectories of the subleading BFKL singularities and eigenfunctions for the running BFKL pomeron in the color dipole representation. We obtain a viable BFKL–Regge expansion of the proton structure function $F_{2p}(x,Q^2)$ in terms of several rightmost BFKL singularities. We find large subleading contributions to $F_{2p}(x,Q^2)$ in the HERA kinematical region which explain the lack of predictive power of GLDAP extrapolations of $F_{2p}(x,Q^2)$ to the region of small x. We point out the relation of our early finding of precocious BFKL asymptotic behavior to the nodal structure of subleading BFKL eigenfunctions. © *1997 American Institute of Physics.*
[S0021-3640(97)00215-6]

PACS numbers: 11.55.Jy, 12.40.Nn

Extrapolation of the proton structure function from the accessible region of x and Q^2 to small x has remained a topical issue ever since the first SLAC experiments on deep inelastic scattering (DIS). The GLDAP evolution[1] has been a standard instrument in these studies. It was soon realized that GLDAP extrapolations are not unique, and equally good fits to the large-x data did invariably, and wildly, diverge with each other and new experimental data, when extrapolated beyond the investigated range of x. For an instructive comparison of the extrapolations of the pre-HERA fits to the proton structure function with the new data from HERA down to $x\sim 10^{-5}$ see Ref. 2. The lack of predictive power at small x is not surprising: the GLDAP evolution describes the future for large Q^2 starting with assumptions on the parton densities in the past, Q_0^2. One needs to assume that the whole function of x will give different futures for different pasts.

At very small x, the assumptions of the GLDAP evolution break down, and it is superseded by the $\log(1/x)$ BFKL evolution.[3] The BFKL evolution is meant to predict the future at small x from the past defined as a function of Q^2 at a sufficiently small x_0. At asymptotically small x the BFKL prediction, $F_2(x,Q^2)=F_{\mathbb{P}}(Q^2)x^{-\Delta_{\mathbb{P}}}$, is unique modulo the total normalization factor. In the BFKL approach, the x dependence of the structure function at moderately small x depends on the spectrum of eigenvalues and on the

eigenfunctions of the BFKL operator. The purpose of the present study[a)] is an evaluation of the contributions from subleading BFKL singularities for the running BFKL pomeron in the color dipole formulation.[5–7]

The BFKL equation for the interaction cross section section $\sigma(\xi,r)$ of the color dipole r with the target reads $\partial\sigma(\xi,r)/\partial\xi=\mathcal{K}\otimes\sigma(\xi,r)$ (where $\xi=\log(1/x)$). Here the kernel $\mathcal{K}$ is related to the squared wave function of the color-singlet $q\bar{q}g$ state with the Weizsäcker–Williams soft gluon. The gluon fields are calculated with the running QCD coupling and perturbative gluons are infrared-regularized, imposing a finite propagation radius $R_c\simeq 0.2-0.3$ fm. The BFKL pole $\mathbb{P}_n$ corresponds to the Regge-behaving solution of the BFKL equation,

$$\sigma_n(\xi,r)=\sigma_n(r)\exp(\Delta_n\xi)=\sigma_n(r)\left(\frac{x_0}{x}\right)^{\Delta_n}, \tag{1}$$

where the eigenfunction $\sigma_n(r)$ and the eigenvalue (intercept) Δ_n are determined from

$$\mathcal{K}\otimes\sigma_n=\Delta_n\sigma_n(r). \tag{2}$$

The behavior of the eigenfunctions at $r\to 0$ and/or $\alpha_S(r)\to 0$ was found in Refs. 6 and 7:

$$\sigma_n(r)=r^2\left[\frac{1}{\alpha_S(r)}\right]^{\gamma_n-1}, \quad \gamma_n\Delta_n=\frac{4}{3}. \tag{3}$$

Useful clues come from experience with the solutions of the eigenvalue problem for the Schrödinger equation. First, the leading eigenfunction $\sigma_0(r)$, found numerically in Refs. 5–7, is node-free. Consequently, the subleading solutions with eigenfunctions $\Delta_n<\Delta_0$ must have nodes. Second, the asymptotic behavior (3) must hold for all eigenfunctions in the region of r beyond all nodes. Third, because of the infrared regularization the $\sigma_n(r)$ saturate at $r\gtrsim R_c$. This suggests that for eigenfunctions with n nodes one must try $\sigma_n(r)=\mathcal{P}_n(z)\sigma_0(r)$, where $\mathcal{P}_n(z)$ is a polynomial of a suitably chosen variable $z\sim[1/\alpha_S(Q^2)]^{\gamma}$. Then we apply the variational principle and minimize the functional

$$\Phi(\sigma_n)=\int\frac{dr}{r}\left|\frac{\mathcal{K}\otimes\sigma_n(r)-\Delta_n\sigma_n(r)}{\sigma_0(r)}\right|^2 \tag{4}$$

in the space of trial functions with the polynomial prefactor $\mathcal{P}_n(z)$. The success of such an unorthodox variational principle for excited states depends on the trial function guessed; examples of astonishingly successful applications can be found in Ref. 8.

With the eigenfunctions $\sigma_n(r)$ thus obtained we can calculate the contributions $F_2^{(n)}(Q^2)$ to the proton structure function using the color dipole factorization[9] and can perform the BFKL–Regge expansion of the proton structure function

$$F_{2p}(x,Q^2)=\sum_n A_nF^{(n)}(Q^2)\left(\frac{x_0}{x}\right)^{\Delta_n}. \tag{5}$$

Our principal findings on solutions of the BFKL equation are as follows.

The running BFKL equation gives rise to a series of moving poles in the complex j plane. The intercepts Δ_n (Fig. 1) very closely, to better than 10%, follow the law

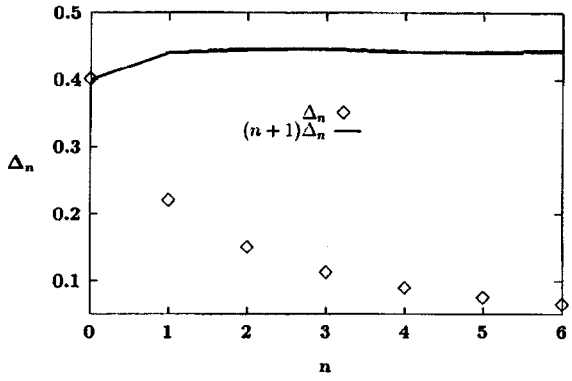

FIG. 1. BFKL eigenvalues.

$$\Delta_n = \frac{\Delta_0}{(n+1)} \tag{6}$$

suggested earlier by Lipatov from quasiclassical considerations.[10] The eigenfunctions found, when plotted as $\mathcal{E}_n(r)=\sigma_n(r)/r$ (Fig. 2), are to a crude approximation, similar to Lipatov's quasi-classical eigenfunctions, which are $\mathcal{E}_n(r)\sim\cos[\phi(r)]$ for $n\gg 1$ (Ref. 10). For a related numerical analysis of the running BFKL equation see Ref. 11. Within our specific infrared regularization the node of $\sigma_1(r)$ is located at $r\simeq 0.05$–0.06 fm. With growing n, the location of the first node moves to a somewhat larger r, and the first nodes accumulate at $r\sim 0.1$–0.15 fm.

The slope α_n' of the Regge trajectory for the pole $\mathbb{P}_n$ can be found using the technique of Refs. 12 and 13 We find $\alpha_n'\simeq 0.07-0.06\ \mathrm{GeV}^{-2}$, with a weak dependence on n.

The structure functions $F_2^{(n)}(Q^2)$ for the $\mathbb{P}_n$ poles are shown in Fig. 3. At large Q^2, far beyond the nodal region, $F_2^n(x,Q^2)\propto(x_0/x)^{\Delta_n}[1/\alpha_S(Q^2)]^{4/3\Delta_n}$. Since the relevant variable is a power of the inverse gauge coupling, which varies with Q^2 very slowly, the

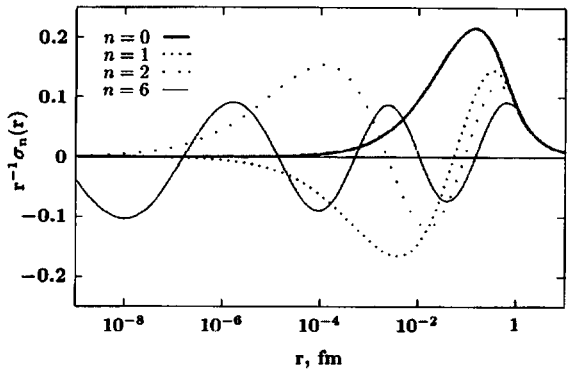

FIG. 2. BFKL eigenfunctions.

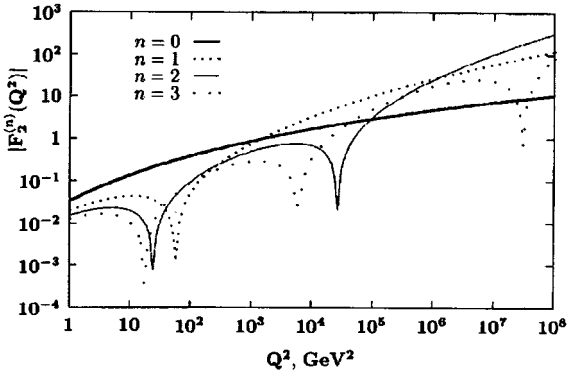

FIG. 3. Modulus of BFKL structure functions.

nodes of $F_2^{(n)}(Q^2)$ are spaced by 2–3 orders of magnitude on the Q^2 scale, and only the first two of them are in the accessible range of Q^2. The first nodes of $F_2^{(n)}(Q^2)$ are located at $Q^2 \sim 20-60$ GeV^2. Hence, only the leading structure function contributes significantly in this region. This explains the precocious BFKL asymptotic behavior for $Q^2 \sim 60$ GeV^2 found earlier from the numerical solution of the color-dipole running BFKL equation.[14]

An interesting finding is that the Born approximation for the dipole cross section, $\sigma_B(r)$, gives a very good quantitative description of the proton structure function at $x_0 \simeq 0.03$ (Ref. 14). The r-dependence of $\sigma_B(r)$ is quite different from that of the leading eigenfunction $\sigma_0(r)$, and expansion of $\sigma_B(r)$ in BFKL eigenfunctions shows that the contribution of subleading terms with $n>0$ makes up to $\sim 60\%$ of $\sigma_B(r)$. Consequently, the Q^2 dependence of the proton structure function at $x=x_0$ and the subsequent x dependence towards smaller x are governed to a large extent by the subleading contributions $F_2^{(n)}(Q^2)$.

At small x only $Q^2 \lesssim 10^3$ GeV^2 are accessible. In this range the structure functions

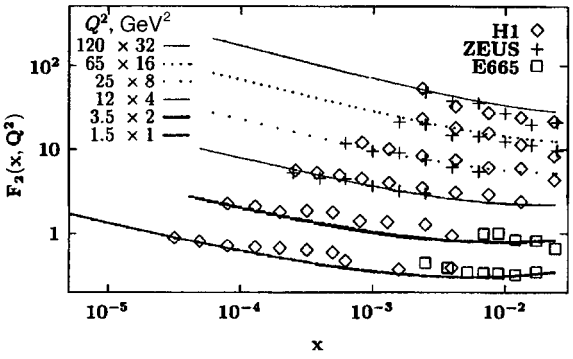

FIG. 4. Three-pole approximation versus the data of H1, ZEUS and E665.

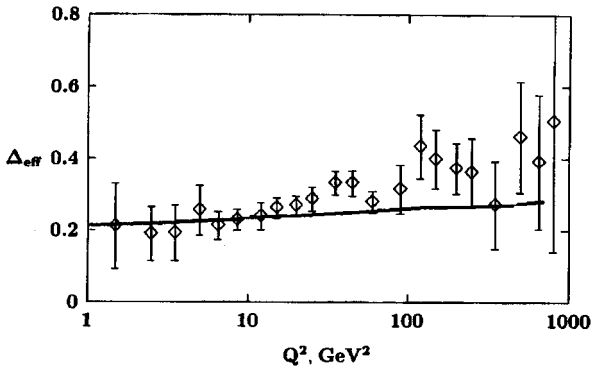

FIG. 5. Effective intercept versus H1 determination.[17]

with $n \geqslant 3$ are hardly distinguishable. Besides, the splitting of intercepts with $n \geqslant 3$ is much smaller than for $n = 0, 1, 2$. Hence, the Regge expansion (5) can be truncated at $n = 2$, and $F_2^{(2)}(Q^2)$ comprises the contributions of all poles with $n \geqslant 2$.

The BFKL equation allows one to determine the intercepts and structure functions $F_2^{(n)}(Q^2)$. In the expansion we put $A_0 = 1$. Then the overall normalization of eigenfunctions, for instance, $\sigma_n(r \gg R_c) = 0.89$ mb, and $A_1 = 0.39$ and $A_2 = 0.33$ are two adjustable parameters which are fixed from the boundary condition at $x = x_0$. With the proper allowance for the valence[15] and nonperturbative[14] corrections to (5) we arrive at the three-pole-approximation, which provides a viable description of the experimental data[16] in a wide kinematical range (Fig. 4). Notice that in the pre-nodal region of $Q^2 \lesssim 20$ GeV^2 the leading and subleading structure functions are very close in shape, and the experimental data in such a limited range of Q^2 are absolutely insufficient for the determination of A_n. This accounts for the failure of the early GLDAP fits.

The effective pomeron intercept

$$\Delta_{\text{eff}} = -\frac{\partial \log F_{2p}(x, Q^2)}{\partial \log x} \tag{7}$$

gives an idea of the role of the subleading singularities. The intercept Δ_{eff} calculated with the experimental kinematic constraints is much smaller than $\Delta_0 = 0.4$, which is expected to dominate asymptotically. The agreement of our numerical estimates with the H1 determination[17] (Fig. 5) is quite satisfactory.

B. G. Zakharov and V. R. Zoller thank J. Speth for the hospitality in the Institut für Kernphysik, Forshungszentrum Jülich, where this work was finished. This work was partly supported by DFG Grant 436-RUS-17/13/97 and INTAS Grant 93-239ext.

[a)]The preliminary results have been reported at the DIS'97 Workshop[4]

[1] V. N. Gribov and L. N. Lipatov, Yad. Fiz. **15**, 781 (1972) [Sov. J. Nucl. Phys. **15**, 438 (1972)]; Yu. L. Dokshitzer, Zh. Éksp. Teor. Fiz. **73**, 1216 (1977) [Sov. Phys. JETP **46**, 641 (1977)]; G. Altarelli and G. Parisi, Nucl. Phys. B **126**, 297 (1977).

[2] H1 Collab., I. Abt *et al.*, Nucl. Phys. B **44**, 515 (1993).
[3] V. S. Fadin, E. A. Kuraev, and L. N. Lipatov, Zh. Éksp. Teor. Fiz. **71**, 840 (1976); [Sov. Phys. JETP **44**, 443 (1976)]; Zh. Éksp. Teor. Fiz. **72**, 377 (1977) [Sov. Phys. JETP **45**, 199 (1977)]; Yu. Yu. Balitsky and L. N. Lipatov, Yad. Fiz. **28**, 1597 (1978) [Sov. J. Nucl. Phys. **28**, 822 (1978)].
[4] V. R. Zoller, *Talk at 5th International Workshop on Deep Inside Inelastic Scattering and QCD (DIS'97), Chicago, April 1997*, Report No. KFA-IKP(TH)-97-12.
[5] N. N. Nikolaev, B. G. Zakharov and V. R. Zoller, JETP Lett. **59**, 8 (1994).
[6] N. N. Nikolaev, B. G. Zakharov, and V. R. Zoller, Zh. Éksp. Teor. Fiz. **78**, 1498 (1994) [JETP **105**, 806 (1994)].
[7] N. N. Nikolaev and B. G. Zakharov, Phys. Lett. B **327**, 157 (1994).
[8] G. Karl and V. Novikov, Phys. Rev. B **51**, 5069 (1995).
[9] N. N. Nikolaev and B. G. Zakharov, Z. Phys. C **49**, 607 (1991); Z. Phys. C **53**, 331 (1992).
[10] L. N. Lipatov, Zh. Éksp. Teor. Fiz. **90**, 1536 (1986) [Sov. Phys. JETP **63**, 904 (1986)].
[11] R. E. Hancock and D. A. Ross Nucl. Phys. B **383**, 575 (1992).
[12] N. N. Nikolaev, B. G. Zakharov and V. R. Zoller, JETP. Lett. **60**, 678 (1994).
[13] N. N. Nikolaev, B. G. Zakharov, and V. R. Zoller, Phys. Lett. B **366**, 337 (1996)
[14] N. N. Nikolaev and B. G. Zakharov, Phys. Lett. B **333**, 250 (1994).
[15] M. Glück, E. Reya, and A. Vogt, Z. Phys. C **67**, 433 (1995).
[16] H1 Collab., T. Ahmed *et al.*, Nucl. Phys. B **439**, 471 (1995); ZEUS Collab., M. Derrick *et al.*, Z. Phys. C **69**, 607 (1996); E665 Collab., M. R. Adams *et al.*, Phys. Rev. D **54**, 3006 (1996).
[17] H1 Collab., S. Aid *et al.*, Nucl. Phys. B **470**, 3 (1996).

Published in English in the original Russian journal. Edited by Steve Torstveit.

Dynamics of excitonic states in GaAs/AlGaAs quantum wells

K. L. Litvinenko,[a] A. Gorshunov, and V. G. Lysenko
Institute of Problems of the Technology of Microelectronics and Ultrapure Materials, Russian Academy of Sciences, 142432 Chernogolovka, Moscow Region, Russia

J. M. Hvam
Mikroelektronik Centret DTU, DK-2800 Lyngby, Denmark

(Submitted 11 June 1997)
Pis'ma Zh. Éksp. Teor. Fiz. **66**, No. 3, 139–144 (10 August 1997)

The influence of photoexcited carriers on the dynamics of the absorption spectra of GaAs/$Al_xGa_{1-x}As$ multilayer quantum wells is investigated experimentally. It is found that at quasiparticle densities all the way up to 10^{11} cm^{-2} the saturation of the excitonic absorption is due to both a decrease of oscillator strength and broadening of the excitonic lines. It is shown that in the case of femtosecond resonance laser excitation the decrease of oscillator strength is due to free electron–hole pairs, while the broadening and energy shift of the excitonic lines are due to the exciton–exciton interaction. The lifetimes of free electron–hole pairs and excitons ($\approx$65 ps and $\approx$410 ps, respectively) are determined from the exponential decrease of the change in the oscillator strength and in the width and energy position of the excitonic lines.
 [S0021-3640(97)00315-0]

PACS numbers: 73.61.Ey, 71.35.Cc, 78.66.Fd

The saturation of excitonic resonance has been studied extensively for the last 10 years. Initially, when the technology for growing multilayer quantum wells (MQWs) had still not been adequately developed, specimens exhibiting excitonic lines with large inhomogeneous broadening were employed in the investigations. Since the photoexcited-carrier density has little effect on inhomogeneous broadening, in the early works[2,3] no change in excitonic linewidths with increasing quasiparticle density was detected, and the saturation of excitonic absorption was attributed exclusively to the decrease in oscillator strength f. In Refs. 2 and 3 it was concluded on the basis of these results that at room temperature excitons are at least twice as effective in lowering f as are thermalized free carriers. However, Schmitt-Rink *et al.*[4] predicted theoretically the completely opposite situation, specifically, that in quasi-two-dimensional media the ''cold'' electron–hole plasma should affect f most effectively.

Wake *et al.*[5] discovered that in high-quality quantum wells with narrow excitonic absorption lines the broadening can be the sole reason for saturation of the excitonic absorption right up to photoexcited-carrier densities of 10^{11} cm^{-2}. Investigations of the phase relaxation time in bulk GaAs[6] and GaAs quantum wells[7] by the four-wave mixing method confirmed that broadening of excitonic lines plays the dominant role. Nonethe-

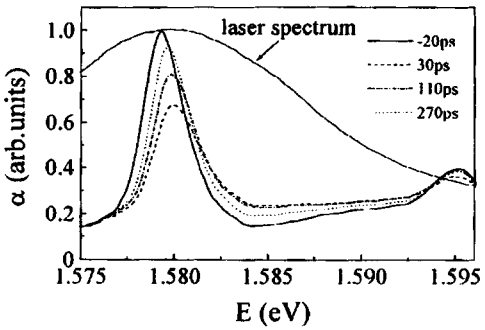

FIG. 1. Change in shape of the excitonic absorption spectrum as a function of the delay time. The solid line represents the spectrum of the exciting laser radiation.

less, recent studies[8] have shown that f is observed to change even at low photoexcited-carrier densities and that the higher the quasiparticle density, the more effectively f influences excitonic absorption.

To determine the role of different excitonic parameters in the change in excitonic absorption and to determine how effectively free and bound quasiparticles influence these parameters, we investigated experimentally the dynamics of the change in the excitonic absorption spectra in GaAs/$Al_{0.3}Ga_{0.7}As$ MQWs by a method employing pump and probe beams.[8]

The experimental MQW was grown by molecular-beam epitaxy and consisted of 20 periods of 80-Å wide GaAs layers and 100-Å wide AlGaAs layers. In all experiments the specimen was placed in a helium optical cryostat and its temperature was maintained close to 5 K. The laser source was a tunable titanium–sapphire laser with 120 fs pulses and a repetition frequency of 76 MHz.

The typical absorption spectra of our experimental sample are displayed in Fig. 1 for different delay times of the probe beam. The initial exciton density was equal to approximately 8.6×10^{10} cm^{-2}. The spectral position of the exciting laser radiation is shown in Fig. 1 (solid thin line). Lines of heavy (1.579 eV) and light (1.595 eV) excitons are clearly seen in the absorption spectra. In the present letter we shall examine the behavior of the heavy excitons.

We analyzed the experimental results by the moment analysis method.[9] This method does not require knowledge of the exact shape of the absorption spectrum and consists of defining all excitonic parameters in terms of integrals. If it is assumed that excitonic absorption is described by an arbitrary symmetric statistical distribution $\alpha(\hbar\omega)$, then f can be expressed in terms of the zeroth moment of this distribution:

$$f\sim\int\alpha(\hbar\omega)d\omega. \tag{1}$$

The spectral position of the excitonic resonance is calculated as the normalized first moment of the distribution $\alpha(\hbar\omega)$

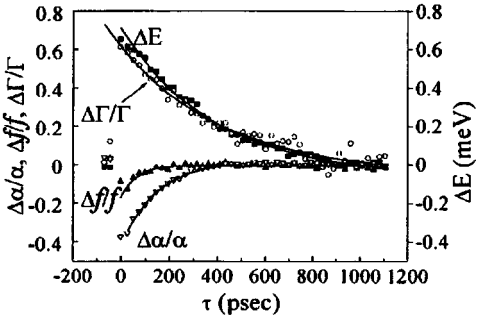

FIG. 2. Relative changes in the oscillator strength, the maximum of the absorption coefficient, and the broadening and energy shift of the excitonic absorption line as functions of the delay time.

$$E_{1s}=\int \hbar\omega\alpha(\hbar\omega)d\omega/f, \tag{2}$$

and the width of the excitonic resonance is described as the normalized centered second moment

$$\Gamma^2=\int (\hbar\omega-\hbar\omega_{1s})^2\alpha(\hbar\omega)d\omega/f. \tag{3}$$

Now, to investigate the dynamics of the change in all excitonic parameters these moments must be calculated for each value of the delay time τ and compared with the corresponding values of these moments for negative τ. The computational results obtained for the data displayed in Fig. 1 are presented in Fig. 2. One can see from Fig. 2 that saturation of excitonic absorption is due to both a change in f and broadening of the excitonic line. These parameters exhibit different behavior in time, and to understand which interaction mechanisms influence f and the broadening and shift of the excitonic line we also investigated the change in each excitonic parameter as a function of the particle density for a fixed delay time $\tau\approx 20$ ps. This time was chosen because all relaxation processes for both free and bound particles should be completed after this time has elapsed.

Figure 3 displays the relative change $\Delta f/f$ in the oscillator strength and the relative change $\Delta\alpha/\alpha$ in the maximum of the absorption coefficient versus the excitonic line shift $\Delta E/E_b$ normalized to the binding energy. Each point of these curves corresponds to different values of the photoexcited particle density at the same value $\tau\approx 20$ ps. To describe these results we used the formulas[4]

$$\delta E/E_b=C^{(f)}\delta f/f_{1s}, \tag{4}$$

$$\delta E/E_b=C^{(\alpha)}\delta\alpha/\alpha, \tag{5}$$

where E_b, f_{1s}, and α are the experimental values of the binding energy, oscillator strength, and absorption maximum of the unperturbed excitonic state and $C^{(f)}$ and $C^{(\alpha)}$are proportionality coefficients. From Fig. 3 we obtained $C^{(\alpha)}=0.20\pm 0.02$ and $C^{(f)}=0.49\pm 0.06$. The value of $C^{(\alpha)}$agrees very well with previously obtained results[10]

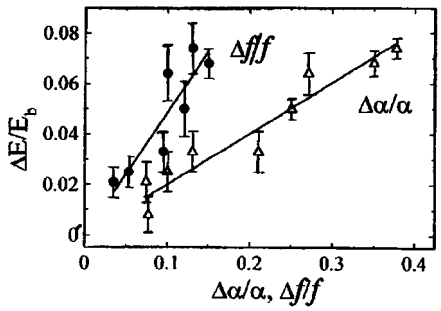

FIG. 3. Energy shift of the excitonic line in units of the binding energy versus the relative change in oscillator strength and versus the relative change in the maximum of the absorption coefficient for a fixed delay time ($\tau \approx 20$ ps) and different electron–hole pair densities.

but differ substantially from $C^{(f)}$. This confirms the incorrectness of the assumption employed in Ref. 10 that the saturation of the excitonic absorption is determined exclusively by a decrease of f. Our value of $C^{(f)}$ is the first experimental determination of this quantity, so that it can be compared only with the results of theoretical calculations. Using the results of Ref. 4, we find for a real quantum well that in the case when cold excitons are responsible for the change in f the proportionality coefficient $C^{(f)}$ equals

$$C_{\rm exc}^{(f)} = 0.45 E_b^{(2{\rm D})}/E_b\,, \tag{6}$$

and in the case when the cold plasma is responsible

$$C_{\rm pl}^{(f)} = 0.22 E_b^{(2{\rm D})}/E_b\,, \tag{7}$$

where $E_b^{(2{\rm D})}$ is the binding energy of an ideal two-dimensional exciton. It should be mentioned that in Ref. 4 the influence of the electron–hole plasma was completely ignored in the calculation of the quasiparticle-density dependence of the magnitude of the blue shift, which we employed to obtain expressions (6) and (7). As a result of the quite wide spectrum of the laser radiation, free charge carriers are generated under our experimental conditions. However, their effect on the energy position of the excitonic line is very small. This effect is expressed as a small deviation of the time dependence of the blue shift from an exponential for small values of τ (see Fig. 2) and leads to an error in the determination of ΔE of only several percent. Substituting into expressions (6) and (7) the value $E_b \approx 10$ meV, we obtain for our MQW $C_{\rm exc}^{(f)} = 0.76$ and $C_{\rm pl}^{(f)} = 0.37$. Comparing these values with the experimental value $C^{(f)} \approx 0.49$, it is easy to conclude that despite their very low density the free electron–hole pairs have the decisive influence on the decrease of f for an excitonic transition. This result confirms the Schmitt-Rink prediction that the influence of free carriers on f is much more effective than that of excitons.[4]

As one can see from Fig. 2, a change in f is observed during the first 120 ps, while the broadening and shift of the excitonic line, which will be shown below to be due to the exciton–exciton interaction, continue for another several hundreds of picoseconds. Such a rapid return of f to its initial value is due to the vanishing of the free carriers from the system of interacting particles. Using an exponential function to describe the behavior of

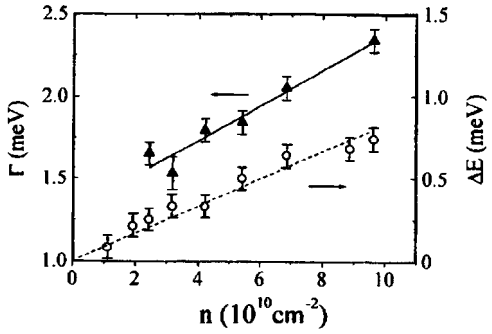

FIG. 4. Width of the excitonic absorption line and energy shift of the absorption maximum versus the electron–hole pair density for constant delay time $\tau \approx 20$ ps.

f, we were able to measure directly the lifetime of the free electron–hole pairs. It was found that this time remains practically unchanged right up to electron–hole pair densities 10^{11} cm^{-2} and equals $T_{1,\mathrm{eh}} = 65 \pm 8$ ps.

The broadening of an excitonic line as a function of the particle density with a fixed delay time ($\tau \approx 20$ ps) is displayed in Fig. 4 (triangles). As one can see from the figure, we obtained a clear linear dependence. This attests to the fact that the exciton–exciton interaction is responsible for the appearance of broadening. Free electron–hole pairs would have produced a square-root dependence.[11] To describe the behavior of the excitonic linewidth, we employ the relation

$$\Gamma_x(n) = \Gamma_x(0) + \gamma E_b a_b^2 n_x, \tag{8}$$

where a_b is the Bohr radius of an exciton in our MQW, n_x is the density of the two-dimensional excitonic gas, and γ is a proportionality coefficient. To determine a_b we shall employ a relation obtained by means of calculations based on a description of quantum wells as a medium with a fractional dimension[12]

$$E_{1S}^{(\alpha)} a_b^{(\alpha)} = \text{const}, \tag{9}$$

where $E_{1S}^{(\alpha)}$ and $a_b^{(\alpha)}$ are the binding energy and Bohr radius of an exciton in a medium of dimension α. A variational calculation[13] also confirms the validity of relation (9). For our MQW it was found that $E_{1S}^{(\alpha)} = E_b \approx 10$ meV ($\alpha \approx 2.3$) and therefore $a_b^{(\alpha)} \approx 59$ Å. Substituting $a_b^{(\alpha)}$ for a_b in Eq. (8) and approximating the experimental results, we find that for our excitation conditions $\gamma = 3.1 \pm 0.4$ and $\Gamma(0) = 1.30 \pm 0.08$. We shall now compare this value to the experimental result obtained in Ref. 14, where the broadening of the excitonic resonance was determined as a function of the particle density in a four-wave mixing experiment with preexcitation ($\tau \approx -20$ ps) of both free electron–hole pairs and excitonic states in the specimen. Using relation (9), we get $\gamma = 2.8 \pm 0.56$ for the case of exciton–exciton scattering from Ref. 14 and $\gamma = 21.8 \pm 3.7$ for scattering by free carriers. Our value of γ confirms unequivocally the conjecture that in the case of resonance excitation the broadening of the excitonic lines is governed by the exciton–exciton interaction.

Let us now compare the experimental scattering efficiency γ with the calculations performed in Ref. 15. It was found there that the exciton–exciton scattering is described by the parameter $\gamma^{(2D)}=0.41$ for an ideal two-dimensional quantum well and by $\gamma^{(3D)}=56.6$ for an ideal bulk semiconductor. Our value $\gamma\approx 3.1$ falls between $\gamma^{(2D)}$ and $\gamma^{(3D)}$, attesting to the fact that we are dealing with an intermediate quasi-two-dimensional case.

The energy shift ΔE of the excitonic line as a function of the photoexcited-carrier density ($\tau\approx 20$ ps) is displayed in Fig. 4. As expected for the case of exciton–exciton interaction, a clear linear dependence is observed. The proportionality coefficient between ΔE and n was found to be $C=0.083$, while for an ideal two-dimensional quantum well it should be $C=0.24$ (Ref. 4). In our opinion, this small discrepancy is due to the interaction of excitons from neighboring quantum wells, as a result of which the wells approach the three-dimensional limit and therefore the magnitude of the blue shift decreases. It follows from the linear dependence of ΔE on the quasiparticle density that the characteristic time of the exponential decrease of ΔE should equal the lifetime $T_{1,\mathrm{exc}}$ of excitonic states. Furthermore, the broadening of the excitonic line also decreases exponentially with the same characteristic time $T_{1,\mathrm{exc}}$(see Fig. 2). Therefore we have found that the lifetime of excitonic states is $T_{1,\mathrm{exc}}=410\pm 14$ ps and remains constant right up to densities of 10^{11} cm^{-2}. The fact that $T_{1,\mathrm{exc}}$ is constant indicates that the range of variation of the exciton density employed in our experiment is much smaller than the Mott-transition density. This justifies using the low-density limit for describing the experimental results.

In the present work we have distinguished the simultaneous contributions of a change in oscillator strength and broadening of excitonic lines to the saturation of excitonic absorption and have shown that, despite the low free-carrier density, for femtosecond resonance laser excitation the change in the oscillator strength is due mainly to free electron–hole pairs, while the broadening and energy shift of the excitonic lines are due to the exciton–exciton interaction. This shows that at low temperatures free carriers influence the oscillator strength much more efficiently than do excitons. The lifetimes of free electron–hole pairs and excitons were determined from the time variation of the values of the excitonic parameters: $T_{1,\mathrm{eh}}=65\pm 8$ ps and $T_{1,\mathrm{exc}}=410\pm 14$ ps, respectively

This work was supported by the Russian Fund for Fundamental Research (Grants Nos. 95-02-05046 and 97-02-16833), INTAS (Grant No. 94-0324), and INTAS-RFBR (Grant No. 95-0576).

[a)]e-mail: kostja@ipmt-hpm.ac.ru

[1] A. Gorshunov, V. I. Grinev, K. L. Litvinenko *et al.*, Zh. Éksp. Teor. Fiz. **109**, 665 (1996) [JETP **82**, 356 (1996)].
[2] N. Peyghambarian and H. M. Gibbs, Phys. Rev. Lett. **53**, 2433 (1984).
[3] W. H. Koch, R. L. Fork, M. C. Downer *et al.*, Phys. Rev. Lett. **54**, 1306 (1985).
[4] S. Schmitt-Rink, D. S. Chemla, D. A. B. Miller *et al.*, Phys. Rev. B **32**, 6601 (1985).
[5] D. R. Wake, H. W. Yoon, J. P. Wolfe *et al.*, Phys. Rev. B **46**, 13452 (1992).
[6] L. Schultheis, J. Kuhl, A. Honold *et al.*, Phys. Rev. Lett. **57**, 1635 (1986).
[7] A. Honold, L. Schultheis, J. Kuhl, and C. W. Tu, Phys. Rev. B **40**, 6442 (1989).
[8] S. Hunsche, K. Leo, H. Kurz, and K. Kohler, Phys. Rev. B **49**, 16565 (1994); V. Grigor'ev, V. I. Grinev,

K. L. Litvinenko *et al.*, Fiz. Tverd. Tela (St. Petersburg) **38**, 184 (1996) [Phys. Solid State **38**, 101 (1996)].
[9] G. Korn and T. Korn, *Mathematical Handbook for Scientists and Engineers*, McGraw-Hill, New York, 1961 [Russian translation, Nauka, Moscow, 1971].
[10] K.-H. Schlaad, Ch. Weber, J. Cunningham *et al.*, Phys. Rev. B **43**, 4268 (1991).
[11] J.-Y. Bigot, M. T. Portella, R. W. Schroenlein *et al.*, Phys. Rev. Lett. **67**, 636 (1991).
[12] P. Lefebvre, P. Christol, and H. Mathieu, Phys. Rev. B **48**, 17308 (1993).
[13] Y. Shinozuka and M. Matsuura, Phys. Rev. B **28**, 4878 (1983); **29**, 3717 (1984).
[14] A. Honold, L. Schultheis, J. Kuhl, and C. W. Tu, Phys. Rev. B **40**, 6442 (1989).
[15] G. Manzke, K. Heneberger, and V. May, Phys. Status Solidi B **139**, 233 (1987).

Translated by M. E. Alferieff

Experimental determination of the rate constant for spin exchange in collisions of polarized metastable helium atoms with ground-state cesium atoms

S. P. Dmitriev, N. A. Dovator, and V. A. Kartoshkin[a)]
A. F. Ioffe Physicotechnical Institute, Russian Academy of Sciences, 194021 St. Petersburg, Russia

(Submitted 16 June 1997)
Pis'ma Zh. Éksp. Teor. Fiz. **66**, No. 3, 145–148 (10 August 1997)

The rate constant for spin exchange in a system consisting of a metastable helium atom and an alkali-metal atom is determined. An experiment on optical orientation of atoms established that the rate constant for spin exchange in a collision of a metastable 2^3S_1 helium atom with a cesium atom in the $6^2S_{1/2}$ ground state equals $(2.8\pm 0.8)\times 10^{-9}$ cm^3 s^{-1}. The rate constant for chemoionization of cesium atoms by metastable helium atoms was determined at the same time to be $(1.0\pm 0.3)\times 10^{9}$ cm^3 s^{-1}. © *1997 American Institute of Physics.* [S0021-3640(97)00415-5]

PACS numbers: 34.50.−s, 82.40.Dm

Investigations of atomic collisions in alkali–helium plasma are of interest not only for atomic physics but also for applications, for example, in the development of new types of quantum magnetometers.[1] Two types of processes occur simultaneously in collisions of metastable helium atoms with alkali atoms — inelastic (chemoionization) and elastic (spin exchange). However, the rate constant for the former process is now well known (see Refs. 2 and 3), whereas the rate constant for spin exchange in collisions of 2^3S_1 metastable helium atoms with $n^1S_{1/2}$ alkali atoms has still not been determined. This is due to the fact that in experiments with polarized particles, which are ordinarily employed for measuring the rate constant for spin exchange,[4] it is difficult to separate two simultaneously occurring spin-dependent processes.

In the present work, the rate constant for spin exchange in a collision of a polarized metastable helium atom with a cesium atom in the ground state was determined experimentally.

In a collision of excited metastable helium atoms in the 2^3S_1 state with cesium atoms in the $6^2S_{1/2}$ ground state, ionization of the cesium atoms occurs as a result of the high internal energy of excitation of the metastable helium atoms ($E=19.82$ eV), i.e., the following reactor occurs:

$$\mathrm{He}(2^3S_1,m_1)+\mathrm{Cs}(6^2S_{1/2},m_2)\rightarrow \mathrm{He}(1^1S_0)+\mathrm{Cs}^+(2^1S_0)+e^-(m_3). \quad (1)$$

The rate of the process (1) is $1/\tau_{ci}$. The reaction (1) is allowed when the total spin of the

system at the start of the reaction equals the total spin at the end of the reaction (here m_i is the projection of the electronic spin of the constituent particle onto a preferred direction).

The second process occuring simultaneously with chemoionization is spin exchange:

$$\mathrm{He}(2^3S_1, m_1) + \mathrm{Cs}(6^2S_{1/2}, m_2) \rightarrow \mathrm{He}(2^3S_1, m_1') + \mathrm{Cs}(6^2S_{1/2}, m_2'). \quad (2)$$

Here $m_1 + m_2 = m_1' + m_2'$, the total spin of the system, is conserved. The rate of the process (2) is $1/\tau_{se}$.

In the present letter we shall study the interaction of ^{133}Cs atoms with optically polarized helium atoms in the 2^3S_1 state. The helium atoms may be aligned or oriented along a static magnetic field H_z. It can be shown[5] that the rate of destruction of the orientation $\langle S_{\mathrm{He}} \rangle^z$ and alignment $\langle Q_{\mathrm{He}} \rangle^{zz}$ of metastable helium atoms depend on collisional processes of the type (1) and (2) as follows:

$$1/\tau_{or} = \pi \delta f_{or} = N_{\mathrm{Cs}}(1/3 \cdot C_{ci} + 1/2 \cdot C_{se}), \quad (3)$$

$$1/\tau_{al} = \pi \delta f_{al} = N_{\mathrm{Cs}}(1/3 \cdot C_{ci} + 3/2 \cdot C_{se}). \quad (4)$$

Here N_{Cs} is the density of cesium atoms, C_{ci} and C_{se} are the chemoionization and spin-exchange rate constants, and $\delta f_{or,al}$ is the contribution of the processes (1) and (2) to the width of the magnetic resonance line for the longitudinal components of the orientation and alignment of the helium atoms.

As one can see from Eqs. (3) and (4), the contribution to the width of the magnetic resonance line for aligned helium atoms should be different from that of oriented helium atoms. This difference makes it possible to determine the rate constants of the two simultaneously occurring processes.

The standard setup for investigating the optical orientation of atoms was employed in the experiment. Optical orientation of the spin moments of the metastable helium atoms was achieved with circularly polarized[b)] pump light and alignment was achieved with unpolarized pump light ($\lambda = 1.08$ μm) propagating along a magnetic field $H_z \cong 35$ mOe produced by Helmholtz coils inside a magnetic shield. The pump source was a helium capillary lamp in which an rf discharge was excited. The metastable state was filled by exciting an rf discharge in the volume of the absorption chamber containing ^{4}He gas ($P = 1$ torr at $T = 300$ K) and metallic cesium. The gas-discharge chamber was placed in a thermostat. The working temperature was determined by means of a thermistor glued onto the coldest part of the absorption chamber. The density of cesium atoms was regulated from 2.7×10^{10} to 2.5×10^{12} cm^{-3} by varying the temperature over the range 393–343 K. An amplitude-modulated rf magnetic field $H_1 = h \sin \Omega t \sin \omega t$, where $\Omega/2\pi = 250$ Hz and $\omega/2\pi \sim 100$ kHz is the rf frequency, was applied perpendicular to the magnetic field H_z in order to excite magnetic resonance in the system of Zeeman sublevels of the 2^3S_1 helium atoms. In the experiment, the change (at the modulation frequency Ω) in the intensity of the pump light passing through the absorption chamber was recorded by scanning the frequency ω near the magnetic resonance frequency $\omega_0 = \gamma H_z$ ($\gamma/2\pi = 2.8$ MHz/Oe). For low values of the rf amplitude $h \leqslant 0.1$ mOe (see Ref. 6) the magnetic resonance line was nearly Lorentzian (for both orientation and alignment of the helium atoms) and the width of the magnetic resonance line depended

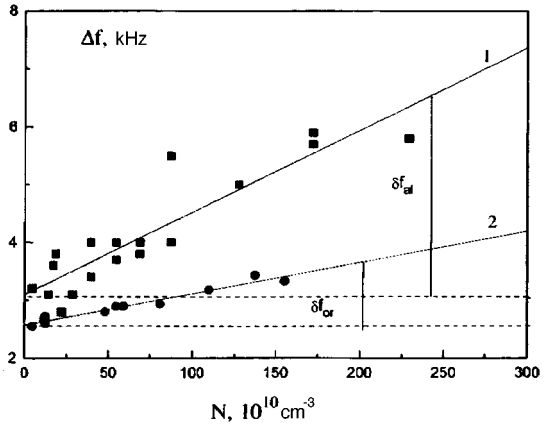

FIG. 1. Magnetic resonance linewidth of oriented (2) and aligned (1) metastable helium atoms versus the density N_{Cs} of ground-state cesium atoms; $\delta f_{or,al}$ is the broadening of the magnetic resonance line due to spin-exchange and chemoionization processes for oriented and aligned atoms.

mainly on relaxational collision processes occurring in the absorption chamber. The linewidth was determined at one-half the maximum amplitude of the magnetic resonance signal.

To find the desired spin-exchange rate constant, in the experiment we determined the increment $\delta f_{or,al}$ of the magnetic resonance linewidth (for both oriented and aligned helium atoms) as the density of cesium atoms increases on heating of the absorption chamber: $\delta f_{or,al}=\Delta f_{or,al}(T)-\Delta f_{or,al}(T_0)$, where $\Delta f_{or,al}(T_0)$ is the linewidth at $T=300$ K ($\sim 2-2$ kHz). To construct the curves of $\delta f_{or,al}$ versus the Cs atom density N_{Cs}, the temperature was converted to the value of N_{Cs} in accordance with the data given in Ref. 7.

In the experiment, several series of measurements were performed for the purpose of determining the dependence $\delta f(N_{\mathrm{Cs}})$ for both orientation and alignment. The data obtained were averaged both within each series and over the whole set of series. An example of the dependences $\delta f_{or,al}(N_{\mathrm{Cs}})$ obtained in one series of experimental measurements is presented in Fig. 1.

As one can see from the figure, the widths of the magnetic resonance lines are substantially different for oriented (2) and aligned (1) atoms.[c)] Indeed, it follows from Eqs. (3) and (4) that

$$\pi(\delta f_{al}-\delta f_{or})=N_{\mathrm{Cs}}C_{se}. \tag{5}$$

The value determined from Eq. (5) is $C_{se}=(2.8\pm 0.8)\times 10^{-9}$ cm^3 s^{-1}. The value obtained for C_{se} was used in Eqs. (3) and (4) to find the chemoionization rate constant $C_{ci}=(1.0\pm 0.3)\times 10^{-9}$ cm^3 s^{-1}. It should be noted that the main error in the present measurements is due to the error in determining the density of alkali atoms. This error is caused by both the presence of temperature gradients at the surface of the chamber and the error in measuring the working temperature of the chamber.

In conclusion, it should be noted that this is the first time that the spin-exchange rate constant has been determined, whereas the chemoionization rate constant, without allowance for the statistical factor $(1/3\cdot C_{ci})$, has been determined several times ($(0.44\pm 0.16)\times 10^{-9}$ cm^3 s^{-1} (Ref. 2) and $(0.45\pm 0.09)\times 10^{-9}$ cm^3 s^{-1}). As one can see from the results presented, our results are in satisfactory agreement with Refs. 2 and 3.

In closing, we thank the Russian Fund for Fundamental Research for supporting this work (Grant No. 95-02-04116-a).

[a)]e-mail: victor@kart.ioffe.rssi.ru

[b)]Both orientation and alignment can appear in the case of pumping by circularly polarized radiation. The relative degree of alignment in the magnetic resonance signal depends on the emission spectrum of the lamp and on the thickness of the optical layer in the absorption chamber. In our experiment this quantity did not exceed 10%.

[c)]It should be noted that the width of the magnetic resonance line of polarized helium atoms also depends on the rate of diffusion, spin exchange with electrons, and so on. In the present experiment the change (with increasing temperature) in the width of the magnetic resonance line as a result of these processes did not exceed the measurement error.

---

[1] E. V. Blinov, B. I. Ginzburg, and R. A. Zhitnikov, Zh. Tekh. Fiz. **54**, 287 (1984) [Sov. Phys. Tech. Phys. **29**, 163 (1984)].
[2] Yu. A. Tolmachev and D. Fogel', Opt. Spektrosk. **48**, 818 (1980) [Opt. Spectrosc. **48**, 451 (1980)].
[3] C. E. Johnson, C. A. Tipton, and P. G. Robinson, J. Phys. B: At. Mol. Phys. **11**, 927 (1978).
[4] W. Happer, Ann. Phys. (Paris) **10**, 645 (1985).
[5] V. A. Kartoshkin, G. V. Klement'ev, and V. D. Mel'nikov, JETP Lett. **39**, 156 (1984).
[6] V. A. Kartoshkin, G. V. Klement'ev, and V. D. Mel'nikov, Opt. Spektrosk. **65**, 792 (1988) [Opt. Spectrosc. **65**, 468 (1988)].
[7] I. Langmuir and J. B. Taylor, Phys. Rev. **51**, 753 (1937).

Translated by M. E. Alferieff

Nonergodicity and nonequilibrium properties of asperomagnets

A. B. Surzhenko and Yu. P. Grebenyuk
Institute of Magnetism, Ukrainian National Academy of Sciences, 252142 Kiev, Ukraine

(Submitted 18 June 1997)
Pis'ma Zh. Éksp. Teor. Fiz. **66**, No. 3, 149–153 (10 August 1997)

The nonequilibrium properties of asperomagnetic systems are studied for the example of the alloy Ni–23 at.% Mn. It is shown that the appearance of a de Almeida–Thouless phase, characterized by astronomic equilibration times $t_{\max} \gg 10^{15}$ s, is preceded by the formation of a Gabay–Toulouse phase, for which $t_{\max}$ is comparable to experimental times. © *1997 American Institute of Physics.*
[S0021-3640(97)00515-X]

PACS numbers: 75.50.Cc, 75.40.Cx

The ergodic hypothesis, i.e., the assumption that the Gibbs average $\langle \ldots \rangle_T$ is equivalent to a time average $\langle \ldots \rangle_t$, is a basic postulate of statistical physics. It is therefore not surprising that nonergodic systems, for which $\langle \ldots \rangle_T \neq \langle \ldots \rangle_t$, have been and continue to be of special interest to investigators.[1] On the basis of the accumulated information once can assert that such properties are inherent only to macroscopically degenerate systems, and the degree of nonergodicity Δ_S of the systems is determined by the observation time t_{obs}, more accurately, by the ratio of the observation and the maximum time $t_{\max}$ of a transition from one degenerate state into another. Specifically, spin glasses (SGs), in which $t_{\max}$ reaches astronomical values $t_{\max} \sim 10^{40}$ s $\gg t_{\text{obs}}$,[2,3] are obviously nonergodic. This property is widely employed for determining the freezing temperature of spin glasses in a magnetic field $H > 0$,[4] when the basic Edwards–Anderson order parameter $q_{ea} = \langle S^2 \rangle$ is nonzero not only in the SG phase but also in the paramagnetic (PM) phase.[2,3] However, the problem of finding the freezing temperature is most urgent for asperomagnetic (ASM) systems, where the SG behavior in the XY plane is accompanied by *spontaneous* ordering ($m_s \neq 0$, $q_{ea} \neq 0$) of the spins in the orthogonal, Z direction, even in the absence of an external field.[2] The solution of this problem is ordinarily reduced to obtaining the temperature dependence of the parameter $\Delta_s(H,T,t)$ from investigations of FC, ZFC curves.[4] In so doing, the error due to the increase in the effective observation time t_{obs} on heating is assumed to be quite small, since $t_{\max} \gg t_{\text{obs}}$. There is no doubt that this inequality is valid below the de Almeida–Thouless crossover line $T < T_{\text{AT}}(H)$,[2] where strong irreversibilities arise along the Z axis. However, near the Gabay–Toulouse (GT) phase line of freezing of the XY component $T_{\text{GT}}(H) \geqslant T_{\text{AT}}(H)$, which is what must actually be determined, $t_{\max}$ decreases catastrophically all the way down to FMR frequencies.[5] This can radically change the results of FC, ZFC experiments ($t_{\text{obs}} \geqslant 1$ s). To avoid this error, we used an approach satisfying the requirement $t_{\text{obs}} = \text{const}$ to study nonequilibrium ASM systems. In what follows, we make a comparative

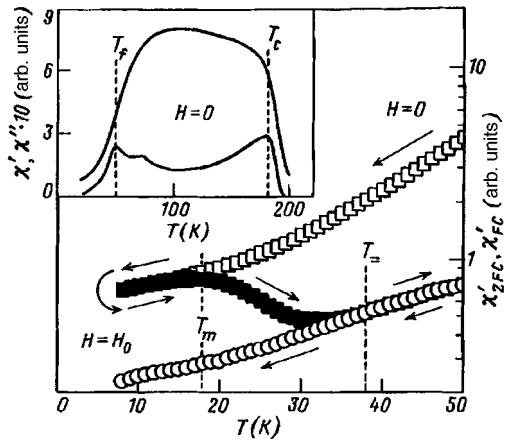

FIG. 1. Thermomagnetic cycle of the alloys Ni–23 at.% Mn: zero-field cooling — $\chi'_{\mathrm{FC=ZFC}}(H=0\ \mathrm{Oe}, T)$ (□), switching on of a magnetic field H_0 and heating — $\chi'_{\mathrm{ZFC}}(H_0,T)$ (□), cooling in a field — $\chi'_{\mathrm{FC}}(H_0,T)$ (○). Experimental conditions: $H_0=140$ Oe, magnetization-reversal frequency and amplitude $f=85$ Hz and $h=0.1$ Oe, heating rate ≈ 2 K/min. Inset: Real $\chi'(0,T)$ and imaginary $\chi''(0,T)$ components of the ac susceptibility ($f=85$ Hz, $h=0.1$ Oe).

analysis of our method and the conventional methods[2,4] and we discuss alternative descriptions of nonergodic systems.

The problem was solved for the particular case of a rapidly quenched alloy Ni–23 at.% Mn, in whose low-temperature phase ($T<T_1=51.2$ K, inset in Fig. 1) long-range ferromagnetic (FM) order and the SG coexist,[6] making it possible to identify the phase as an ASM phase. This latter capability makes the system of Ni–Mn alloys a classic object for checking theoretical ideas.[2] Another important consideration was the fact that thermomagnetic prehistory effects in a sample of roughly similar composition had been studied by ac methods,[7] in addition to the now-customary dc experiments. The quantity $\chi'_{\mathrm{ZFC}}(H_0,T)$ (see Fig. 1, curve) relaxes monotonically from one equilibrium value $\chi'_{\mathrm{FC}}(0,T)$ (□) to another $\chi'_{\mathrm{FC}}(H_0,T)$ (○) during heating. For sufficiently high measuring fields H_0, this gives rise to additional maxima. Thus two characteristic points, $T=T_m$, corresponding to a maximum of $\chi'_{\mathrm{ZFC}}(H_0,T)$, and $T=T_=$, above which $\chi'_{\mathrm{ZFC}}=\chi'_{\mathrm{FC}}$, can be distinguished on the curve $\chi'_{\mathrm{ZFC}}(H_0,T)$. Considering the strong dependence of any ZFC curve and therefore also of $T_m(t)$ and $T_=(t)$ (Fig. 1) on the heating rate dT/dt,[2,3] it can be asserted that the formal identification of the latter temperatures with T_{AT} and T_{GT}, as proposed in Ref. 7, is inadmissible. An objective assessment requires a nonergodicity criterion that does not depend on the observation time. The use of the time $t_{\max}$ required for the system to reach its equilibrium state, $\Delta_S(H,T,t_{\max})=0$, confers this advantage. To evaluate it experimentally it is more convenient to introduce a normalized function of the form

$$\Delta(t)|_{H,T=\mathrm{const}}=[\chi'_{\mathrm{ZFC}}(t)-\chi'_{\mathrm{ZFC}}(\infty)]/[\chi'_{\mathrm{ZFC}}(0)-\chi'_{\mathrm{ZFC}}(\infty)]|_{H,T=\mathrm{const}}, \qquad (1)$$

which, while retaining the physical meaning of the classical definition[4] of Δ_S, is more universal ($0\leqslant\Delta\leqslant 1$).

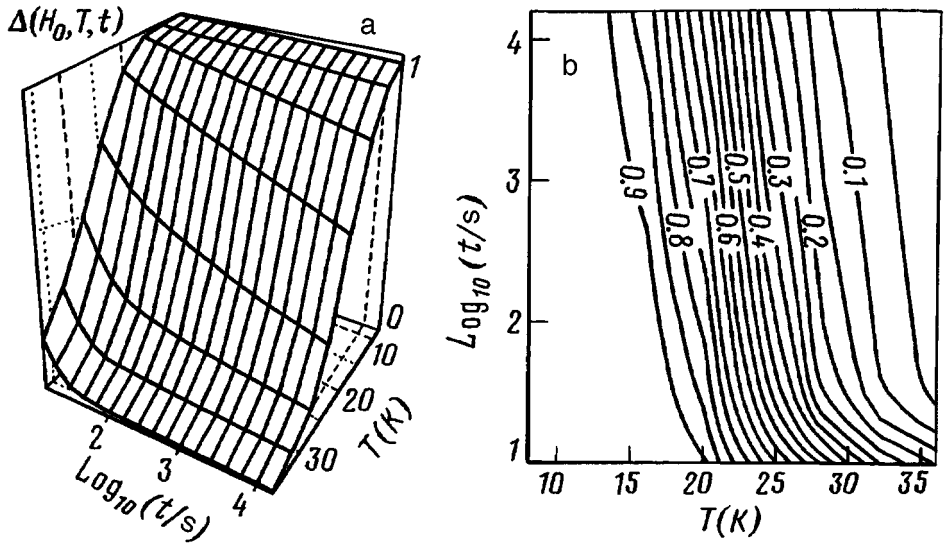

FIG. 2. Parameter of nonequilibrium $\Delta(H_0=140\ \text{Oe}, T, t)$ of the alloy Ni–23 at.% Mn represented as a surface (a) and its topographic projection (b).

Since the problem of recording the temperature dependences $\Delta(H_0,T,t)$ instantaneously ($t=$ const) cannot be solved by direct methods, we employed a method in which t can be strictly controlled — the study of relaxation curves followed by analysis of the temperature sections $\Delta(H_0,T,t=$ const). For convenience, a value $H_0=140$ Oe was chosen, which is such that the regions of strong ($T<T_m$) and weak ($T_m<T<T_=$) irreversibilities of the longitudinal response of the ASM are approximately equal. The correctness of the experiments was ensured by adhering to a single thermomagnetic prehistory: The sample was cooled from room temperature to the required value of T in a zero magnetic field and held under these conditions for 1 h (to eliminate any influence of a different cooling rate). Then a magnetic field $H_0=140$ Oe was switched on and the quantity $\chi'_{\text{ZFC}}(t)$ was recorded. Since an equilibrium state was usually not attained over the finite time of an experiment (~ 4 h), the function (1) was calculated in the approximation $\chi'_{\text{ZFC}}(H_0,T,t\to\infty)=\chi'_{\text{FC}}(H_0,T)$ (Fig. 1).

Let us examine the surface $\Delta(H_0,T,t)$ and its topographic projection, which are displayed in Figs. 2a and 2b, respectively. The small distortions observed at short times $\text{Log}(t/\text{s})<1.5$, which are due to the integration constant ≈ 1 s of the output cascade of the apparatus, on the whole, cannot change the general conclusion that the relaxation curves are logarithmic. The logarithmic time metric is due to the ultrametric topology of the phase space of SGs and is a consequence of the anomalously wide and practically uniform spectral distribution of their relaxation times.[3] It is obvious that the desired quantity $t_{\max}$ is the upper limit of the width of this spectrum. To calculate it, both the time sections $\Delta(t)$ and temperature sections $\Delta(T)\sim\tau^{\beta}$ (Ref. 4) of the surface $\Delta(H_0,T,t)$ were used. While the extrapolation of the lines $\Delta[\text{Log}(t_{\max})]$ to zero did not present any difficulties, in the second case an additional procedure was required — it was necessary

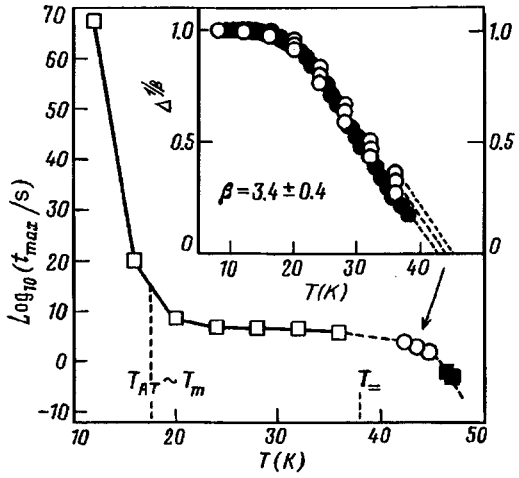

FIG. 3. Temperature dependence of the time $t_{\max}(H_0=140$ Oe, $T)$ for the alloy Ni–23 at.% Mn to reach its equilibrium state. The points were obtained by extrapolating the time (□) and temperature (○) curves $\Delta(H_0,T,t_0)$, the squares □ correspond to the temperature maxima of $\chi''_{\rm FC}(H_0,T)$ observed with different magnetization reversal frequencies $f=85$ and 850 Hz. Inset: Linearized dependence $\Delta(H_0=140$ Oe, T, $t_0=$const) (top to bottom: $\mathrm{Log}(t_0/\mathrm{s}=2,3,4)$ (○)), obtained by a section of the surface in Fig. 2, and the quantity $\Delta(H_0=140$ Oe, $T, t\neq$ const) (●) calculated from the results $\chi'_{\rm ZFC}$ and $\chi'_{\rm FC}$ of the thermomagnetic cycle in Fig. 1.

to find the exponent β that gave the optimal linearization of the curves $[\Delta(T)]^{1/\beta}$. It is important that the system of parallel straight lines (top to bottom in the inset in Fig. 3 (○): $\tau=10^2$, 10^3, 10^4 s) obtained in the process ($\beta=3.4\pm0.4$) is *intersected* by the curve $[\Delta(T)]^{1/\beta}$ (●) constructed from the results for $\chi'_{\rm FC}$ and $\chi'_{\rm ZFC}$ (Fig. 1) in the standard approximation $\chi'_{\rm ZFC}(t=0)=\chi'_{\rm FC}(H=0,T)$, $\chi'_{\rm ZFC}(t\to\infty)=\chi'_{\rm FC}(H_0,T)$.[2,3] This fact clearly reflects an increase in the effective observation time on heating of the specimen in the course of a standard FC, ZFC experiment and the unavoidable error, associated with this increase, in determining the temperature $T_{\rm GT}$.[4] Finally, besides the above-described methods, which yield information mainly about the macroscopic times $t_{\max}$, the appearance of a weak irreversibility can be judged according to the temperature of the maximum of the imaginary part $\chi''(H_0,T)$. It is clearly seen from Fig. 3 that the points (□) corresponding to the magnetization-reversal frequencies $f=85$ and 850 Hz fit in reasonably well and supplement helpfully the overall picture of the evolution of the ASM.

The results obtained give every reason to doubt the validity of the prevailing opinion that the freezing temperature of a SG decreases as the observation time $t_{\rm obs}$ increases. Indeed, the fact that an equilibrium state $t_{\rm obs}\geqslant t_{\max}(T)$ is reached does not at all mean that the GT phase as such vanishes. Then, even the temperature $T_=(t_{\rm obs})$, whether determined in the course of ZFC, FC measurements[4] ($t_{\rm obs}=1-10^4$ s) or by ac[2] ($t_{\rm obs}=10^{-6}-10^{-1}$ s) or resonance[2,5] ($t_{\rm obs}=10^{-12}-10^{-8}$ s) methods should be regarded not as a phase transition but only as a boundary separating the equilibrium $T>T_=(t_{\rm obs})$ and nonequilibrium $T<T_=(t_{\rm obs})$ states. The latter temperature will coincide with the temperature $T_{\rm GT}$ and/or

T_{AT} only for an appropriate choice of the threshold criterion $T_{GT/AT}(T_=)$ for weak/strong nonergodicity. Unfortunately, the m-vector model[2] of a SG does not give any estimates for this, and very few experiments have been done to study the distribution of the relaxation times in the SG phase. Essentially the only results[8] have been obtained in an investigation of the dilute SG $Cu_{96}Mn_4$ in zero field. Nonetheless, the use of these results for $H \neq 0$, $T < T_{AT}$ is entirely justified, since below the AT line the SG dynamics is essentially independent of the strength of the magnetic field. This is indicated by the reasonable agreement between the ''universal'' value $d\mathrm{Log}(T_1)/d\mathrm{Log}(\omega) = 2.2 \times 10^{-3}$ obtained in a study of the frequency dependence (2.6 Hz $< \omega <$ 1.33 kHz) of the maximum of $\chi'(H=0,T_1)$ for the alloys $Cu_{1-x}Mn_x$ $(0.0094 < x < 0.064)$[9] and our estimate $[dT_=/d\mathrm{Log}(t_{max})]/T_f \approx (-2.0 \pm 0.2) \times 10^{-3}$ ($H_0 = 140$ Oe, $16 > T > 8$ K, $10^{20} < t_{max}(\mathrm{s}) < 10^{110}$). According to Ref. 8, at $T = 0.9T_{AT}$ $t_{max} \approx 10^{20}$ s, whence it is possible to reconstruct the temperature $T_{AT} = 17.6$ K and a corresponding criterion for strong nonergodicity $t_{AT}(T_{AT}) \approx 10^{16}$ s. As expected, on account of the slow relaxation of $\chi'_{ZFC}(H_0, T \leqslant T_{GT})$ (see Fig. 1) the value $T_m = 18 \pm 1$ K is a quite good approximation for T_{AT}. In the case $T_{AT} < T < T_{GT}$, however, the relaxation processes are much faster. For example, for $10^2 < t(\mathrm{s}) < 10^4$ the characteristic slope of the isolines $[dT/d\mathrm{Log}(t)] \approx 1.2$ K $\approx -0.024T_f$ (see Fig. 2b) is practically constant and is approximately an order of magnitude greater than the same indicator for $T < T_{AT}$. This makes the temperature T_{GT} extremely sensitive to the choice of threshold $t_{GT}(T_=)$. However, since the absolute values of $t_{max}(T_{AT} < T < T_{GT})$ depend on the anisotropy of the experimental object and can vary from one specimen to another,[2] there apparently does not exist a universal value of $t_{GT}(T_=)$. Nonetheless, to avoid the error due to different observation times in constructing the $H-T$ phase diagrams it is essential to adhere to a single, separately specified criterion — for our case it is reasonable to choose $t_{GT}(T_=) = 1$ s.

In closing, we note that the results of an investigation of asperomagnetism which were presented above should not be regarded as isolated and unique. They undoubtedly could be helpful for understanding complicated evolution processes in classical spin glasses in a magnetic field as well as a wide class of other nonergodic systems (structural, dipole, vortex glasses and so on).

We thank G. A. Takzeĭ for helpful discussions.

[1] R. G. Palmer, Adv. Phys. **31**, 669 (1982).
[2] K. Binder and A. P. Young, Rev. Mod. Phys. **58**, 801 (1986).
[3] S. L. Ginzburg, *Irreversible Processes in Spin Glasses* [in Russian], Nauka, Moscow, 1989.
[4] Y. Yeshurun, Philos. Mag. B **50**, 285 (1983).
[5] G. A. Takzei, M. V. Gavrilenko, A. B. Surzhenko, and S. V. Tarapov, J. Magn. Magn. Mater. **140–144**, 221 (1995).
[6] Yu. P. Grebenyuk and G. A. Takzeĭ, Metallofiz. Noveĭshie Tekhnologii **16**, 3 (1994).
[7] H. Kunkel, R. M. Roshko, W. Ruan, and G. Williams, J. Appl. Phys. **69**, 5060 (1991).
[8] L. Lundgren, P. Svedlindh, P. Nordblad, and O. Beckman, Phys. Rev. Lett. **51**, 911 (1983).
[9] C. A. M. Mulder, A. J. van Duyneveldt, and J. A. Mydosh, Phys. Rev. B **23**, 1384 (1981).

Translated by M. E. Alferieff

Resistivity of 2D electrons with $\nu=1/2$ in a zero magnetic field

G. M. Gusev, Z. D. Kvon, and E. B. Ol'shanetskiĭ
Institute of Semiconductor Physics, Siberian Branch of the Russian Academy of Sciences, 630090 Novosibirsk, Russia

J. C. Portal and D. K. Maude
LCMI–CNRS, F38042 Grenoble, France

(Submitted 19 December 1996; resubmitted 26 June 1997)
Pis'ma Zh. Éksp. Teor. Fiz. **66**, No. 3, 154–158 (10 August 1997)

The dependence of the resistivity of 2D electrons with Landau level filling factor $\nu=1/2$ in a zero magnetic field is studied experimentally as a function of the carrier density. It is found that the ratio of the resistivity for $B=0$ and $\nu=1/2$ is a linear function of the carrier density, as predicted by a theory based on the scattering of composite fermions by spatial fluctuations of the effective static magnetic field. [S0021-3640(97)00615-4]

PACS numbers: 73.40.Hm, 71.70.Di

A new approach for describing the electronic properties of the fractional quantum Hall effect by means of the Chern–Simon gauge field theory was recently proposed in Ref. 1. According to this theory, near a Landau filling factor $\nu=1/2$ electrons are bound with two magnetic flux quanta and form a new quasiparticle — a composite fermion. For $\nu=1/2$ the external magnetic field is completely compensated and the composite fermions move in a nonuniform effective magnetic field induced by fluctuations of the impurity potential. In Refs. 1 and 2 the resistivity of composite fermions due to scattering by fluctuations of the magnetic field was calculated. Assuming that each charged impurity produces a local fluctuation of the effective magnetic field, it was shown that the scattering of composite fermions by a fluctuating magnetic field predominates over Coulomb scattering by the same impurities. It was found that the ratio of the resistivity R_{xx}^{CF} of the composite fermions to the resistivity R_{xx}^{e} of the electrons in a field $B=0$ equals $(k_F ds)^2$, where k_F is the electron Fermi wave number equal to $(2\pi N_s)^{1/2}$, N_s is the electron density, and ds is the distance between uncorrelated charged impurities and 2D electrons. For the case $k_F ds \gg 1$ it was found to be possible to explain the experimental fact that the resistivity of composite fermions in a field $B=0$ is many times greater than that of electrons.[3] However, a detailed comparison of the resistivity of composite fermions with a theoretical calculation was not made.

In the present work these measurements were performed on samples for which the resistivity of the electrons and composite fermions could be varied via the gate voltage. It was found that over more than an order-of-magnitude variation of the resistivity of the fermions, the ratio $R_{xx}^{\mathrm{CF}}/R_{xx}^{e}$ depends linearly on the density, in accordance with the theoretical predictions.[1]

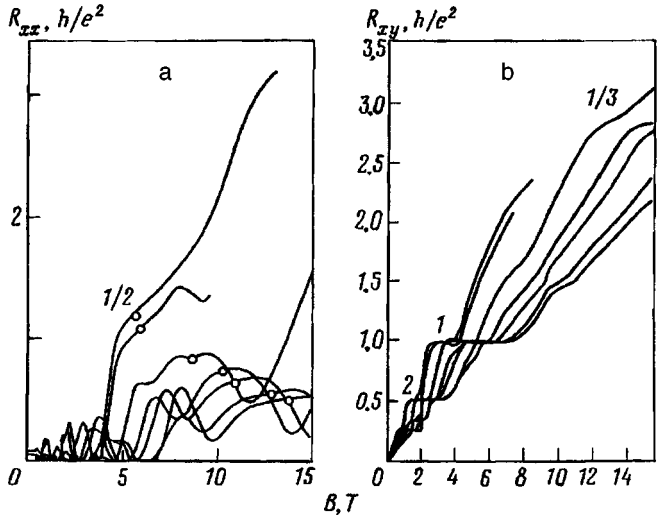

FIG. 1. $T=200$ mK; gate voltage $V_g=0.1$–0.4 V; a — $R_{xx}(B)$; the dots represent the resistivity for $\nu=1/2$; b — $R_{xy}(B)$.

The specimens consisted of AlGaAs/GaAs heterostructures with a 2D electron gas. The Hall bridges had dimensions of 50×100 μm and were coated with a gold and nickel gate. The density was varied over the range $(0.4$–$1.8)\times10^{11}$ cm^{-2}. The undoped AlGaAs region (spacer) was 60 nm wide. The mobility varied from 15 to 65 m^2/V$\cdot$s. The measurements were performed with an ac current not exceeding 10^{-8} A and at a frequency of 6.6 Hz in magnetic fields up to 15 T. The temperature was varied from 50 mK up to 1 K. Two specimens were investigated. The measurement results obtained for one specimen are presented in detail.

Figure 1 displays typical curves of the diagonal (a) and Hall (b) resistivities versus the magnetic field for different gate voltages (0–0.4 V). The points give the resistivity $R_{xx}^{\rm CF}$ at a Landau-level filling factor $\nu=1/2$. One can see that $R_{xx}^{\rm CF}$ decreases with increasing density and magnetic field. Minima at fractional filling factors of 1/3 and 2/3 are visible. One can also see that $R_{xx}^{\rm CF}$ increases logarithmically with decreasing temperature for $T<300$ mK.[4] It was recently shown that these temperature corrections could be due to the interaction between the composite fermions in the presence of a scattering potential.[5] To take account of only the T-independent component of the scattering of composite fermions, we measured the resistivity $R_{xx}^{\rm CF}$ for $T>200$ mK (Fig. 1). For $T=50$ mK the minima at 2/3 and 1/3 vanish, and flat plateaus are observed. Nonetheless, the T-dependent corrections did not exceed 10% of the total resistivity as the temperature varied from 50 mK to 1 K. Figure 2a shows the low-field part of the magnetoresistivity for different gate voltages. For clarity, the same dependence is shown on a logarithmic scale in Fig. 2b. One can see that the resistivity for $B=0$ changed by not more than an order of magnitude, but the Shubnikov–de Haas oscillations arose at the same fields 0.25 T irrespective of density (Fig. 2b). The resistivity in a zero magnetic field is determined by the transport relaxation time, which is more than an order of magnitude greater than

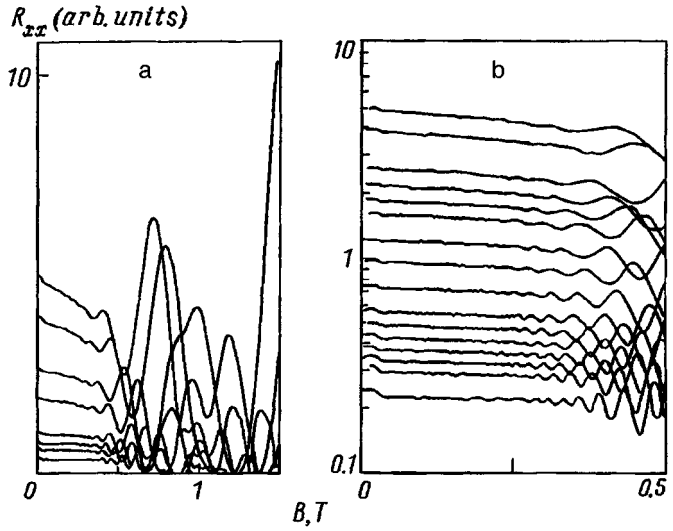

FIG. 2. $R_{xx}(B)$ near $B=0$ on linear (a) and logarithmic (b) scales.

the quantum relaxation time, which determines the amplitude of the Shubnikov oscillations in a magnetic field.[6] This attests to the long-range character of the impurity potential. In the case of a short-range impurity the transport and quantum times are equal to each other.[7] In contrast to the transport relaxation time, for a long-range impurity potential the quantum time has been studied comparatively little (see the discussion in Ref. 7). As the temperature decreased, the resistivity of the electrons in zero magnetic field also increased logarithmically on account of weak localization effects.[8] However, since $R^e_{xx} \ll h/e^2$, these corrections were less than 1%.

Figure 3a displays the experimental density dependences of the resistivity of the electrons (squares) and composite fermions for $\nu=1/2$ (circles). Up to $N_s \sim 1.2\times 10^{11}$ cm^{-2} a power-law decrease of the resistivity with increasing density is observed for electrons and for composite fermions with $\nu=1/2$; this is described to a high degree of accuracy by the relations $\rho^e_{xx} \sim N_s^{-5/2}$ and $\rho^{\mathrm{CF}}_{xx} \sim N_s^{-3/2}$, respectively. As the carrier density increases further, in both cases the rate of decrease of the resistivity decreases. We note that the relation $\mu \sim N_s^{-3/2}$ for electrons near $B=0$ was also observed earlier.[9] Figure 3a also displays several values of the resistivity for $\nu=3/2$ (triangles) in the range $N_s=(0.753\text{–}1.97)\times 10^{11}$ cm^{-2}. For $\nu=3/2$, this density range in the experimental specimens is a transitional range from an integer to a fractional quantum Hall effect and, as one can see, the dependence of the resistivity in this case is substantially different from the corresponding dependences for electrons in a field $B=0$ and composite fermions with $\nu=1/2$. Figure 3b shows the ratio of the resistivity of the composite fermions to the resistivity of the electrons as a function of the density; this function is linear up to $N_s \sim 1.2\times 10^{11}$ cm^{-2}.

Let us now compare the experimental results with theory. In Ref. 1 the resistivity of electrons with $B=0$ (scattering by fluctuations of the Coulomb field) and the resistivity

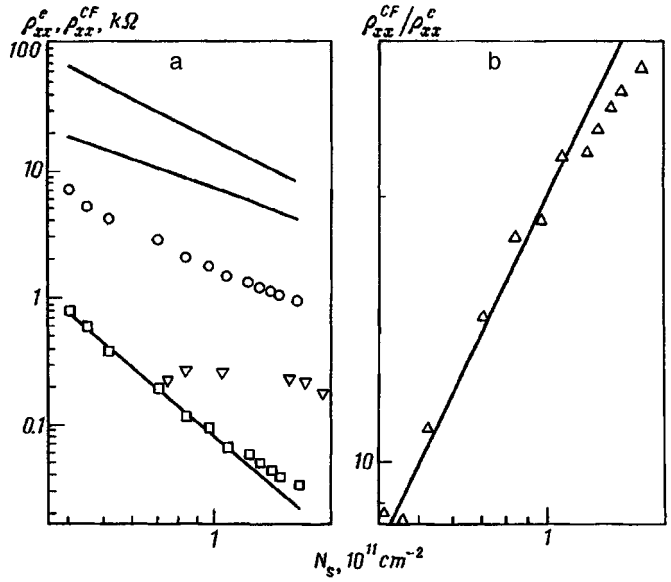

FIG. 3. a — Experimental curves of ρ_{xx}^{e} (squares) and ρ_{xx}^{CF} (circles) versus the electron density. The resistivity for $\nu=3/2$ (triangles). *1*, *2*, *3* — Curves constructed using Eqs. (1), (2), and (3), respectively, for $N_{\mathrm{imp}}=1.5\times10^{11}$ cm^{-2} and $ds=40$ nm. b — Ratio $\rho_{xx}^{\mathrm{CF}}/\rho_{xx}^{e}$ (dots — experiment, straight line — $\rho_{xx}^{\mathrm{CF}}/\rho_{xx}^{e}\sim N_s$).

of composite fermions with $\nu=1/2$ (scattering by fluctuations of the magnetic field) was calculated. The formulas were derived in the Born approximation for electron transport in a heterojunction, where a spacer separates the two-dimensional carrier gas from the scattering impurities. The relation

$$\rho_{xx}^{e}=\frac{h}{e^2}\frac{N_{\mathrm{imp}}}{N_s}\frac{1}{16(k_F ds)^3} \tag{1}$$

was obtained for electrons.[1] Correspondingly, for composite fermions

$$\rho_{xx}^{\mathrm{CF}}=\frac{h}{e^2}\frac{N_{\mathrm{imp}}}{N_s}\frac{2}{k_F' ds}. \tag{2}$$

We note that k_F and k_F' differ by a factor of $\sqrt{2}$, since the electrons are spin-degenerate, while the composite fermions are spin polarized. Substituting in Eqs. (1) and (2) the expression for the wave number in terms of the electron density, we obtain precisely the power-law dependences which, as we noted above, describe the experimental dependences in Fig. 3a. Therefore the theory of Ref. 1 gives the correct functional description of the experimental curves. To make a quantitative comparison of Eqs. (1) and (2) with experiment it is necessary to obtain more accurate values of the parameters N_{imp} and ds in these equations. Since in our case the electron mobility is much lower than in other specimens with approximately the same spacer thickness,[10] it can be conjectured that a large number of residual impurities are present in the spacer which effec-

tively decrease the spacer thickness. Taking $N_{\rm imp}=1.5\times10^{11}$ cm^{-2}, a fit of Eq. (1) to the experimental dependence of the resistivity for electrons gives an effective spacer thickness $ds=40$ nm. Figure 3a displays the curves corresponding to Eqs. (1) and (2) for $N_{\rm imp}=1.5\times10^{11}$ cm^{-2} and $ds=40$ nm. For these values of the parameters a numerical discrepancy is observed between Eq. (2) and the experimental dependence for composite fermions.

As we have said, Eqs. (1) and (2) were obtained in the Born approximation. Whereas this approximation is correct for electrons in the entire experimental density range, for composite fermions it is valid, strictly speaking, only in the limit $N_s \gg N_{\rm imp}$ (Ref. 2). A new approach that makes it possible to solve the Boltzmann equation without using the Boltzmann approximation was developed in Ref. 2. Specifically, the following relation was obtained for composite fermions near $\nu=1/2$:

$$\rho_{xx}^{\rm CF}=\frac{h}{e^2}\,\frac{1}{k_F' ds}\,\frac{1}{\exp(\alpha)K1(\alpha)}. \tag{3}$$

This relation is displayed in Fig. 3a for $N_{\rm imp}=1.5\times10^{11}$ cm^{-2} and $ds=40$ nm. Like Eq. (2), for these values of the parameters Eq. (3) gives too high a value of the resistivity of composite fermions, but the quantitative discrepancy with the experimental results is smaller in this case. The slope of the function (3) differs from that of the experimental dependence for $N_s<1.2\times10^{11}$ cm^{-2} but equals the experimental slope for higher densities, i.e., in the region where the discrepancy with the theory of Ref. 1 appears.

In summary, in this study we have investigated experimentally the electron-density dependence of the resistivity of composite fermions with $\nu=1/2$ and electrons in a field $B=0$. A comparison was made with the theories of Refs. 1 and 2. It was shown that for $N_s<N_{\rm imp}$ the theory of Ref. 1 gives the correct functional description of the behavior of the experimental dependences for both electrons and composite fermions. At the same time, a numerical discrepancy between experiment and the theories of Refs. 1 and 2 is observed. In the theory of Ref. 1 this discrepancy cannot be eliminated simultaneously for electrons and composite fermions by adjusting the parameters.

This work was supported in part by the INTAS program (Grant No. 94-668).

[1] B. I. Halperin, P. A. Lee, and N. Read, Phys. Rev. B **47**, 7312 (1993).
[2] D. V. Khveshchenko, cond-matter/9604165 (1996).
[3] R. L. Willet, R. R. Ruel, K. W. West, and L. N. Pfeiffer, Phys. Rev. Lett. **71**, 3846 (1993).
[4] L. P. Rokhinson *et al.*, Phys. Rev. B **52**, 11588 (1995).
[5] D. V. Khveshchenko, Phys. Rev. Lett. **77**, 362 (1996).
[6] P. T. Coleridge, Phys. Rev. B **44**, 3793 (1991).
[7] B. Laikhtman and E. L. Altshuler, Ann. Phys. **232**, 332 (1994).
[8] P. A. Lee and T. V. Ramakrishnan, Rev. Mod. Phys. **57**, 287 (1985).
[9] K. Hirakawa and H. Sakaki, Phys. Rev. B **33**, 8291 (1986).
[10] W. Kang, Song He, H. L. Stromer *et al.*, Phys. Rev. Lett. **75**, 4106 (1995).

Translated by M. E. Alferieff

Weak ferromagnetism and oxygen ordering in La_2CuO_{4+x} single crystals

A. A. Nikonov, O. E. Parfenov, and A. A. Zakharov
Kurchatov Institute Russian Science Center, 123182 Moscow, Russia

(Submitted 26 June 1997)
Pis'ma Zh. Éksp. Teor. Fiz. **66**, No. 3, 159–162 (10 August 1997)

The changes produced in the magnetic properties and structure of La_2CuO_{4+x} ($0<x<0.015$) single crystals by doping with oxygen are investigated by differential magnetic susceptibility and x-ray diffraction methods. It is found that the appearance of a weak ferromagnetism in weak fields $H<50$ Oe is accompanied by a lowering of lattice symmetry as a result of the oxygen ordering. © *1997 American Institute of Physics.* [S0021-3640(97)00715-9]

PACS numbers: 75.50.Cc, 75.40.Cx

In our preceding work[1] we observed weak ferromagnetism (FM) in lightly doped La_2CuO_{4+x} crystals in fields $H<50$ Oe. At the same time, it is well known that in stoichiometric La_2CuO_4 a spontaneous FM moment cannot appear in zero and weak magnetic fields on account of the difference of the magnetic and crystallographic unit cells. In Ref. 2 it was determined on the basis of a symmetry analysis that stoichiometric La_2CuO_4 possesses a weakly noncollinear antiferromagnetic (AFM) structure. It was shown that a first-order transition into a weak-FM phase is possible in a high magnetic field. In a high magnetic field the copper magnetic symmetry increases as a result of spin flipping and agrees with the crystallographic symmetry, as a result of which a weak $10^{-3}\mu_b$/Cu FM moment directed along the c axis appears.[3] However, lattice matching can be achieved through a lowering of the symmetry of the crystal lattice by an ordering of the impurity oxygen along definite positions in the La_2CuO_4 unit cell.

Our objective in the present work is to establish, by measuring the magnetic susceptibility $\chi_{ac}(T)$ in a low magnetic field and by x-ray crystallographic analysis, a correlation between the anomalous magnetic properties of La_2CuO_{4+x} single crystals and the structural changes produced in the crystal lattice by doping with oxygen.

The magnetic susceptibility was measured by a double synchronous detection method.[7] During the measurements the specimen was placed in a low ac field $h=h_0\sin(\omega t)$, with $h_0=3$ Oe and $f=3$ kHz. The temperature was varied in the range $80<T<350$ K. X-ray diffraction analysis was performed with an automated DRON-3 diffractometer using CuK_α radiation, a special system of collimators, and a LiF monochromator. To suppress the higher-order harmonics the voltage on the x-ray tube was set at 16 kV, since $U(\lambda/2)=17.7$ kV.

The measurements were performed on the same crystals N1 and N2 as in Ref. 1. As shown by means of magnetic and resistance measurements and x-ray crystallographic analysis in Ref. 4 and also by neutron scattering in Ref. 5, the N1-type crystals, grown

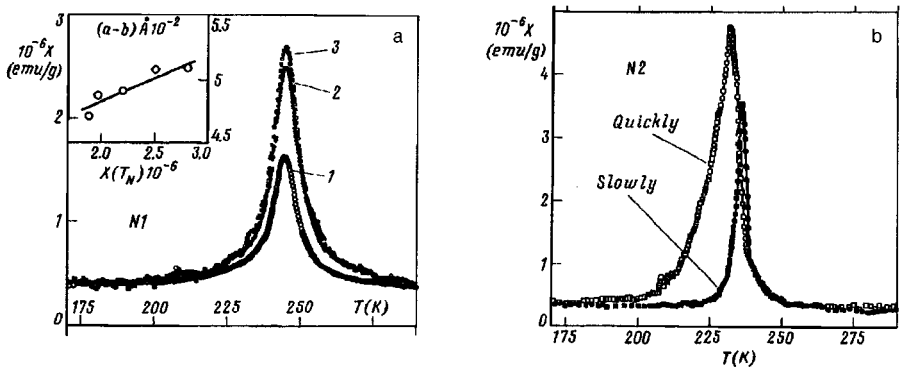

FIG. 1. a) $\chi(T)$ of the specimen N1 measured at different times in the course of one year. *1* — 0, *2* — 4920, *3* — 6048 h. Inset: Correlation of the height of a magnetic peak and the orthorhombic distortion $a-b$. b) $\chi(T)$ obtained for specimen N2 at different chill rates.

from a fluxed melt, possess a high degree of perfection, as a result of which the oxygen mobility is very low. The N2 sample was grown by the floating-zone method. The crystals grown by this method are structurally less perfect and the mobility of the excess oxygen in them is higher. In this specimen, phase separation into an AFM insulator and a metallic phase occurs at temperatures $T<280$ K, and the specimen becomes superconducting at $T_c=30$ K. The excess oxygen concentration in the crystals was determined by x-ray crystallographic analysis according to the lattice parameters c measured at room temperature using the data of Ref. 6. The values $x_1\approx 0.01$ and $x_2\approx 0.015$ were obtained for $c_1=13.144(1)$ and $c_2=13.148(1)$. The Néel temperatures determined according to the maxima of $\chi(T_N)$ were $T_{N1}=245$ K and $T_{N2}=235$ K. The masses of the specimens were $m_1=0.19$ and $m_2=0.14$ g.

Our measurements of $\chi(T)$ for lightly doped La_2CuO_{4+x} single crystals[1] in low fields $1<H<100$ Oe showed the appearance of a residual FM moment directed along the c axis. The value of this moment is $\approx 0.1\%$ of the weak-FM moment obtained in a high field in Ref. 3. Analysis of the dependences $\chi(T,H)$ suggests that the anomaly observed near T_N is a manifestation of a magnetic phase transition which is distinct from the well-known magnetic transition to an AFM phase with latent weak ferromagnetism.

While performing the measurements of $\chi(T)$ in the specimen N1, we observed that the anomaly depends on the time and temperature of low-temperature annealing in a manner correlated with the change in the lattice parameters. The fact that the superstoichiometric-oxygen redistribution processes are substantially slowed down in specimen N1 enabled us to observe the time dependence of the anomaly. Multiday anneals at temperatures below the tetra–ortho structural transition temperature $T<T_{T-O}\cong 220$ °C (Ref. 4) lead to a slow growth of the height of the peak without any changes in T_N or the width of the peak. But annealing for only 1 h at $T>T_{T-O}$ is sufficient to decrease the height of the peak by more than a factor of 2. Figure 1a displays the change in the anomaly over a 1-yr period for the specimen N1 stored in air. The height of the magnetic peak correlates with the change in the orthorhombic distortion $a-b$ with $c=$ const (see inset in Fig. 1a). Assuming that the change in the anomaly is due

to the motion of oxygen and using the method of Ref. 8, we obtained from the time dependence of the height of the peak at different annealing temperatures the values of the oxygen diffusion activation energy $E_a \cong 0.2$ eV. This agrees with the values obtained in Ref. 9 for the energy E_a for oxygen diffusion in the *ab* plane.

Oxygen moves very easily in the specimen N2. This results in a phase separation into an oxygen-depleted AFM phase and an oxygen-enriched metallic phase.[10] For this reason, in contrast to specimen N1, a strong dependence of the anomaly on the rate of cooling at temperatures $T < 295$ K exists in specimen N2; this is shown in Fig. 1b. Rapid chilling suppresses the formation of the metallic phase and increases the AFM volume. Slow cooling to liquid-nitrogen temperature was conducted at a rate of less than 0.5 K/min. Rapid chilling was accomplished by abruptly immersing a room-temperature specimen directly into liquid nitrogen. Ideally, quenching should shift the anomaly to a temperature corresponding to T_N for the more uniform oxygen distribution with $x = 0.015$ ($T_N \cong 200$ K). But since oxygen becomes mobile at temperatures $T > 180$ K,[11] a partial phase separation occurs during the measurements. Apparently, this is why the anomaly acquires a tail in the temperature interval 200 K $< T < T_N$.

As we have already mentioned, in order for a ferromagnetic moment to appear in an antiferromagnet the symmetry of the magnetic and crystal lattices must match. But the magnetic lattice of stoichiometric La_2CuO_4 is primitive and the crystal lattice is base-centered (*Abma*). Ordering of the impurity oxygen can result in a lowering of the crystal symmetry from *Abma* to primitive, which in turn should result in the appearance of ''superstructural'' (forbidden for *Abma*) reflections. Room-temperature x-ray structural analysis of the specimens N1 and N2 confirmed the change in symmetry accompanying doping with oxygen. The analysis indicated the appearance of (330) type reflections which are characteristic for the primitive orthorhombic Bravais lattice. Figure 2 displays the (330) reflections for samples N1 and N2. Superstructural reflections (103) and (309) destroying the *A* base-centered structure were found for the crystal N2. The ratio of the intensities of the superstructural reflections and the main Bragg peaks was of the order of 2×10^{-5}–10^{-4}. Assuming that the broadening of the superstructural reflections is due to the dimensions of the domains of the new phase, the coherence length in the *ab* plane and along the *c* axis can be estimated for N2 as 200 Å and 100 Å, respectively, using the Scherrer formula. At the level of sensitivity of the apparatus ($< 10^{-7}$% of the main Bragg peaks), no superstructural reflections were found in the directions $(h00)$, $(0k0)$, $(00l)$, and $(q0q)$.

In summary, it has been shown in the present letter that the behavior of the anomalies in $\chi(T)$ measured in a low field is determined not only by the amount of impurity oxygen but also by the distribution of impurity oxygen in the orthorhombic crystal lattice of La_2CuO_4. The following mechanism of oxygen ordering in La_2CuO_4 is possible. Two nonequivalent, primarily with respect to rotation of the octahedra of two neighboring planes, positions in the unit cell exist in the orthorhombic phase (*Abma*) for nonstoichiometric oxygen.[12] In a tetragonal lattice all the oxygen sites are equivalent. Annealing at temperatures above T_{T-O} has the effect that oxygen occupies all possible sites with equal probability. Below T_{T-O} such a distribution can become energetically unfavorable, and oxygen becomes ordered over the lattice by means of diffusion. The redistribution of oxygen over two sites produces a nonequivalence of the magnetic sublattices as well,

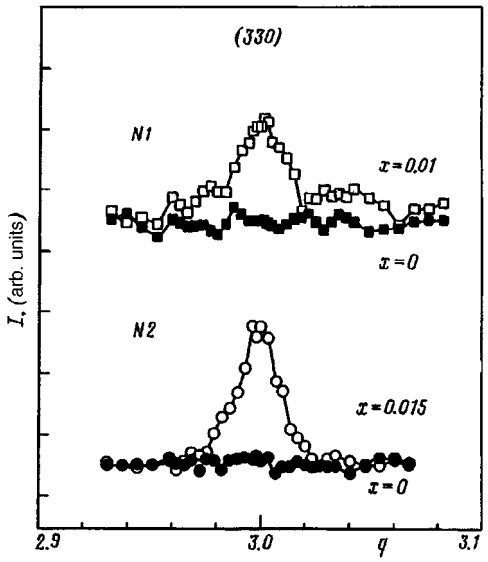

FIG. 2. X-ray crystallographic reflections (330) for the specimens N1 and N2 with different oxygen content. The profiles were measured in the $[qq0]$ direction.

thereby giving rise to an uncompensated moment along the *c* axis.

Thus, doping of La_2CuO_4 crystals with a small amount of oxygen gives rise to a structural transformation that changes the lattice symmetry from base-centered to primitive orthorhombic. The exact crystallographic group has not yet been determined, but in our opinion it should satisfy the condition for the existence of ferromagnetism in a low magnetic field with a spontaneous FM moment directed along the *c* axis. To clarify this question we intend to continue the investigation of the structure by x-ray crystallographic analysis and neutron scattering.

We thank A. N. Bazhan, E. P. Krasnoperov, É. L. Nagaev, and M. B. Tsetlin for their interest and for valuable remarks. This work was performed as part of Project No. 96019 ''Microstratification'' of the State Program on High-T_c Superconductors.

[1] A. A. Zakharov, A. A. Novikov, and O. E. Parfenov, JETP Lett. **64**, 162 (1996).
[2] A. S. Borovik-Romanov, A. I. Buzdin, N. M. Kreĭnes, and S. S. Krotov, JETP Lett. **47**, 697 (1988).
[3] A. N. Bazhan, V. N. Bevz, V. A. Merzhanov *et al.*, JETP Lett. **48**, 21 (1988); Tineke Thio, T. R. Thurston, N. W. Preyer *et al.*, Phys. Rev. **38**, 905 (1988); K. Fukuda, M. Sato, S. Samato *et al.*, Solid State Commun. **63**, 811 (1987); D. C. Johnston *et al.*, Physica C **153–155**, 572 (1988); S-W. Cheong, J. D. Thompson, and Z. Fisk, Phys. Rev. B **37**, 5916 (1988).
[4] A. A. Zakharov, A. A. Nikonov, and O. E. Parfionov *et al.*, Physica C **223**, 157 (1994).
[5] A. M. Balagurov, V. Yu. Pomjakushin, V. G. Simkin, and A. A. Zakharov, Physica C **272**, 277 (1996).
[6] J. C. Grenier, N. Lagueyte, A. Wattianx *et al.*, Physica C **202**, 209 (1992).
[7] A. A. Nikonov, Instrum. Exp. Tech. **38**, 807 (1995).
[8] F. C. Chou and D. C. Johnston, Phys. Rev. B **54**, 572 (1996).
[9] A. P. Reyes, P. C. Hammel, E. T. Ahrens *et al.*, J. Phys. Chem. Solids **54**, 1393 (1993); S. Rubini, F. Borsa, and P. Canfield, Physica C **235–240**, 1717 (1994).
[10] E. L. Nagaev, Z. Phys. B **98**, 59 (1995).

[11] P. C. Hammel, A. P. Reyes, S-W. Cheong *et al.*, Phys. Rev. Lett. **71**, 440 (1993).
[12] B. Morosin, G. H. Kwei, J. E. Schinber *et al.*, Phys. Rev. B **44**, 7673 (1991).

Translated by M. E. Alferieff

Luminescence of short-lived color centers induced in LiF crystals by a pulsed microwave discharge

G. M. Batanov, V. A. Ivanov, M. E. Konyzhev,[a] and A. A. Letunov
Institute of General Physics, Russian Academy of Sciences, 117942 Moscow, Russia

(Submitted 2 July 1997)
Pis'ma Zh. Éksp. Teor. Fiz. **66**, No. 3, 163–167 (10 August 1997)

A new phenomenon — intense luminescence of noncolored lithium fluoride (LiF) crystals excited by an electrodeless pulsed microwave discharge at the prebreakdown stage of development — is observed. This luminescence consists of the luminescence of short-lived aggregate F_2 and F_3^+ color centers at room temperature. It is shown that the density of short-lived color centers induced in the surface layer of LiF crystals by a microsecond microwave discharge reaches values of $\sim 10^{19}$–10^{20} cm^{-3}. © *1997 American Institute of Physics.* [S0021-3640(97)00815-3]

PACS numbers: 78.55.Fv, 78.60.Ya

INTRODUCTION

At the prebreakdown stage an electrodeless pulsed microwave discharge developing on the surface of dielectric crystals in vacuum consists of a secondary-emission discharge (SED) which gives rise to a high density of excitation of a thin surface layer of the crystals. In the process, an induced electrical conductivity and strong microwave absorption arise in the layer, giving rise to the formation of a contracted discharge and to electrical breakdown of dielectric crystals in the microwave radiation field.[1,2] A sequence of SED pulses acting on the crystals produces an optically dense colored surface layer, containing a high density of long-lived F, F_2, and F_3^+ color centers that are stable at room temperature.[3,4] To explain the observed phenomena we proposed the concept of accumulation and relaxation of short-lived color centers generated in the surface layer of dielectric crystals during each SED.[1,2,5] Our objective in the present work was to observe the short-lived color centers experimentally and to estimate their density in the surface layer of noncolored and colored LiF crystals according to the spectral and dynamic characteristics of their SED-induced luminescence.

EXPERIMENTAL CONDITIONS AND PROCEDURE

The microwave discharge (SED) was initiated on the surface of cleaved $70\times10\times5$ mm LiF crystals grown in air and placed at the maximum of the electric field of a TE_{10} standing wave excited in a 120×57 mm rectangular metal waveguide by pulsed microwave radiation from a magnetron (oscillation frequency $\nu=1960$ MHz, pulse power $P_0=1.65$ MW, pulse duration τ up to 30 μs, pulse repetition frequency f up to 2 Hz). The layout of the experimental apparatus is presented in Ref. 1. The waveguide was evacuated with oil-free pumps to a pressure of 10^{-4} Pa. The spectral and dynamic

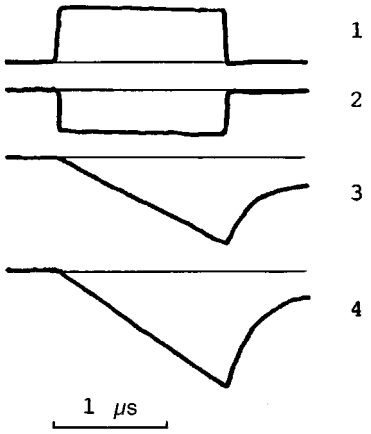

FIG. 1. Oscillograms of signals obtained in the investigation of a microwave discharge (SED) ($P_0 = 1.65$ MW, $\tau = 1.5$ μs, $f = 0.1$ Hz) on the surface of noncolored LiF crystals: *1* — Envelope of the incident microwave radiation pulse; *2* — electronic current from the region of the microwave discharge; *3*, *4* — optical luminescence of LiF crystals at wavelengths near 540 ± 2 nm and 670 ± 2 nm.

characteristics of the luminescence of the LiF crystals were investigated with a MDR-2 monochromator (with a 600 lines/mm diffraction grating) and interference light filters. The optical radiation detectors consisted of FÉU-79 photomultipliers. The temporal resolution of the detecting apparatus was equal to 50 ns. A relative spectral calibration and an estimate of the absolute sensitivity of the optical measuring channel of the MDR-2 monochromator and the FÉU-79 photomultipliers in the wavelength 400–700 nm were performed using a certified SI-8 tungsten ribbon lamp and a helium-neon laser. The optical absorption spectra of the LiF crystals (both noncolored and colored in the microwave discharge) were recorded with a SF-56 spectrophotometer. The electron current emitted from the SED region was monitored with a multigrid electrostatic analyzer. The incident and reflected microwave signals were detected with directional waveguide decouplers. All experiments were performed at room temperature.

The spectral measurements were performed using two optical channels. Luminescence in the region 686 ± 10 nm was recorded in the first (reference) channel with the aid of a light filter and luminescence in the region 400–700 nm was recorded in the second (measuring) channel using the MDR-2 monochromator with a step of 11 nm and a resolution of 4 nm. The spectral intensity of the luminescence of the LiF crystals was determined by dividing the values of the luminescence intensity recorded simultaneously in the measuring and the reference channels. Averaging was performed over five pulses. Control measurements showed that the luminescence spectrum remained unchanged over the period of time required to record it. The procedure employed made it possible to perform amplitude measurements of the luminescence spectrum of the crystals with a relative error not exceeding 5%.

EXPERIMENTAL RESULTS AND THEIR INTERPRETATION

Figure 1 displays characteristic oscillograms of the signals. For the noncolored LiF

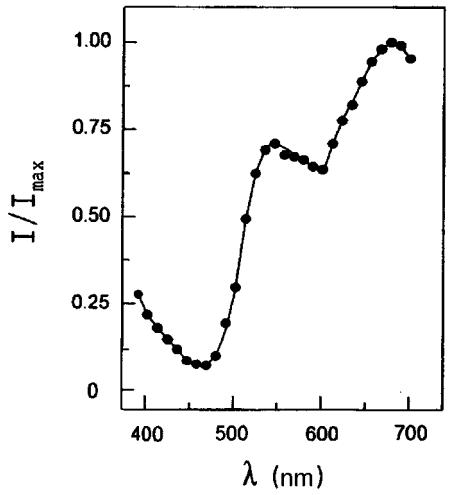

FIG. 2. Luminescence spectrum of noncolored LiF crystals excited by a pulsed microwave discharge (SED) ($P_0 = 1.65$ MW, $\tau = 1.5$ μs, $f = 0.1$ Hz).

crystals (with stable preradiation F_2 and F_3^+ color center density less than 1×10^{14} cm^{-3} and impurity oxygen color center density not exceeding 1×10^{16} cm^{-3}) the dynamics of the variation of the electron current from SED region is virtually instantaneous with respect to the dynamics of the variation of the pulse power of the incident microwave radiation: The observed signals are characterized by sharp leading edges with duration ~ 0.1 μs. In contradistinction to this, the intensity of the luminescence of the crystals rises and falls with characteristic times ~ 1 μs. Therefore for the noncolored LiF crystals only the slow (lagging) components of the luminescence are recorded in the wavelength range 400–700 nm. The luminescence spectrum of the crystals is displayed in Fig. 2. In the region 400–500 nm a minimum of luminescence is observed near 450 nm and two wide intense luminescence bands with maxima near 540 nm and 670 nm are observed in the region 500–700 nm. On the basis of the results obtained in Ref. 4 (where the luminescence spectra of stable F_2 and F_3^+ color centers induced in the surface layer of LiF crystals colored in the microwave discharge were recorded under excitation with laser radiation) we conclude that the radiation bands shown in Fig. 2 with maxima at 540 nm and 670 nm correspond to the luminescence of F_3^+ and F_2 centers, respectively. It follows from the optical absorption spectra of LiF crystals that the density of stable F_2 and F_3^+ centers induced during the measurement time of the luminescence spectrum (150–200 discharge pulses) once again does not exceed 1×10^{14} cm^{-3} (i.e., a noncolored LiF crystal remains noncolored after the luminescence spectrum is measured). An estimate of the absolute intensity of the luminescence recorded in our experiments from a 1 cm^2 surface area of the noncolored LiF crystals corresponds to a flux of $\sim 2 \times 10^{17}$ photons/s emitted into a solid angle of 4π sr in the luminescence bands of F_2 and F_3^+ centers. Further estimates show that in the case when LiF crystals are excited by a SED the density of induced F_2 and F_3^+ color centers is several orders of magnitude higher than that of stable preradiation F_2 and F_3^+ color centers. Therefore we have established that the

observed luminescence spectrum of noncolored LiF crystals corresponds to the luminescence of induced short-lived F_2 and F_3^+ centers generated in the surface layer of LiF crystals during each microsecond SED.

The luminescence dynamics of the SED-excited crystals changes substantially after prolonged coloring of the LiF crystals (using a train of microwave discharge pulses): At wavelengths of 540 and 670 nm there appear, together with slow components of luminescence, fast components (instantaneous) with characteristic intensity rise and fall times ~ 0.1 μs. After a LiF crystal has been exposed to 60000 microwave discharge pulses (SED) ($P_0 = 1.65$ MW, $\tau = 30$ μs, $f = 2$ Hz, external constant magnetic field $H_0 \approx 0.5$ kG) the amplitudes of the slow and fast luminescence components become almost equal to one another. Since the fast luminescence components are due to luminescence of stable centers and the slow components are due to the luminescence of short-lived centers, we conclude from the equality of these amplitudes that the density of stable F_2 and F_3^+ color centers (accumulated in the surface layer of the crystal as a result of prolonged coloring) is comparable to that of short-lived F_2 and F_3^+ centers (generated during each microwave discharge pulse (SED)). The corresponding total density of stable F_2 and F_3^+ color centers equals $\sim 6 \times 10^{19}$ cm^{-3}, calculated according to Smakula's formula (Eq. (2.47) in Ref. 6) using the optical absorption spectrum of a colored LiF crystal. The optical density of the LiF crystal in the absorption band with a maximum near 450 nm (absorption by F_2 and F_3^+ centers) equals 0.07 and the thickness of the colored layer is estimated to be 0.05 μm.

We note that after a LiF crystal is exposed to 30000 microwave discharge pulses (SED) ($P_0 = 1.65$ MW, $\tau = 30$ μs, $f = 2$ Hz, and $H_0 \approx 0.5$ kG) the luminescence spectrum of a crystal colored in this manner is identical to that of a noncolored crystal to within the limits of measurement error, and the intensity of the luminescence of the colored crystal decreases to a level which is 2.5 times lower than the initial luminescence intensity of the noncolored crystal.

DISCUSSION

When noncolored LiF crystals were excited by x-rays or high-current electron beams,[7] luminescence of the crystals was observed only in the emission band of impurity oxygen centers, with a maximum near 440 nm, and the luminescence of F_2 and F_3^+ centers was not detected. In the present work, on the contrary, a strong luminescence of induced short-lived F_2 and F_3^+ centers was recorded from noncolored LiF crystals excited by a microwave discharge (SED) and no luminescence was observed from the impurity oxygen centers in the region 420–460 nm. The new phenomenon which we discovered — intense luminescence of induced short-lived aggregate F_2 and F_3^+ color centers in noncolored LiF crystals — is due to the fact that short-lived color centers with high density $\sim 10^{19}$–10^{20} cm^{-3}, which is 3 to 4 orders of magnitude higher than the residual density of impurity color centers, are generated in the surface layer of crystals excited by a microwave discharge (SED). Therefore the weak luminescence of stable oxygen centers is not observed against the background of the strong luminescence of the induced short-lived F_2 and F_3^+ color centers.

A comparison of the estimated specific energy inputs confirms the analysis performed above. Indeed, the excitation of the surface layer of LiF crystals by low-energy electrons from a microwave discharge (SED) with a characteristic electron energy of 1

keV, electron density 1×10^{10} cm^{-3}, and microwave discharge pulse duration 1 μs is characterized by a specific input energy density $\sim$500 J/cm^3. This is two orders of magnitude higher than the corresponding value $\sim$5 J/cm^3 in the case when LiF crystals are excited with a 200 keV pulsed electron beam with current density 50 A/cm^2 and pulse duration 5 ns.[7]

CONCLUSIONS

1. Intense luminescence of induced short-lived aggregate F_2 and F_3^+ color centers in a thin surface layer of noncolored LiF crystals excited by a pulsed microwave discharge (SED) at room temperature was observed.

2. It was shown that a pulsed microwave discharge (SED) developing on the surface of LiF crystals gives rise to a high excitation density of the surface layer of the crystals. The total density of the short-lived F_2 and F_3^+ color centers generated in the layer reaches $\sim10^{19}$–10^{20} cm^{-3}.

We are grateful to Professor T. T. Basiev and Professor D. I. Vaĭsburd for helpful discussions and consultations and S. M. Satunin for assisting in the computer analysis of the results.

This work was supported by the Russian Fund for Fundamental Research (Project No. 96-02-17647-a).

[a)]e-mail: konyzhev@fpl.gpi.ru

---

[1] G. M. Batanov, V. A. Ivanov, and M. E. Konyzhev, JETP Lett. **59**, 690 (1994).
[2] G. M. Batanov, V. A. Ivanov, and M. E. Konyzhev, Proc. ICPIG XXII **4**, 143 (1995).
[3] G. M. Batanov, V. A. Ivanov, M. E. Konyzhev *et al.*, Pis'ma Zh. Tekh. Fiz. **19**, 42 (1993) [Tech. Phys. Lett. **19**, 653 (1993)].
[4] V. V. Ter-Mikirtychev, T. Tsuboi, M. E. Konyzhev, and V. P. Danilov, Phys. Status Solidi B **196**, 269 (1996).
[5] G. M. Batanov, V. A. Ivanov, and M. E. Konyzhev in *Strong Microwaves in Plasmas*, Vol. 1, edited by A. G. Litvak, Institute of Applied Physics, Nizhny Novgorod, 1996.
[6] W. B. Fowler (ed.), *Physics of Color Centers*, Academic Press, New York, 1968.
[7] V. I. Baryshnikov, T. A. Kolesnikov, E. F. Martynovich, and L. I. Shchepina, Zh. Prikl. Spectrosk. **47**, 301 (1987).

Translated by M. E. Alferieff

Unconventional metallic state in a two-dimensional system with broken inversion symmetry

V. M. Pudalov
Institute of High-Pressure Physics, 142092 Troitsk, Moscow Region, Russia

(Submitted 2 June 1997; resubmitted 2 July 1997)
Pis'ma Zh. Éksp. Teor. Fiz. **66**, No. 3, 168–172 (10 August 1997)

We present a model that explains two phenomena, recently observed in high-mobility Si-MOS structures: (1) the strong enhancement of metallic conduction at low temperatures, $T<2$ K, and (2) the occurrence of a metal–insulator transition in the 2D electron system. Both effects are ascribed to the spin–orbit interaction anomalously enhanced by the broken inversion symmetry of the confining potential well. © *1997 American Institute of Physics.* [S0021-3640(97)00915-8]

PACS numbers: 72.20.Fr, 71.30.+h

INTRODUCTION

Recently, in experiments with high-mobility Si-MOS structures, a strong drop in resistivity $\rho(T)$ has been found[1] as the temperature decreases below $\simeq 2$ K. This effect is evidently in disagreement with the conventional interpretation of the one-parameter scaling theory (OPST),[2] according to which all states in a 2D system at zero magnetic field should be localized in the limit $T\rightarrow 0$. A subsequent scaling analysis of the temperature and electric-field dependences of the conductivity[3] has revealed critical behavior typical of a metal–insulator transition. Finally, convincing evidence for the existence of extended states in 2D systems at zero field has been obtained in experiments in magnetic fields, in studies of the quantum-Hall-effect-to-insulator transitions.[4] The extended states, which at high magnetic fields are located at the center of the corresponding Landau bands, were found to remain in a finite energy range on decreasing field, giving rise to a mobility edge.

The experimental results thus suggest the existence of a true metallic state and a metal–insulator (M–I) transition in 2D. These results are in apparent contradiction with the conventional OPST, and the origin of the metallic state remains puzzling. In this work, both experimental findings are explained as being a consequence of the spin–orbit interaction enhanced by the broken inversion symmetry. The suggested model provides a good agreement with the experimental data on the temperature dependence of the resistivity $\rho(T)$.

ANALYSIS OF THE EXPERIMENTAL RESULTS

Figure 1 shows a set of ρ versus T curves typical for the high-mobility samples,[1] at different electron densities n_s. At $T\gtrsim 2$ K, the resistivity ρ increases slowly as the

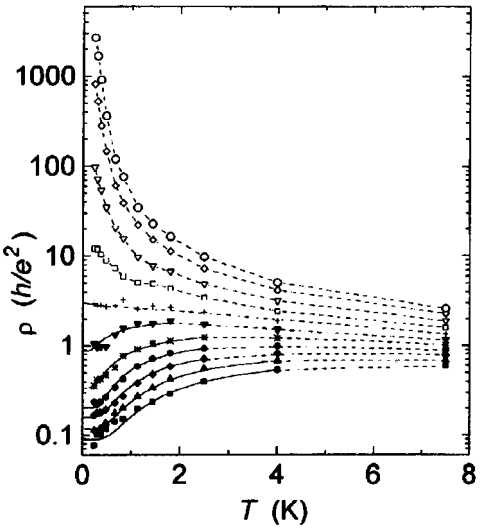

FIG. 1. Typical temperature dependences of the resistivity for a high-mobility sample.[1,3] The electron density, from bottom to top, is equal to 13.69, 12.81, 12.15, 11.50, 10.84, 10.18, 9.53 8.87, 8.21, 7.55, 7.12 $\times 10^{10}$ cm^{-2} (Refs. 1 and 3). The solid lines are the results of simulations, as discussed in the text.

temperature decreases; such behavior is characteristic of a weakly localized regime. At lower temperatures, ρ drops sharply for all curves belonging to the ''metallic'' range of densities, $n_s > n_c$.

The resistance drop is observed at densities in the range from n_c to $\approx 1.4 n_c$. The critical density n_c is sample dependent and is equal to 9.2×10^{10} cm^{-2} for the sample shown in Fig. 1. The drop in $\rho(T)$ diminishes with decreasing sample mobility, and is almost replaced by a conventional rise in ρ at $T \to 0$ in the sample with 8 times lower mobility, $\mu = 5000$ cm^2/V·s. The latter behavior is consistent with that reported in earlier studies on low-mobility samples.[5]

EMPIRICAL FIT OF THE DATA

The $\rho(T)$ curves in Fig. 1 may be fitted well by an empirical dependence which summarizes the scattering probabilities of two processes:

$$\rho(T) = \rho_0 + \rho_1 \exp(-T^*/T). \tag{1}$$

The first term is independent of temperature, while the second one describes a scattering through an energy gap $\Delta = k_B T^*$. The curves shown in Fig. 1 by the heavy continuous lines were obtained using two fitting parameters for each density, ρ_1/ρ_0 and T^*.

POSSIBLE MICROSCOPIC MECHANISMS

As seen from Fig. 1, the characteristic temperature T^* is of the order of 2 K in the high-mobility samples. Searching for a proper microscopic mechanism, we find two small energy gaps intrinsic to Si-MOS structures at $H=0$: the valley splitting $\Delta_v \approx 2.4$ K and the zero-field spin gap $\Delta_s(H=0) \approx 3.6$ K.[6]

It seems attractive to link the resistance drop to transitions between the two electron valleys located close to the X points in the Brillouin zone.[7] However, intervalley ''umklapp'' scattering would hardly occur, since it requires a combination of reciprocal lattice vectors of very high order. On the other hand, the phonon-induced intervalley transition would require participation of high-energy phonons, $E_{\rm ph} \sim 10^4$ K, and is therefore unlikely at low temperatures. Electron tunneling, as the intervalley transition mechanism, would not lead to a strong temperature dependence of scattering.

SPIN-ORBIT SPLITTING AND INTERACTION EFFECTS

In the one-electron approximation, the spin–orbit interaction is described by the Hamiltonian:[7]

$$H_{so} = \frac{\hbar^2}{4m^2c^2}[\nabla V(\mathbf{r}) \times \mathbf{p}]\sigma, \tag{2}$$

where $\mathbf{p}$ and σ are the momentum and spin operators, correspondingly. For the 2D electron system in Si, the contribution of the bulk crystal potential in ∇V is small ($g^* \approx 2$), and the lack of inversion symmetry of the triangular confining potential $U(z)$ plays the major role.

This lifts the spin degeneracy at zero magnetic field and gives rise to a linear term in the energy spectrum of 2D electrons:[8]

$$E^{\pm}(k) = \frac{\hbar^2 k^2}{2m^*} \pm \alpha k. \tag{3}$$

The corresponding spin gap

$$\Delta_s = E^+ - E^- = 2\alpha k_F, \tag{4}$$

can be viewed as the difference in energy for electron states with spin directed in the plane but to the left and right side of $\mathbf{k}_F$, or, equivalently, along and opposite to the effective magnetic field $\mathbf{H}^* \sim (1/m^*c)[\mathbf{k}_F \times \nabla U]$ in the frame tied to electrons moving in the 2D plane at the Fermi velocity.

We suggest that the empirically determined energy gap Δ originates from Δ_s and is equal to $p\Delta_s$ (where $p \sim 1$), whereas the temperature-independent contribution to the resistivity, ρ_0, is related to the spin-independent scattering. The finite quantum relaxation time τ_q and the corresponding level broadening $\hbar/\tau_q$ should reduce the effective gap:

$$k_B T^* = p\Delta_s - \hbar/\tau_q. \tag{5}$$

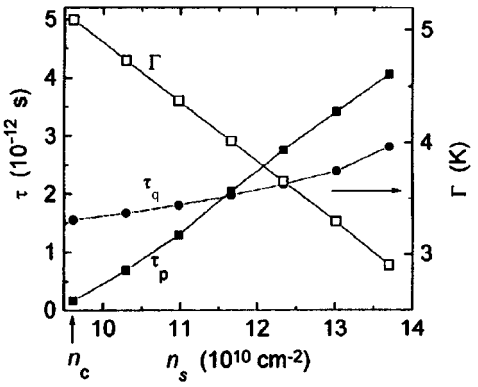

FIG. 2. Level broadening Γ and relaxation times, as determined from a fit (Fig. 1) in the vicinity of n_c.

COMPARISON OF THE MODEL WITH THE EXPERIMENTAL RESULTS

The spin splitting $\Delta_s(H=0)=3.6$ K for the same Si-MOS structures was determined from the magnitude of the quantum oscillations of the chemical potential ,[6] extrapolated to zero field. It is clear from Eqs. (3) and (4), that this value corresponds to $E_{\min}^{-}=-2m^*\alpha/\hbar^2$. With this result we obtain $\alpha=1.79\times10^{-5}$ K·cm, and the total energy spectrum becomes known.

In order to estimate the quantum level broadening $\Gamma=\hbar/\tau_q$, the temperature dependence of the diagonal resistance was measured in the quantum-Hall-effect regime with the Fermi energy adjusted to the Zeeman energy gap at $\nu=6$ in a field of $H=0.75$ T. As a result, we obtained an estimate, $\Gamma=2.8$ K, for $n_s=10.84\times10^{10}\mathrm{cm}^{-2}$ (here we have assumed Gaussian level broadening and take Γ to be the full width). Comparing the model effective energy gap $\Delta=p\Delta_s-\Gamma$ with the empirical value $T^*=0.96$ K obtained in the fit at $n_s=10.84\times10^{10}$ (the 5th curve from the bottom in Fig. 1), we ultimately find $p=0.46$.[9]

The empirical energy gap k_BT^* decreases to zero at $n_s=n_c$, as seen in Fig. 1. In the above model, Eq. (5), this occurs because (i) the level broadening increases, $\Gamma\propto1/n_s$, and (ii) the spin splitting, $\Delta_s=2\alpha k_F$, diminishes $\propto n_s^{1/2}$. The empirical fitting parameter Γ shown versus the electron density in Fig. 2 does indeed increase as the density decreases. The total fit in Fig. 1 is in surprisingly good agreement with the experimental data, despite the very simplified character of the above model.

As n_s decreases and approaches n_c, the resistance drop starts at lower temperatures. The weak decrease in $\rho(T)$ noticeable at $T>4$ K is presumably due to the weak-localization corrections $\delta\rho\propto-\log(T/T_0)$ (Ref. 10). This effect was ignored in the above model, and the $\rho(T)$ points corresponding to the negative $\partial\rho/\partial T$ were not fitted; these points are connected by dashed lines in Fig. 1.

Figure 2 shows also two relaxation times: τ_p, calculated from the mobility in the $T=0$ limit, and $\tau_q=\hbar/\Gamma$. It is noteworthy that both τ_p and τ_q decrease almost linearly and independently of each other as the density decreases (but with $n_s>n_c$) . The momentum relaxation time τ_p provides the necessary resistivity value $\rho\sim h/e^2$ at the critical

density,[1,3] whereas τ_q provides an effective spin gap equal to 0 at $n_s = n_c$. As a result, τ_p decays faster and becomes smaller than τ_q with decreasing n_s. At the critical density, μ is of the order of 0.1 m^2/Vs and $\Gamma \simeq 5$ K, which corresponds to $\tau_p = 0.17 \times 10^{-12}$ s, and $\tau_q \simeq 1.5 \times 10^{-12}$ s. The conclusion that the two curves $\tau_q(n_s)$ and $\tau_p(n_s)$ intersect is model independent, although the numerical values of $\tau_q(n_s)$ and the intersection point depend on the model chosen for level broadening. For instance, the intersection occurs at 11.5 or 13×10^{10} cm^{-2} for Gaussian or Lorenzian broadening, respectively.

METAL-INSULATOR TRANSITION AT $H=0$: SPIN-ORBIT INTERACTION AND SYMMETRY EFFECTS

Not only does the low-temperature resistance drop depend strongly on the symmetry, so does the total scaling behavior. The corresponding universality classes of the symmetry for random systems were established by Dyson.[11] In the presence of the spin–orbit (SO) interaction, the orthogonal symmetry of the system is replaced by symplectic symmetry. Correspondingly, the level-repulsion exponent in the random matrix statistics[11] changes from $\omega = 1$ to $\omega = 4$. It appears therefore, that states are less easily localized in systems with large ω.

The effect of the spin–orbit interaction on weak localization has been studied both theoretically and experimentally.[12] For the strong localization regime, there have been suggestions[13] that M–I transition can occur in the presence of a strong SO interaction. The scaling function in 2D was found to behaves asymptotically as $\beta(G) \sim -a/G$ in the high-conductance limit $G \gg 1$, with $a > 0$ in the orthogonal and $a < 0$ in the symplectic case.[14] The β function in the symplectic case may thus become positive at sufficiently large G. As the disorder increases and the conductance G decreases, all states will be localized even in the symplectic case. The critical level of disorder and the critical conductance G_c correspond to the point at which $\beta(G_c) = 0$.

The behavior of the symplectic $\beta(G)$ function in 2D is qualitatively consistent with the experimental data in the vicinity of n_c (see Fig. 1). As the temperature or the broadening increases, the energy relaxation time τ_ϵ appears as a cutoff parameter, and $1/\tau_\epsilon$ may become larger than the inverse spin relaxation time, $1/\tau_\epsilon \gg 1/\tau_s$. Then the system would again behave as in the orthogonal symmetry case. The natural measure of the SO interaction strength is the spin–orbit gap Δ_s given by Eqs. (4) and (5), and as an estimate for the disorder we adopted $\hbar/\tau_s \approx \hbar/\tau_q = \Gamma$. Thus, one may expect that the M–I transition would be manifested in those samples for which $\Delta_s/\Gamma \geqslant 1$, which is also consistent with occurrence of the transition in the samples with peak mobility larger than 5000 $cm^2/V \cdot s$.[15]

DISCUSSION

The above model explains why the resistance drop is seen only in low-disorder samples with large τ_q values.[15] The effect is also dependent on the symmetry of the potential well. This provides a key for testing the driving mechanism. As to other systems, the zero-field spin gap in GaAs/Al(Ga)As is smaller by a factor of 10–100, due to the smaller g^* factor and the much smaller value of ∇U (Ref. 16). Thus, even in ideal samples with zero broadening, the resistance drop may occur at temperatures 10–100

times lower than those for the Si-MOS structures. In accord with this, no signatures of the resistance drop were revealed in recent measurements on GaAs/Al(Ga)As heterojunctions at temperatures down to 20 mK.[17]

Recently, there have been suggestions on other possible collective mechanisms, such as Coulomb interaction,[18] spin-triplet pairing,[19] and non-Fermi-liquid behavior.[20] However, the corresponding models are not developed yet to provide a comparison with the experimental data.

SUMMARY

It seems likely that the recently observed metal–insulator transition in high-mobility Si-MOS structures is the first experimental manifestation of the spin–orbit-interaction-induced transition in 2D. The enhancement of the metallic conduction in these samples at low temperatures fits the same framework. A strong SO interaction energy relative to the level broadening and broken inversion symmetry are favorable for the 2D metallic state. The Coulomb interaction in this model provides the small level broadening at density down to n_c. In the recent experiments[21,22] the 2D metallic phase was found to be easily destroyed by an in-plane magnetic field; this is a strong evidence for the spin-related origin of the 2D metal.

The author acknowledges the hospitality of the Institut für Halbleiter Physik at the Universität Linz, where the work was partly performed. The author appreciates valuable discussions with G. Bauer, G. Brunthaler, M. V. Entin, V. Kravtsov, I. M. Suslov, E. I. Rashba, and V. Volkov. This study was supported by the Russian Fund for Fundamental Research (Grant 97-02-17387), by the Programs on ''Physics of solid-state nanostructures'' and ''Statistical physics,'' and by a grant from NWO, The Netherlands.

[1] S. V. Kravchenko, G. V. Kravchenko, J. E. Furneaux *et al.*, Phys. Rev. B **50**, 8039 (1994).
[2] E. Abrahams, P. W. Anderson, D. C. Licciardello, and T. V. Ramakrishnan, Phys. Rev. Lett. **42**, 673 (1979).
[3] S. V. Kravchenko, W. E. Mason, G. E. Bowker *et al.*, Phys. Rev. B **51**, 7038 (1995); S. V. Kravchenko, D. Simonian, M. P. Sarachik *et al.*, Phys. Rev. Lett. **77**, 4938 (1996).
[4] V. M. Pudalov, M. D'Iorio, and J. W. Campbell, Surf. Sci. **305**, 107 (1994).
[5] M. J. Uren, R. A. Davies, M. Kaveh, and M. Pepper, J. Phys. Ç: Solid State Phys. **14**, 5737 (1981).
[6] V. M. Pudalov, S. G. Semenchinskii, and V. S. Edel'man, Zh. Éksp. Teor. Fiz. **89**, 1870 (1985) [Sov. Phys. JETP **62**, 1079 (1985)].
[7] B. K. Ridley, *Quantum Processes in Semiconductors*, Oxford: Clarendon Press, 1993.
[8] Yu. A. Bychkov and E. I. Rashba, JETP Lett. **39**, 78 (1984).
[9] From the classical viewpoint, the $p=0.5$ value means that the average scattering angle is $\approx \pi/2$ for transitions between $\pm$ branches of the spectrum (2).
[10] B. L. Altshuler and A. G. Aronov, in *Electron Electron Interaction in Disordered Systems*, A. L. Efros and M. Pollak, eds., Amsterdam: North-Holland, 1985.
[11] F. J. Dyson, J. Math. Phys. **3**, 140 (1962); **3**, 157 (1962); **3**, 166 (1962); **3**, 1191 (1962); **3**, 1199 (1962).
[12] F. G. Pikus and G. E. Pikus, cond-mat/9606108; W. Knap, C. Skierbiszewski, A. Zduniak *et al.*, Phys. Rev. B **53**, 3912 (1996).
[13] T. Ando, Phys. Rev. B **40**, 5325 (1989).
[14] S. Hikami, A. I. Larkin, and Y. Nagaoka, Prog. Theor. Phys. **63**, 707 (1980); S. Hikami, *ibid.* **64**, 1425 (1980).
[15] V. M. Pudalov, in *Proc. Intern. Conf. on Electron Localization and Quant. Transport in Solids*, Ed. T. Dietl, Inst. of Physics PAN, Warsaw, p. 34, 1996.
[16] J. P. Eisenstein, H. L. Störmer, V. Narayanamurti *et al.*, Phys. Rev. Lett. **53**, 2579 (1984).
[17] F. W. Van Keuls, X. L. Hu, H. Mathur *et al.*, *op. cit.* 15, p. 33.
[18] F. G. Pikus and A. L. Efros, *op. cit.* 15, p. 10.
[19] D. Belitz and T. R. Kirkpatrick, cond-mat/9705023.

[20] V. Dobrosavljevic, E. Abrahams, E. Miranda, and S. Chakravarty, cond-mat/9704091.
[21] D. Simonian, S. V. Kravchenko, and M. P. Sarachik, cond-mat/9704071.
[22] V. M. Pudalov, G. Brunthaler, A. Prinz, and G. Bauer, JETP Lett. **65**, 932 (1997).

Published in English in the original Russian journal. Edited by Steve Torstveit.

Redistribution of the hole spectral weight due to long-range spin correlations in the three-band Hubbard model

A. F. Barabanov, E. Žąsinas, and O. V. Urazaev
Institute of High Pressure Physics, 142092 Troitsk, Moscow Region, Russia

L. A. Maksimov
Kurchatov Institute Russian Research Center, 123182 Moscow, Russia

(Submitted 3 July 1997)
Pis'ma Zh. Éksp. Teor. Fiz. **66**, No. 3, 173–177 (10 August 1997)

The spectrum of the spin-polaron hole exitation is investigated in the framework of the three-band model for the CuO_2 plane in high-temperature superconductors. The problem is treated taking into account the coupling of a local polaron with the antiferromagnetic spin wave with $\mathbf{Q}=(\pi,\pi)$. This leads to fundamental changes in the lowest polaron band $\epsilon_1(\mathbf{k})$ and to a strong redistribution of the bare electron filling. © *1997 American Institute of Physics.*
[S0021-3640(97)01015-3]

PACS numbers: 74.20.Mn

In order to understand the nature of high-temperature superconductors it is important to describe properly the motion of a hole in the CuO_2 plane.[1,2] This motion takes place against the antiferromagnetic (AFM) spin background of the copper spins and must be treated as the correlated motion of a hole coupled to spin excitations (a spin polaron). Usually the spin polaron is studied within the frameworks of the t-J model[1] and the three-band Hubbard model.[3–5] In the previous works the spin polaron problem was studied mainly in the approximation of a small-radius polaron (an analog of a Zang–Rise polaron). In the present work, for the first time, the long-range order of the AFM background is taken into account by introducing an additional new spin polaron of infinite radius — a bound state of a charge exitation and a spin wave with $\mathbf{Q}=(\pi,\pi)$. We shall show that the introduction of such a polaron leads to a substantial decrease in the filling of the lowest band by bare holes. As a result, the area of the Fermi surface strongly increases and its form becomes more complex.

The effective Hamiltonian of the three-band Hubbard model of the CuO_2 plane has the following form (in the conventional notation):[3,6,5]

$$\hat{H}=\hat{T}+\hat{h}+\hat{J},\quad \hat{T}=\tau\sum_{\substack{\mathbf{R},\mathbf{a}_1,\mathbf{a}_2,\\ \sigma_1,\sigma_2}} X_{\mathbf{R}}^{\sigma_1\sigma_2} c^{+}_{\mathbf{R}+\mathbf{a}_2,\sigma_2} c_{\mathbf{R}+\mathbf{a}_1,\sigma_1},$$

$$\hat{h}=-h\sum_{\mathbf{R},\mathbf{a},\mathbf{b},\sigma} c^{+}_{\mathbf{R}+\mathbf{a},\sigma} c_{\mathbf{R}+\mathbf{a}+\mathbf{b},\sigma},\quad \hat{J}=\frac{J}{2}\sum_{\mathbf{R},\mathbf{g}} \hat{\mathbf{S}}_{\mathbf{R}}\hat{\mathbf{S}}_{\mathbf{R}+\mathbf{g}}. \tag{1}$$

Here the CuO_2 plane is described by a square sublattice with lattice constant g and two O sites per Cu unit cell; $\mathbf{R}$ stands for the position vectors of Cu sites, $\mathbf{R}+\mathbf{a}$ are the four vectors of the O sites nearest to Cu site $\mathbf{R}$, $\mathbf{a}=\pm\mathbf{a}_x,\pm\mathbf{a}_y$, $\mathbf{a}_x=g(1/2,0)$, $\mathbf{a}_y=g(0,1/2)$. We assume $g=1$. In Eq. (1) we have adopted the following notation: $\mathbf{b}$ are the nearest-neighbor vectors for the oxygen sublattice; $\mathbf{g}=2\mathbf{a}$ and $\mathbf{d}=2\mathbf{b}$ are the nearest and second-nearest neighbors for the Cu sublattice; the operators c_σ^+ and $X^{\sigma 0}$ create a hole with spin $S=1/2$ and spin projection $\sigma/2$ ($\sigma=\pm 1$) at the O and Cu sites, respectively, and $X_{\mathbf{R}}^{\sigma_1\sigma_2}$ are the Hubbard projection operators, which are convenient for excluding doubly occupied Cu sites.

The first term $\hat{T}$ in Eq. (1) describes the effective hole hopping with an amplitude from O to O sites through the intervening Cu sites, the term $\hat{J}$ corresponds to the AFM interaction between Cu sites, and $\hat{h}$ represents the direct O–O nearest-neighbor hopping.

Let us discuss the hole excitations with spin $S=1/2$ and the spin projection $\sigma/2$. We shall restrict ourselves to a finite number of site operators $A_{\mathbf{R},j}$ ($1\leqslant j\leqslant 12$), in each unit cell $\mathbf{R}$.

In order to treat the hole excitations in the framework of the spin-polaron concept we introduce for each unit cell $\mathbf{R}$ six site operators which describe the local polaron of small radius:

$$A^+_{\mathbf{R},\sigma,1(2)}=c^+_{\mathbf{R}+\mathbf{a}_x(\mathbf{a}_y),\sigma},\quad A^+_{\mathbf{R},\sigma,3(4)}=\sigma\sum_{\gamma=\pm 1}\gamma X^{\overline{\gamma\sigma}}_{\mathbf{R}}c^+_{\mathbf{R}+\mathbf{a}_x,(\mathbf{a}_y),\gamma},$$

$$A^+_{\mathbf{R},\sigma,5(6)}=\sigma\sum_{\gamma=\pm 1}\gamma X^{\overline{\gamma\sigma}}_{\mathbf{R}+\mathbf{g}_x,(\mathbf{g}_y)}c^+_{\mathbf{R}+\mathbf{a}_x,(\mathbf{a}_y),\gamma},\quad \overline{\sigma}=-\sigma, \tag{2}$$

$$A^+_{\mathbf{k},\sigma,j}=\frac{1}{\sqrt{N}}\sum_{\mathbf{R}} e^{i\mathbf{k}\mathbf{R}}A_{\mathbf{R},\sigma,j}.$$

$A^+_{\mathbf{k},\sigma,j}$ are the Fourier transforms of $A^+_{\mathbf{R},\sigma,j}$.

We might mention that in our previous investigations[7] this basis of local spin-polaron operators led to the proper description of the important experimentally observed features of the hole spectrum of the CuO_2 plane: the extended saddle point and isotropic band bottom.

In this paper we want to investigate the role of the delocalized spin polarons, which correspond to the coupling of the local polarons to the AFM spin wave with momentum $\mathbf{Q}=(\pi,\pi)$, usually called Q-polarons. If the spin subsystem is found in the state with AFM long-range order, then the average value of the amplitude $\langle\mathbf{S_Q}\rangle$ of the spin wave with $\mathbf{q}=\mathbf{Q}$ (the Q wave) has a macroscopically large value and has properties analogous to the amplitude of a Bose particle with zero momentum in the superfluid Bose gas. As a result, for many problems this amplitude can be treated as a c number.[8] Then the coupling of the Q wave to local electron states does not represent new states but leads, as mentioned above, to the mixing of the states with momenta $\mathbf{k}$ and $\mathbf{k}+\mathbf{Q}$. This treatment is usually based on the widely used Néel-type state of the spin subsystem with two sublattices.

But for the $S=1/2$ spin system the quantum fluctuations are very important and lead to the spherically symmetric homogeneous Néel state at any small but finite temperature. Against this background even at $T=0$ the average value $\langle \mathbf{S_Q} \rangle = 0$, and the above-mentioned simple approach for the hybridization of the $\mathbf{k}$ and $\mathbf{k}+\mathbf{Q}$ states fails. In the homogeneous Néel state only $\langle \mathbf{S_Q S_Q} \rangle$ can be treated as a macroscopic quantity. Then the coupling of local polaron states to $\mathbf{S_Q}$ corresponds to new delocalized states. In order to take these states into account we introduce six additional operators on the basis of Eq. (2):

$$A^{+}_{\mathbf{R},\sigma,j} = \sigma \sum_{\gamma=\pm 1} \gamma Q^{\overline{\gamma\sigma}}_{\mathbf{R}} A^{+}_{\mathbf{R},\gamma,i}, \quad A^{+}_{\mathbf{k},\sigma,\gamma} = \sigma \sum_{\gamma} \gamma A^{+}_{\mathbf{k}+\mathbf{Q},\gamma,i} \mathbf{S}^{\overline{\gamma\sigma}}_{\mathbf{Q}}, \tag{3}$$

$$Q^{\overline{\gamma\sigma}}_{\mathbf{R}} \equiv e^{i\mathbf{QR}} S^{\overline{\gamma\sigma}}_{\mathbf{Q}} = N^{-1} \sum_{\mathbf{R}_1} e^{i\mathbf{Q}(\mathbf{R}+\mathbf{R}_1)} X^{\overline{\gamma\sigma}}_{\mathbf{R}_1}, \quad j = i+6, \quad i = (1-6).$$

In order to determine the spin polaron spectrum $\varepsilon_i(\mathbf{k})$ of 12 quasiparticle bands we use the two-time retarded matrix Green's functions $G_{i,j}(t,\mathbf{k})$ for the operators $A_{\mathbf{k},\sigma,i}$:

$$G_{i,j}(t,\mathbf{k}) \equiv \langle A_{\mathbf{k},i}(t) | A^{+}_{\mathbf{k},j}(0) \rangle = -i\Theta(t) \langle \{ A_{\mathbf{k},i}(t), A^{+}_{\mathbf{k},j}(0) \} \rangle. \tag{4}$$

We solve the system of the equations of motion for $G_{i,j}(\omega,\mathbf{k})$ by using the standard Mori–Zwanzig projection technique and restricting ourselves to the above chosen basis of operators $\{A_{\mathbf{k},\sigma,i}\}$ from Eqs. (2) and (3). Then the Green's functions and the spectrum are determined from the equations

$$(\omega - DK^{-1})G = K, \quad \det | K\varepsilon(\mathbf{k}) - D | = 0, \tag{5}$$

$$D_{i,j}(\mathbf{k}) = \langle \{ B_{\mathbf{k},i}, A^{+}_{\mathbf{k},l} \} \rangle, \quad K_{i,j} = \langle \{ A_{\mathbf{k},i}, A^{+}_{\mathbf{k},j} \} \rangle, \quad B_{\mathbf{k},i} = [A_{\mathbf{k},i}, H]. \tag{6}$$

The matrix elements of D and K are expressed both through short-range spin-correlation functions of the Cu subsystem and the long-range-order correlation function $\langle \mathbf{S_Q S_Q} \rangle$. The Cu spin subsystem is described by the $S=1/2$ Heisenberg model at $T=0$. For the value of the correlation functions we use the results of Ref. 9 where this model was treated in the framework of spherically symmetrical Green's functions theory. It is important that we take into account that $\langle \mathbf{S_Q S_Q} \rangle$ is a macroscopic quantity which is equal to the square of the effective sublattice magnetization:

$$\langle \mathbf{S_Q S_Q} \rangle = \lim_{\mathbf{R}_1 \to \infty} | \langle \mathbf{S_R S_{R+R_1}} \rangle | = M^2. \tag{7}$$

Note that the dependence of the spin polaron excitation spectrum on the long-range correlation function $\langle \mathbf{S_Q S_Q} \rangle$ appears only on account of treatment of the Q-polaron states (3). Below we take the following numerical values of the spin correlation functions: $\langle \mathbf{S_R S_{R+g}} \rangle = -0.3521$, $\langle \mathbf{S_R S_{R+d}} \rangle = 0.229$, $\langle \mathbf{S_R S_{R+2g}} \rangle = 0.2$, $M^2 = 0.0914$. The matrix elements were calculated in the low-hole-doping limit, $n \ll 1$, where n is the total number of oxygen holes per unit cell. The detailed expressions of matrices D and K will be published elsewhere.

As a result the Green's functions have the form

$$G_{i,j}(\omega,\mathbf{k})=\sum_{l=1}^{12}\frac{Z_{(i,j)}^{(l)}(\mathbf{k})}{\omega-\varepsilon_l(\mathbf{k})}. \tag{8}$$

In particular, the value of $Z_h(\mathbf{k})=Z_{(1,1)}^{(1)}(\mathbf{k})+Z_{(2,2)}^{(1)}(\mathbf{k})$ corresponds to the number of bare oxygen holes with fixed spin σ and momentum $\mathbf{k}$ in the state $|\mathbf{k},\sigma\rangle$ of the lowest quasiparticle band $\varepsilon_1(\mathbf{k})$. Let us remark that residue $Z_{(i,j)}(\mathbf{k})$ satisfies the sum rule $\Sigma_s Z_{(i,i)}^{(s)}(\mathbf{k})=1$, $i=1, 2$. This means that in this model the Luttinger theorem does not hold, and the maximum number of holes per cell is equal to four despite the presence of twelve bands.

The results of the most interesting, two lowest bands $\varepsilon_1(\mathbf{k})$ and $\varepsilon_2(\mathbf{k})$ for realistic values of the model parameters $J_1=0.2\tau$, $h=0.4\tau$ (all the energy parameters below are expressed in units of τ) are presented in Fig. 1a. Also shown in this figure is the spectrum of the lowest of six bands $\underline{\varepsilon}_1(\mathbf{k})$, calculated in the approximation of the six operators (2). In Fig. 1b the spectrum $\varepsilon_1(\mathbf{k})$ is presented by the equal-energy lines $\varepsilon_1(\mathbf{k})=\text{const}$. Let us mention that the Q-polarons may lead to a rather complex form of the Fermi surface. This circumstance can give nontrivial behavior of the Hall effect on doping and can even cause inversion of the Hall constant if the Fermi energy is close to $\varepsilon_1(\mathbf{k})=-4.5$.

As is seen from Fig. 1a, the inclusion of the Q-wave qualitatively leads to the decoupling of the lowest band of the local small polaron excitations, and $\varepsilon_1(\mathbf{k})$ is close to $\underline{\varepsilon}_1(\mathbf{k})$. This means that the main features of the lowest-band excitations previously calculated in the local polaron approximation[7] are preserved.

The importance of the treatment of the Q-wave polarons may be seen if we discuss the filling of the lowest band by bare holes. In Fig. 1c the filling of the $\varepsilon_1(\mathbf{k})$ and $\underline{\varepsilon}_1(\mathbf{k})$ are shown, i.e., the residues $Z_h(\mathbf{k})$ and $\underline{Z}_h(\mathbf{k})$ (the underlined values correspond to local polaron approximation). One can see that the introduction of the Q-polarons leads to a substantial decrease in the hole filling along the lines $X-M$ and $M-N$. This redistribution of the bare hole spectrum weight explains the results of photoemission experiments, where a ''flat band region'' is observed along the direction $X-\Gamma$ but not along the line $X-M$. Figure 1d demonstrates that the local polaron concept (the six operators (2)) leads to a strong decrease of the filling under the Fermi surface. This implies a violation of the Luttinger theorem by approximately four times (an analogous effect was found in Ref. 10). But the inclusion of Q-polaron states (3) leads to an addition substanntial reduction of the filling, by approximately 1.5 times. The maximum $\varepsilon_1(\mathbf{k})$-band filling is equal to $n=0.22$, and the smallness of this value justifies our low-density approximation.

Formula (3) points out that the Q-polaron $A_{\mathbf{k},\sigma,7(8)}^{+}$ contains a bare hole state $c_{\mathbf{k}+\mathbf{Q},\sigma}^{+}$. This means that the residues $Z_{\mathbf{Q}}$ of the corresponding Green's function $G_{\mathbf{Q}}(\mathbf{k})=\mathbf{G}_{7,7}+\mathbf{G}_{8,8}$ are responsible for the ''shadow band'' effect.[11]

We note that the Q-polaron scenario reproduces the substantial decrease in width of the lowest band with decrease of the AFM constant J. Usually such an effect is obtained only in the self-consistent Born approximation.[12]

In conclusion we want to mention that the above-described properties of the spin polaron are mainly preserved if we suppose that the spin subsystem has no long-range order but that the spin correlation length L is large. Then, in the matrix elements of D and

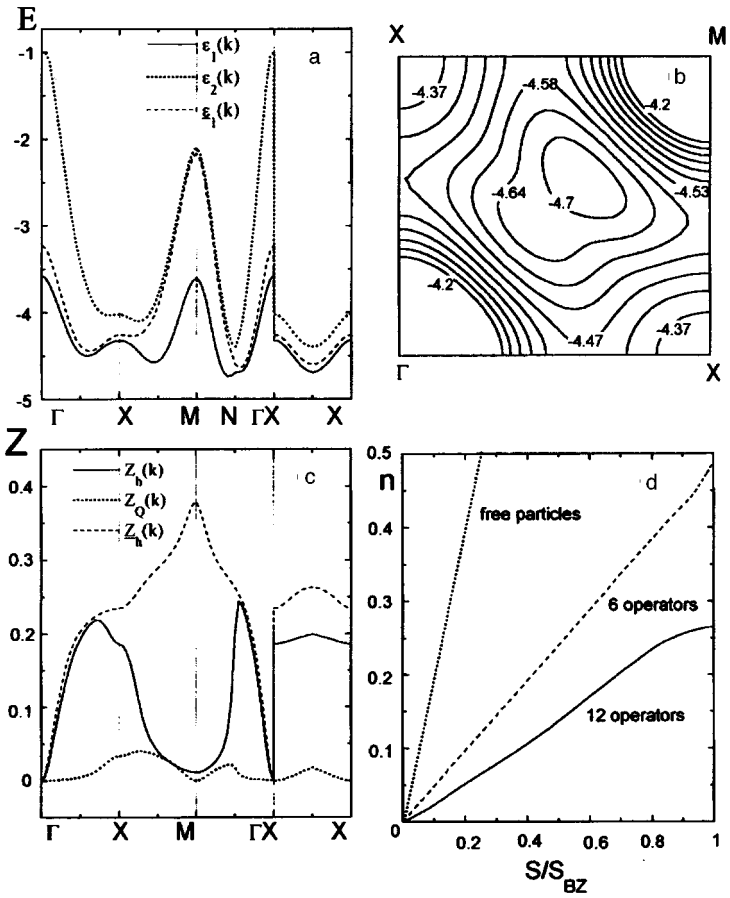

FIG. 1. a: The spectra $\varepsilon_1(\mathbf{k})$ and $\varepsilon_2(\mathbf{k})$ calculated for the basis (2), (3), and the spectrum $\underline{\varepsilon}_1(\mathbf{k})$ calculated for the basis (2). The spectra are given along symmetry lines Γ–X–M–N–Γ and X–N–X; $\Gamma=(0,0)$; $X=(\pi,0),(0,\pi)$, $M=(\pi,\pi)$; $N=(\pi/2,\pi/2)$. b: Spectrum equal-energy lines $\varepsilon_1(\mathbf{k})=$const. c: $Z_h(\mathbf{k})$ and $\underline{Z}_h(\mathbf{k})$ are the number of bare holes (the residues of corresponding Green's functions) in the quasiparticle excitations for the spectra $\varepsilon_1(\mathbf{k})$ and $\underline{\varepsilon}_1(\mathbf{k})$; $Z_Q(\mathbf{k})$ is the residue of the lowest pole $\varepsilon_1(\mathbf{k})$; for the Green's function $G_{11,11}(\omega,\mathbf{k})+G_{12,12}(\omega,\mathbf{k})$, which characterize the ''shadow band'' effect. d: The dependence of the number of holes n per unit cell on the value of the Fermi surface area S (S_{BZ} is the the area of the first Brillouine zone): thick line — for the spectrum $\varepsilon_1(\mathbf{k})$; dashed line — for the spectrum $\underline{\varepsilon}_1(\mathbf{k})$; solid straight line — the case of noninteracting-particle filling.

K we must replace the long-range correlation function $\langle S_{\mathbf{Q}} S_{\mathbf{Q}}\rangle$ by the following expression:

$$\sum_{|\mathbf{q}|<\delta q} \langle S_{\mathbf{Q}+\mathbf{q}} S_{\mathbf{Q}+\mathbf{q}}\rangle \quad \delta q \approx 1/L, \quad L \gg 1. \tag{9}$$

We are grateful to L. B. Litinski for valuable discussions and comments. This work was supported, in part, by INTAS-PFBR (Project 95-0591), by RSFR (Grant 95-02-

04239-a), by the Russian National Program on Superconductivity (Grant 93080), by the Dutch Organization for Scientific Research (Grant NWO-07-30-002), and by the International Soros Science Education Program.

[1] E. Dagotto, Rev. Mod. Phys. **66**, 763 (1994).
[2] W. Brenig, Phys. Rep. **251**, 4 (1995).
[3] V. J. Emery, Phys. Rev. Lett. **58**, 2794 (1987); V. Emery and G. Reiter, Phys. Rev. B **38**, 4547 (1988).
[4] F. C. Zhang and T. M. Rice, Phys. Rev. B **37**, 3759 (1988).
[5] A. F. Barabanov, L. A. Maksimov, and G. V. Uimin, JETP Lett. **47**, 622 (1988); Zh. Éksp. Teor. Fiz. **96**, 655 (1989) [Sov. Phys. JETP **69**, 371 (1989)]; A. F. Barabanov, R. O. Kuzian, and L. A. Maksimov, J. Phys.: Condens. Matter **3**, 9129 (1991).
[6] H. Matsukava and H. Fukuyama, J. Phys. Soc. Jpn. **58**, 2845 (1989).
[7] A. F. Barabanov, V. M. Berezovsky, L. A. Maksimov, and E. Zhasinas, Physica C **252**, 308 (1995); Zh. Éksp. Teor. Fiz. **110**, 1480 (1996) [JETP **83**, 819 (1996)].
[8] J. R. Schrieffer, J. Low Temp. Phys. **99**, 397 (1995).
[9] A. F. Barabanov and V. M. Berezovsky, Phys. Lett. A **186**, 175 (1994); Zh. Éksp. Teor. Fiz. **106**, 1156 (1994) [JETP **79**, 627 (1994)].
[10] R. Hayn, V. Yushankhai, and S. Lovtsov, Phys. Rev. B **47**, 5253 (1993).
[11] A. P. Kampf and J. R. Schrieffer, Phys. Rev. B **42**, 7967 (1990).
[12] G. Martinez and P. Horsch, Phys. Rev. B **44**, 317 (1991).

Published in English in the original Russian journal. Edited by Steve Torstveit.

Hopf term in the action for vortices/skyrmions with odd filling of Landau levels

S. V. Iordanskiĭ
L. D. Landau Institute of Theoretical Physics, Russian Academy of Sciences, 142432 Chernogolovka, Moscow Region, Russia

(Submitted 5 June 1997; resubmitted 3 July 1997)
Pis'ma Zh. Éksp. Teor. Fiz. **66**, No. 3, 178–183 (10 August 1997)

A term in the action that is of third order in the derivatives of the rotation matrix is calculated. A direct diagrammatic method in the limit of high magnetic fields is used. It is shown that the action contains the standard Hopf invariant with a coefficient corresponding to fermionic behavior of vortices/skyrmions. © *1997 American Institute of Physics.* [S0021-3640(97)01115-8]

PACS numbers: 12.39.Dc, 71.70.Di

For odd fillings of the Landau levels (taking account of spin splitting) the ground state of two-dimensional electrons in a high magnetic field is ferromagnetic. Therefore states with a gradual change in the direction of the average spin in space could possibly form. This change can be very slow in the case when the Zeeman energy is low compared with the Coulomb energy; this is the basis for using a gradient expansion. This approach has been used in many theoretical works.[1–4] These works all employ an approximation in which the wave functions are assumed to be projected onto a set of functions belonging to the same fixed Landau level. In Ref. 5 it was shown that this approximation is insufficient for obtaining an adequate description and calculating the energy of vortices/skyrmions. In the case when the perturbation theory in the derivatives of the rotation matrix is valid, it was shown that the formation of such vortices is thermodynamically favored. A more detailed paper should appear in *JETP*.

A topological term in the action for skyrmions that is of third order in the derivatives was calculated in Ref. 6. The calculations were performed in the projected-wave-function approximation. However, in this approximation the rotation matrix becomes nonlocal and it is unitary only if some total derivatives are neglected. This could be the reason why the corresponding terms in the action are of an unconventional form. This work was criticized in the Ref. 7, where an expression with a Hopf invariant in the action is presented. The coefficient of the Hopf invariant was obtained on the basis of a quasiclassical calculation (probably valid in the limit of a large number of filled Landau levels), previously performed by the authors for another physical system without using the projected-functions approximation. On the whole, the debate is not over, and it is of interest to find the topological term in the action directly without using any approximations other than the assumptions that the ratio of the cyclotron energy to the Coulomb interaction energy is large and that the g factor is small.

To describe vortices/skyrmions we introduce a 2×2 rotation matrix $U(\mathbf{r},t)$ that

transforms electronic spinors to a local spin coordinate system $\psi = U\chi$, where the spinor χ is almost ferromagnetic with one ''up'' component and the spinor ψ is a spinor in the laboratory coordinate system. In this case the Lagrangian for the spinors χ assumes the form

$$L = \int \left[i\chi^+ \frac{\partial \chi}{\partial t} - \frac{1}{2m}\chi^+(-i\nabla - \mathbf{A}_0 - iU^+\nabla U)^2 + i\chi^+ U^+ \frac{\partial U}{\partial t}\chi \right] d^2r dt$$
$$+ \frac{1}{2}\int V(\mathbf{r}-\mathbf{r}')\chi^+(\mathbf{r})\chi^+(\mathbf{r}')\chi(\mathbf{r}')\chi(\mathbf{r}) d^2r' d^2r dt,$$

where the potential energy is invariant under a local rotation, and $\mathbf{A}_0$ is the vector potential of a uniform external magnetic field H_0. We employ a system of units with $\hbar = H_0 = l_H = 1$, where l_H is the magnetic length.

We assume that the derivatives of the rotation matrix are small, and we treat the quantities $-iU^+\nabla U = \vec{\Omega}^l \sigma_l$ and $-iU^+\partial_t U = \Omega_t^l \sigma_l$, where σ_l are Pauli matrices, as small perturbations in the Hamiltonian. Thus, we can separate the Hamiltonian into three parts: (i) an unperturbed part which in the Hartree–Fock approximation has the form

$$H = \frac{1}{2m}\int \chi^+(-i\nabla - \mathbf{A}_0)^2 d^2r + \int V(\mathbf{r}-\mathbf{r}')\rho(\mathbf{r}')\chi^+(\mathbf{r})\chi(\mathbf{r}) d^r d^2r' + \int V(\mathbf{r}-\mathbf{r}')$$
$$\times \langle \chi_\alpha^+(\mathbf{r}')\chi_\beta(\mathbf{r})\rangle \chi_\beta^+(\mathbf{r})\chi_\alpha(\mathbf{r}') d^2r d^2r';$$

(ii) a first-order perturbation

$$H_1 = \frac{1}{m}\int \chi^+ \vec{\Omega}^l \sigma_l \cdot (-i\nabla - \mathbf{A}_0)\chi d^2r - \int \chi^+ \Omega_t^l \sigma_l \chi d^2r; \tag{1}$$

and, (iii) a second-order perturbation

$$H_2 = \frac{1}{2m}\int \chi^+ [(\vec{\Omega}^l)^2 - i\nabla \cdot \vec{\Omega}^l \sigma_l]\chi d^2r. \tag{2}$$

Here we have introduced the average density ρ and the average value $X_{\alpha\beta} = \langle \chi_\alpha^+(\mathbf{r})\chi_\beta(\mathbf{r}')\rangle$. In what follows, we employ a local approximation for the exchange energy, introducing the exchange constant γ

$$\int V(\mathbf{r}-\mathbf{r}')\langle \chi_\alpha^+(\mathbf{r}')\chi_\beta(\mathbf{r})\rangle \chi_\beta^+(\mathbf{r})\chi_\alpha d^2r d^2r' \to \int \gamma \chi^+(\mathbf{r})\sigma_z \chi(\mathbf{r}) d^2r$$

and we neglect the direct interaction. Apparently, the use of this model is unimportant for final results but it substantially simplifies the calculations.

Let

$$\langle \chi_\alpha^+ \chi_\beta\rangle = \langle \chi_\alpha^+ \chi_\beta\rangle^0 + \delta\langle \chi_\alpha^+ \chi_\beta\rangle,$$

where the first term corresponds to a uniform situation neglecting all Ω^l, i.e., the leading term in the decomposition of the Hamiltonian; the second term includes all corrections for the nonuniformity of the rotation matrix. The action with the Hubbard–Stratonovich field taken into account has the form

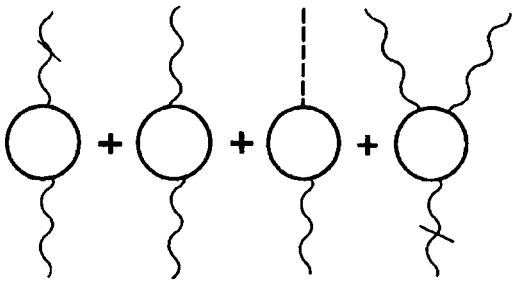

FIG. 1. A wavy line corresponds to H_1 with spatial derivatives. A wavy line with a line through it corresponds to the part of H_1 that contains a time derivative. The dashed line corresponds to H_2. A solid line denotes the electronic Green's function.

$$S=\int \chi^{+}\left[i\partial_t-\frac{1}{2m}(-i\nabla-\mathbf{A}_0+\vec{\Omega}^l\sigma_l)^2-\Omega_t^l\sigma_l+\gamma X^0_{\alpha\beta}\right]\chi d^2r dt$$
$$+\gamma\int \delta X_{\alpha\beta}\chi^{+}_{\beta}\chi_{\alpha}d^2r dt-\frac{\gamma}{2}\int (X^0_{\alpha\beta}+\delta X_{\alpha\beta})(X^0_{\beta\alpha}+\delta X_{\beta\alpha})d^2r dt.$$

Since in the mean-field approximation $X_{\alpha\beta}=\langle\chi^{+}_{\alpha}\chi_{\beta}\rangle$, it is easy to obtain for the action in the mean-field approximation

$$S=S_0(\chi,\Omega)+\frac{\gamma}{2}\int \delta\langle\chi^{+}_{\alpha}\chi_{\beta}\rangle\,\delta\langle\chi^{+}_{\beta}\chi_{\alpha}\rangle d^2r dt, \tag{3}$$

where the first term corresponds to the action $X^0_{\alpha\beta}=\langle\chi^{+}_{\alpha}\chi_{\beta}\rangle^0$ for the spinors χ^{+} and χ in a uniform field with the nonuniformity of the rotation matrix, i.e., of all the Ω in the Hamiltonian, taken into account. We shall calculate first the topological terms in the skrymion effective action generated by S_0. The second term is determined completely by the electronic Green's function, likewise corresponding to the action S_0, and as will be shown below it does not contain the topological Hopf invariant. To find the effective action for vortices/skyrmions, an integration must be performed over the fermion field in the expression for the partition function generated by the action S_0; this is equivalent to a calculation of the free energy of the electrons in terms of the fields Ω^l. For this reason, the effective action has the well-known form $S=i\ \mathrm{Tr}\ \ln G$, where G is the electronic Green's function in a field Ω^l and the trace is calculated over all variables, including the time and the spatial coordinates.

In the present letter we shall calculate only the topological Hopf term in action that contains all three components Ω_t, Ω_x, and Ω_y. Therefore we must find the contribution of four diagrams (see Fig. 1). For the first two diagrams, which are formally second-order diagrams, we must find the contribution which is of third order in Ω. The unperturbed Green's function has the form

$$G_0(\mathbf{r},\mathbf{r}',t-t')=-i\langle T\chi(\mathbf{r},t)\chi^{+}(\mathbf{r}',t')\rangle$$

$$= \sum_s \int \frac{d\omega}{2\pi} \frac{dp}{2\pi} g_s(\omega) e^{-i\omega(t-t')} \Phi_{sp}(\mathbf{r}) \Phi^*_{sp}(\mathbf{r}').$$

Here T is the time-ordering operator for Fermi operators, s is the index of the Landau level, and Φ_{sp} are oscillator wave functions in the Landau gauge which we are employing. The matrices $g_s(\omega)$ correspond to a completely filled (all p) bottom spin sublevel $s=0$, and the other spin sublevel and all states with $s\neq 0$ are empty:

$$g_0(\omega) = \frac{1+\sigma_z}{2(\omega+\gamma-i\delta)} + \frac{1-\sigma_z}{2(\omega-\gamma+i\delta)}, \tag{4}$$

$$g_s(\omega) = \frac{1+\sigma_z}{2(\omega-s\omega_c+\gamma+i\delta)} + \frac{1-\sigma_z}{2(\omega-s\omega_c-\gamma+i\delta)}. \tag{5}$$

We have introduced the chemical potential $\mu=\omega_c/2$, so that this energy does not appear in the expressions for g_s.

In order for the perturbation theory in Ω^l to be valid, the corrections $\delta E \sim (\Omega^2/m)$ to the single-electron energies[5] must be small compared with the smallest exchange gap $\gamma\rho \sim (e^2/l_H)$. This results in the strong inequality $L_c \gg l_H \sqrt{\hbar\omega_c l_H/e^2}$, where L_c is the size of the vortex core. The core size is determined by the minimum of the sum of the core Coulomb energy $\sim e^2/L_c$ and the additional Zeeman energy $\sim gH\rho L_c^2$; this gives $L_c^3 \sim e^2/(gH\rho)$. Therefore the perturbation theory in Ω is valid if the g factor is sufficiently small.

We obtain to third order inclusively

$$S = i\ \mathrm{Tr}\Big[\ln G_0 + H_1 G_0 + H_2 G_0 + \frac{1}{2} H_1 G_0 H_1 G_0 + H_2 G_0 H_1 G_0 + \frac{1}{3} H_1 G_0 H_1 G_0 H_1 G_0\Big],$$

using the standard perturbation theory for the Green's function and expanding the logarithm. This corresponds to the diagrams in Fig. 1.

We start with the second-order term corresponding to the first diagram in Fig. 1,

$$S_2^1 = \frac{i}{m}\mathrm{Tr} \int \sigma_l g_s \sigma_{l'} g_{s'} e^{i\omega\delta} \frac{d\omega}{2\pi} \Omega_t^l(\mathbf{r},t) \Phi_{sp}(\mathbf{r}) \Phi^*_{sp}(\mathbf{r}') \times [\Omega_+^{l'}(\mathbf{r}',t')\pi^- + \Omega_-^{l'}(\mathbf{r}',t')\pi^+] \Phi_{s'p'}(\mathbf{r}') \Phi^*_{s'p'}(\mathbf{r}) d^2r' d^2r dt.$$

Here δ is an infinitesimal positive quantity. The expression $\vec{\Omega}^l \cdot (-i\nabla - \mathbf{A}_0)$ is written using the quantities $\Omega_+^l = (-i\Omega_x^l - \Omega_y^l)/2$ and $\Omega_-^l = (i\Omega_x^l - \Omega_y^l)/2$ and also the Landau-index raising and lowering operators $\pi^+ \Phi_{sp} = \sqrt{2(s+1)}\Phi_{s+1,p}$ and $\pi^- \Phi_{sp} = \sqrt{2s}\Phi_{s-1,p}$, respectively. The time derivatives of $\vec{\Omega}^l$ can be neglected in the above expression, since the Hopf invariant does not contain a term with two time derivatives. The corresponding expression contains three terms with $s=s'=0$ and two other terms with $s=1$, $s'=0$ and $s=0$, $s'=1$.

Introducing the new integration variables $\mathbf{R}=(\mathbf{r}+\mathbf{r}')/2$ and $\vec{\rho}=(\mathbf{r}'-\mathbf{r})$ and expanding in powers of $\vec{\rho}$, we easily find that

$$S_2^1=\frac{1}{4m\gamma}\sum_{l\neq z}\int[i\Omega_t^l\nabla\cdot\vec{\Omega}^l-i\vec{\Omega}^l\times\nabla\Omega_t^l-\Omega_t^l\nabla\times\vec{\Omega}^l-\vec{\Omega}^l\times\nabla\Omega_t^l]\frac{d^2rdt}{2\pi}$$
$$+\frac{1}{2}\int(\Omega_t^l\nabla\times\vec{\Omega}^l+\vec{\Omega}^l\times\nabla\Omega_t^l)\frac{d^2rdt}{2\pi}+\frac{1}{4}\,\mathrm{Tr}\,\sigma_l\sigma_{l_1}\sigma_z$$
$$\times\int(-i\Omega_t^l\nabla\cdot\vec{\Omega}^{l_1}+i\vec{\Omega}^{l_1}\cdot\nabla\Omega_t^l)\frac{d^2rdt}{2\pi}. \tag{6}$$

The part of the action that corresponds to the second diagram in Fig. 1 is calculated analogously. The second-order term, which does not appear in the Hopf invariant, can be dropped, and only terms with one time derivative are important. The general formula is close to the corresponding formula in the preceding case. We are interested in the terms corresponding to $s=1$, $s'=0$ and $s=0$, $s'=1$; all other terms contain extraneous spatial derivatives. Introducing the new variables of integration $T=(t+t')/2$ and $\tau=t'-t$, we obtain after expanding in powers of τ

$$S_2^2=-i\,\mathrm{Tr}\,\frac{\sigma_l\sigma_{l_1}(1+\sigma_z)}{2}\int\left(\Omega_-^{l_1}\frac{\partial\Omega_+^l}{\partial T}-\Omega_+^l\frac{\partial\Omega_-^{l_1}}{\partial t}\right)\frac{d^2rdt}{2\pi}.$$

Using the expressions for Ω_+^l and Ω_-^l and the identity $\partial_t\Omega_k^l=\partial_k\Omega_t^l+2e^{ljm}\Omega_t^j\Omega_k^m$, where e^{ljm} is a completely antisymmetric unit tensor, this relation can be rewritten in the form

$$S_2^2=-\frac{1}{2}\int(\vec{\Omega}^l\times\nabla\Omega_t^l+2e^{ljm}\Omega_t^j\vec{\Omega}^l\times\vec{\Omega}^m)\frac{d^2rdt}{2\pi}$$
$$-\frac{i}{2}\,\mathrm{Tr}\,\sigma_{l_1}\sigma_l\sigma_z\int(\vec{\Omega}^l\cdot\nabla\Omega_t^{l_1}+2e^{l_1jm}\vec{\Omega}^l\cdot\vec{\Omega}^m\Omega_t^j)\frac{d^2rdt}{2\pi}. \tag{7}$$

It is easy to obtain the contribution of the third diagram (Fig. 1):

$$S_{21}=-\frac{i}{2m\gamma}\sum_{l\neq z}\int\Omega_t^l\nabla\cdot\vec{\Omega}^l\frac{d^2rdt}{2\pi}. \tag{8}$$

The general expression for the contribution of the last diagram in Fig. 1 has the form

$$S_3=\frac{i}{m^2}\int\mathrm{Tr}\sigma_l g_s\sigma_{l_1}g_{s_1}\sigma_{l_2}g_{s_2}e^{i\omega\delta}\int\Omega_t^l\Phi_{sp}(\mathbf{r})\Phi_{sp}^*(\mathbf{r}_1)(\Omega_+^{l_1}\pi^-+\Omega_-^{l_1}\pi^+)$$
$$\times\Phi_{s_1p_1}(\mathbf{r}_1)\Phi_{s_1p_1}^*(\mathbf{r}_2)(\Omega_+^{l_2}\pi^-+\Omega_-^{l_2}\pi^+)\Phi_{s_2p_2}(\mathbf{r}_2)\Phi_{s_2p_2}(\mathbf{r})\Phi_{s_2p_2}^*(\mathbf{r})$$
$$\times\frac{d\omega}{2\pi}d^2rd^2r_1d^2r_2dt.$$

Only terms with $s=s_2=0$, $s_1=1$ and $s=s_2=1$, $s_1=0$ are important. All derivatives of Ω can be neglected. The calculations are similar to the preceding calculations and we obtain

$$S_3^0 = -\frac{i}{m\gamma}\sum_{l\neq z}\mathrm{Tr}\ \sigma_l\sigma_{l_1}\sigma_{l_2}\int \Omega_t^l\vec{\Omega}^{l_1}\times\vec{\Omega}^{l_2}\frac{d^2rdt}{2\pi} + \frac{i}{4}\mathrm{Tr}\ \sigma_z\sigma_{l_1}\sigma_{l_2}$$
$$\times\int \Omega_t^z\vec{\Omega}^{l_1}\times\vec{\Omega}^{l_2}\frac{d^2rdt}{2\pi} \tag{9}$$

for terms of the first type and

$$S_3^1 = \frac{1}{2}\int\left[\Omega_t^z\sum_{l\neq z}[(\vec{\Omega}^l)^2-(\vec{\Omega}^z)^2]-\sum_{l\neq z}\Omega_t^l\vec{\Omega}^z\cdot\vec{\Omega}^l\right]\frac{d^2rdt}{2\pi} + \frac{i}{4}\mathrm{Tr}\ \sigma_l\sigma_{l_1}\sigma_{l_2}$$
$$\times\int \Omega_t^l\vec{\Omega}^{l_1}\vec{\Omega}^{l_2}\frac{d^2rdt}{2\pi} \tag{10}$$

for the contribution of the second type.

The sum of all third-order terms (6)–(10) gives the desired Hopf term in the action. We shall clarify some results of such a summation. All terms possessing a factor $1/(m\gamma)$ can be combined together into the total derivative

$$\frac{1}{4m\gamma}\sum_{l\neq z}\int[-i\nabla\cdot(\Omega_t^l\vec{\Omega}^l)-\nabla\times(\Omega_t^l\vec{\Omega}^l)]\frac{d^2rdt}{2\pi}=0,$$

which gives zero, since $\vec{\Omega}^l$ for $l\neq z$ approach zero exponentially at large distances. The symmetric differential terms in S_2^1 and S_2^2 also combine into a total derivative

$$\frac{(-i)}{4}\mathrm{Tr}\ \sigma_l\sigma_{l_1}\sigma_z\int\nabla\cdot(\Omega_t^l\vec{\Omega}^{l_1})\frac{d^2rdt}{2\pi}=0,$$

which gives zero for the same reason. The symmetric nondifferential terms in S_2^2 and S_3^1 cancel one another, and we obtain the completely antisymmetric expression in the action

$$S_3 = \frac{i}{4}\mathrm{Tr}\ \sigma_l\sigma_{l_1}\sigma_{l_2}\int\Omega_t^l\vec{\Omega}^{l_1}\times\vec{\Omega}_{l_2}\frac{d^2rdt}{2\pi} + \frac{1}{2}\int\Omega_t^l\nabla\times\vec{\Omega}^l\frac{d^2rdt}{2\pi} - e^{ljm}$$
$$\times\int\Omega_t^j\vec{\Omega}_l\vec{\Omega}^m\frac{d^2rdt}{2\pi}.$$

Calculating the trace and using the identity $\nabla\times\vec{\Omega}^l = e^{ljm}\vec{\Omega}^j\times\vec{\Omega}^m$, we write the answer in the form

$$S_3 = \frac{1}{2\pi}e^{ljm}\int\Omega_t^l\vec{\Omega}^j\times\vec{\Omega}^m d^2rdt = \frac{1}{2\pi}\int\Omega_t^l\frac{\mathbf{H}}{H}\cdot\nabla\times\vec{\Omega}^l d^2rdt,$$

where we have introduced the external magnetic field explicitly. We note that the final expression has all symmetry elements that are characteristic of the exchange interaction: $t\to(-t)$, $\mathbf{H}\to(-\mathbf{H})$; $x\rightleftharpoons y$; and, rotation of the orbital space around the direction of the magnetic field and rotation of the spin space. Therefore the form of S_3 is dictated by symmetry considerations, and the other terms consequently vanish.

Returning to the complete equation (3) for the action, we note that the second term in this equation with the interaction does not possess the required symmetry in the terms

that could appear in the Hopf invariant, since they necessarily contain only Ω_t^l with $l \neq z$; this can be easily shown by calculating the corresponding $\delta\langle\chi_\alpha^+\chi_\beta\rangle$. Therefore the different terms of the required form must cancel one another, and the Hopf invariant gives only S_3. The Hopf invariant can be expressed in terms of Ω according to Ref. 8 in the form

$$H=\frac{1}{2(\pi)^2}e^{ljm}\int \Omega_t^l\vec{\Omega}^j\times\vec{\Omega}^m d^2r\,dt$$

and therefore

$$S_H=\pi H.$$

This result confirms the expression in Ref. 7 and is different from the answer obtained in Ref. 6 for the case $s=0$. The latter assertion follows from the following considerations. The Hopf invariant H assumes arbitrary integer values corresponding to the linking number between the curves $\mathbf{n}(\mathbf{r},t)=$ const, $|\mathbf{n}|=1$ for the map of $S_3 \rightarrow S_2$. In this case Ω approaches zero for large $\mathbf{r}$, t, since infinity of R_3 should correspond to a single point in order to represent S_3. In this case the degree of the map of any section $t=$ const must equal the degree of the map for $t\rightarrow\infty$, and therefore it must equal zero. This means that the quantities Ω^l decrease more rapidly than $1/r$. The expression obtained in Ref. 6 is an integral of the total spatial derivative and vanishes in this case, in contrast to the Hopf invariant, which takes on arbitrary integer values. It should also be noted that this expression does not possess the complete symmetry of the problem.

The result obtained for S_H signifies, according to the current point of view, that vortices/skyrmions correspond to fermions.[9]

I thank G. E. Volovik for valuable discussions.

This investigation was supported in part by Grant No. RP1-273 from the US Civilian Research and Development Foundation for the Independent States of the Former Soviet Union. It was also supported in part by INTAS Grant No. 95-1/RU-675.

[1] S. Sondhi, A. Kalrede, S. Kivelson, and E. Rezai, Phys. Rev. B **47**, 16418 (1993).
[2] H. Fertig, L. Brey, R. Cote, and A. MacDonald, Phys. Rev. B **50**, 11018 (1994).
[3] K. Moon, H. Mori, K. Yang *et al.*, Phys. Rev. B **51**, 5138 (1995).
[4] Yu. Bychkov, T. Maniv, and I. Vagner, Phys. Rev. B **53**, 10148 (1996).
[5] S. Iordanskiĭ and S. Plyasunov, JETP Lett. **65**, 259 (1997).
[6] W. Apel and Yu. Bychkov, Phys. Rev. Lett. **78**, 2188 (1997).
[7] G. Volovik and V. Yakovenko, cond-mat/9703228.
[8] G. Volovik and V. Yakovenko, J. Phys.: Condens. Matter **1**, 5263 (1989).
[9] F. Wilczek and A. Zee, Phys. Rev. Lett. **51**, 2250 (1983).

Translated by M. E. Alferieff

Properties of a magnetic impurity in a metal

Yu. N. Ovchinnikov,[a] A. M. Dyugaev,[a] and P. Fulde
Max-Planck-Institut für Physik komplexer Systeme, 01187 Dresden, Germany

V. Z. Kresin
Lawrence Berkeley Laboratory, University of California, 94720 California, USA

(Submitted 2 July 1997)
Pis'ma Zh. Éksp. Teor. Fiz. **66**, No. 3, 184–189 (10 August 1997)

The effect of a polarized conduction-electron cloud back on a magnetic impurity dissolved in a metal is studied. It is shown that at a temperature T_c much higher than the Kondo temperature the system becomes unstable against symmetry breaking and that a state with $\langle S_z\rangle \neq 0$ is established. The behavior of $\langle S_z\rangle$ is derived for all temperatures and magnetic fields except for a very narrow region around T_c and for very low temperatures. The minute role of Kondo-type processes in establishing the symmetry-broken state is pointed out. © *1997 American Institute of Physics.* [S0021-3640(97)01215-2]

PACS numbers: 75.30.Hx, 72.15.Qm

The problem of a magnetic impurity embedded in a sea of conduction electrons is a well-studied one.[1–4] In spite of this, the effect of the induced conduction electron polarization cloud acting back on the impurity has been treated only incompletely, and we want to reconsider this problem here. The model investigated is that of an impurity coupled via an exchange interaction to a system of noninteracting conduction electrons. Both signs of the exchange interaction are considered. It is well known that for an antiferromagnetic coupling (Kondo Hamiltonian) a perturbation expansion leads to diagrams which diverge in the low temperature limit. Despite this, as we shall show, the effect of the polarization cloud back on the impurity leads at a relatively high temperature T_c to an instability of the isotropic state against a symmetry-broken one with $\langle S_z\rangle \neq 0$. Here S_z is the z-component of the spin of the magnetic impurity. The divergent diagrams are of little importance for the value of T_c.

The starting point is a Hamiltonian of the form

$$H = H_0 - \sum_{\alpha} \int d^3r \Psi_{\alpha}^{+}(\mathbf{r})(V_1(\mathbf{r}) + V_2(\mathbf{r})(\mathbf{S}\cdot\boldsymbol{\sigma}))\Psi_{\alpha}(\mathbf{r}) = H_0 + H_{\text{int}}. \tag{1}$$

Here H_0 is the Hamiltonian of the conduction electrons and of a free impurity spin in an applied external magnetic field $\mathbf{H}$, i.e., H_0 contains a Zeeman contribution of the form

$$H_{Ze} = -\mu \mathbf{S}\cdot\mathbf{H} - \frac{\mu_e}{2}\boldsymbol{\sigma}\cdot\mathbf{H}. \tag{2}$$

Note that usually $\mu_e = 2\mu_B$.

The quantities $V_1(\mathbf{r})$ and $V_2(\mathbf{r})$ represent short-range potentials of the impurity and, as usual, $V_2 \ll V_1$. We shall not consider the ordinary scattering potential $V_1(\mathbf{r})$ here, but rather limit ourselves to the magnetic part $V_2(\mathbf{r})$, for which we make the approximation

$$V_2(\mathbf{r}) = g\,\delta(\mathbf{r}). \tag{3}$$

As usual, the $\Psi_\alpha(\mathbf{r})$, $\Psi_\alpha^+(\mathbf{r})$ in Eq. (1) are conduction-electron field operators.

Our aim is to calculate $\langle S_z \rangle$. Consider first the case when $g=0$. The partition function of the impurity is then given by

$$Z_0 = \sum_{S_z} e^{(\mu H S_z/T)} = \frac{\sinh\left[\left(S+\frac{1}{2}\right)\mu H/T\right]}{\sinh[\mu H/(2T)]}, \tag{4}$$

and

$$\langle S_z \rangle_0 = T\frac{\partial \ln Z_0}{\partial(\mu H)} = \left(S+\frac{1}{2}\right)\coth\left[\left(S+\frac{1}{2}\right)\mu H/T\right] - \frac{1}{2}\coth(\mu H/(2T)), \tag{5}$$

which is the well-known Brillouin function.

In order to determine $\langle S_z \rangle$ up to second order in g we also need

$$\begin{aligned}
&\langle T_\tau\, \mathbf{S}(\tau)\cdot\mathbf{S}(0)\rangle_0 = \langle S_z^2\rangle_0 + (S(S+1)-\langle S_z^2\rangle_0)\cosh(\mu H\tau) - \sinh(\mu H|\tau|)\langle S_z\rangle_0,\\
&\langle T_\tau\, S_z(0)(\mathbf{S}(\tau)\cdot\mathbf{S}(0))\rangle_0 = -(\cosh(\mu H\tau)-1)\langle S_z^3\rangle_0\\
&\qquad\qquad + S(S+1)\cosh(\mu H\tau)\langle S_z\rangle_0 - \sinh(\mu H|\tau|)\langle S_z^2\rangle_0.
\end{aligned} \tag{6}$$

The averages $\langle S_z^2\rangle_0$ and $\langle S_z^3\rangle_0$ are obtained from

$$\begin{aligned}
&\langle S_z^2\rangle_0 = \frac{T^2}{Z_0}\frac{\partial^2 Z_0}{\partial(\mu H)^2} = \langle S_z\rangle_0^2 + T\frac{\partial\langle S_z\rangle_0}{\partial(\mu H)},\\
&\langle S_z^3\rangle_0 - \langle S_z\rangle_0\langle S_z^2\rangle_0 = T\frac{\partial\langle S_z^2\rangle_0}{\partial(\mu H)}.
\end{aligned} \tag{7}$$

The following combination will be required below

$$\begin{aligned}
&\langle T_\tau\, S_z(0)(\mathbf{S}(\tau)\cdot\mathbf{S}(0))\rangle_0 - \langle S_z\rangle_0\langle T_\tau\, \mathbf{S}(\tau)\cdot\mathbf{S}(0)\rangle_0\\
&\quad = (-\cosh(\mu H\tau)+1)\left(T\frac{\partial\langle S_z^2\rangle_0}{\partial(\mu H)}\right) - \sinh(\mu H|\tau|)\left(T\frac{\partial\langle S_z\rangle_0}{\partial(\mu H)}\right).
\end{aligned} \tag{8}$$

Note that these terms are the ones giving rise to the Kondo effect when a perturbation expansion is made.

We also need the Green's function of the conduction electrons, which for $g=0$ can be written in the form of a (2×2) matrix as

$$G^{(0)}(\tau) = \frac{1}{2}(G_+(\tau)+G_-(\tau))E + \frac{1}{2}(G_+(\tau)-G_-(\tau))\tau_z, \tag{9}$$

where τ_z is the Pauli matrix and

$$G_{\pm}(\omega_n)=\frac{1}{i\omega_n-(\epsilon\mathbf{p}-\epsilon_F\mp\mu_e H/2)};\quad \omega_n=2\pi T\left(n+\frac{1}{2}\right). \tag{10}$$

In the presence of the exchange interaction, i.e., for $g\neq 0$ we must evaluate the expression[5]

$$\langle S_z\rangle=-\frac{T_r\left\{e^{-(H_0-\epsilon_F N)/T}T_\tau\, S_z(0)\sigma\left(\frac{1}{T}\right)\right\}}{T_r\left\{e^{-(H_0-\epsilon_F N)/T}\sigma\left(\frac{1}{T}\right)\right\}} \tag{11}$$

with $\sigma(1/T)$ given by

$$\sigma\left(\frac{1}{T}\right)=T_\tau\, e^{-\int_0^{1/T}d\tau_1 H_{\rm int}(\tau_1)}. \tag{12}$$

In order to calculate $\langle S_z\rangle$ to second order in g we first determine $G(\tau)$ to first order in g, using

$$G_{\alpha\beta}(\tau)=-\frac{T_\tau\left\{e^{-(H_0-\epsilon_F N)/T}T_\tau\Psi_\alpha(\tau_1)\Psi^+_\beta(0)\sigma\left(\frac{1}{T}\right)\right\}}{T_r\left\{e^{-(H_0-\epsilon_F N)/T}\sigma\left(\frac{1}{T}\right)\right\}}. \tag{13}$$

This gives

$$G(\tau)=G^{(0)}(\tau)-g\langle S_z\rangle I(\tau)\tau_z, \tag{14}$$

where $\langle S_z\rangle$ is the *exact* expression for the impurity spin and

$$I(\tau)=\int_0^{1/T}d\tau_1 G(\tau-\tau_1)G(\tau_1). \tag{15}$$

For the local exchange interaction (3) considered here

$$I(0)=-\frac{mp_F}{2\pi^2}A=-N(0)A, \tag{16}$$

where A is of order unity and depends on the hitherto neglected potential V_1. As usual, m is the electron mass and p_F is the Fermi momentum. The effect of the impurity spin polarization on the electrons as contained in Eq. (14) was studied in Ref. 2. Here we need only $I(0)$ as given by Eq. (16). If instead of Eq. (3) a potential $V_2(\mathbf{r})$ with a short but finite range is used, the function $I(\tau)$ is replaced by the more general one

$$I(\mathbf{r},\mathbf{r}',\tau)=\frac{1}{g}\int_0^{1/T}d\tau_1\int d^3r_1 G(\mathbf{r},\mathbf{r}_1,\tau-\tau_1)V_2(\mathbf{r}_1-\mathbf{r_a})G(\mathbf{r}_1,\mathbf{r}',\tau_1),$$

where $\mathbf{r_a}$ is the position of the impurity. The corrections in $\langle S_z\rangle$ to order g^2 follow from Eq. (11), i.e., from the numerator as well as denominator.

The denominator is simply given by the partition function, which to order g^2 is

$$Z = Z_0 \Bigg\{ 1 + \frac{g}{T}(n_+ - n_-)\langle S_z\rangle - \frac{2g^2}{T}\langle S_z\rangle^2 I(0)$$
$$- g^2 \int_0^{1/T} d\tau_1 \int_0^{1/T} d\tau_2 G(\tau_1 - \tau_2) G(\tau_2 - \tau_1) \langle T_\tau(\mathbf{S}(\tau_1)\mathbf{S}(\tau_2))\rangle \Bigg\}. \tag{17}$$

The quantities $n_\pm$ are the densities of spin up and spin down electrons. They are given by

$$n_\pm = n \pm N(0)\frac{\mu_e H}{2}. \tag{18}$$

The third term on the right-hand side of Eq. (17) comes from the correction of the electron Green's function. When the numerator of Eq. (11) is similarly evaluated we find

$$\langle S_z\rangle = \langle S_z\rangle_0 + \frac{\partial\langle S_z\rangle_0}{\partial(\mu H)}(gN(0)\mu_e H - 2g^2 I(0)\langle S_z\rangle)$$
$$- g^2 \int_0^{1/T} d\tau_1 \int_0^{1/T} d\tau_2 G(\tau_1 - \tau_2) G(\tau_2 - \tau_1)(\langle T_\tau\, S_z(0)(\mathbf{S}(\tau_1)\mathbf{S}(\tau_2))\rangle_0$$
$$- \langle T_\tau(\mathbf{S}(\tau_1)\mathbf{S}(\tau_2))\rangle_0). \tag{19}$$

It is important to realize, and in fact has been pointed out before, that the right-hand sides of Eqs. (17) and (19) contain the exact expectation value $\langle S_z\rangle$ rather $\langle S_z\rangle_0$. This is because these terms should be considered as a Hartree-like contribution to the electron Green's function. Some further justification is given below. Note also that the product $G(\tau)G(-\tau)$ in Eq. (19) consists of a singularity of the form $\delta(\tau)$ plus a smooth function of τ. Therefore, multiplying it by integer powers of $|\tau|$ yields integrals of order $\max\{T,\mu H\}/\epsilon_F$. By making use of Eq. (4) we obtain the following result

$$\langle S_z\rangle - \langle S_z\rangle_0 = \frac{\partial\langle S_z\rangle_0}{\partial(\mu H)}(gN(0)\mu_e H - 2g^2\langle S_z\rangle I(0))$$
$$+ 2g^2 \int_0^{1/T} d\tau_1 \int_0^{\tau_1} d\tau G(\tau)G(-\tau)\Bigg[(\cosh(\mu H\tau) - 1)\left(T\frac{\partial\langle S_z^2\rangle_0}{\partial(\mu H)}\right)$$
$$+ \sinh(\mu H\tau)\left(T\frac{\partial\langle S_z\rangle_0}{\partial(\mu H)}\right)\Bigg]. \tag{20}$$

The last term yields the Kondo-type corrections. As shown below they are smaller by a factor of order $(\max\{T,\mu H\}/\epsilon_F)\ln(\epsilon_F/\max\{T,\mu H\})$ than the second term on the right-hand side on that equation. To see this we use Eq. (9) to obtain

$$\int_0^{1/T} d\tau_1 \int_0^{\tau_1} d\tau G(\tau)G(-\tau)\sinh(\mu H\tau)$$
$$= \int \frac{d^3p\, d^3p'}{(2\pi)^6}\left\{\frac{1}{2}\left(\frac{1}{T} + \sinh\left(\frac{\mu H}{T}\right)\frac{\partial}{\partial(\mu H)}\right)\coth\left(\frac{\epsilon_{\mathbf{p}} - \epsilon_{\mathbf{p}'}}{2T}\right)\right.$$

$$-\cosh^2\left(\frac{\mu H}{2T}\right)\frac{\partial}{\partial(\mu H)}\Bigg\}\frac{f_{\mathbf{p}}-f_{\mathbf{p}'}}{\epsilon_{\mathbf{p}}-\epsilon_{\mathbf{p}'}-\mu H},$$

$$\int_0^{1/T}d\tau_1\int_0^{\tau_1}d\tau G(\tau)G(-\tau)(\cosh(\mu H\tau)-1)$$

$$=\int\frac{d^3p\,d^3p'}{(2\pi)^6}\Bigg\{\frac{f_{\mathbf{p}}-f_{\mathbf{p}'}}{2T}\left(\frac{1}{\epsilon_{\mathbf{p}}-\epsilon_{\mathbf{p}'}-\mu H}-\frac{1}{\epsilon_{\mathbf{p}}-\epsilon_{\mathbf{p}'}}\right)$$

$$+\left(\sinh^2\left(\frac{\mu H}{2T}\right)\coth\left(\frac{\epsilon_{\mathbf{p}}-\epsilon_{\mathbf{p}'}}{2T}\right)-\frac{1}{2}\sinh\left(\frac{\mu H}{T}\right)\right)\frac{\partial}{\partial(\mu H)}\left(\frac{f_{\mathbf{p}}-f_{\mathbf{p}'}}{\epsilon_{\mathbf{p}}-\epsilon_{\mathbf{p}'}-\mu H}\right)\Bigg\}. \tag{21}$$

Here $f_{\mathbf{p}}$ denotes the Fermi function. Within logarithmic accuracy we can write

$$\int_0^{1/T}d\tau_1\int_0^{\tau_1}d\tau G(\tau)G(-\tau)\sinh(\mu H\tau)$$

$$=-[N(0)]^2\left(\frac{\mu H}{T}+\sinh\frac{\mu H}{T}\right)\cdot\ln\left(\frac{\epsilon_F}{\max(T,\mu H)}\right)$$

$$\times\int_0^{1/T}d\tau_1\int_0^{\tau_1}d\tau G(\tau)G(-\tau)(\cosh(\mu H\tau)-1)$$

$$=-2[N(0)]^2\sinh^2\left(\frac{\mu H}{2T}\right)\cdot\ln\left(\frac{\epsilon_F}{\max(T,\mu H)}\right). \tag{22}$$

When these results are inserted into Eq. (20) we finally obtain

$$\langle S_z\rangle-\langle S_z\rangle_0=(gN(0)\mu_e H-2g^2I(0)\langle S_z\rangle)\frac{\partial\langle S_z\rangle_0}{\partial(\mu H)}$$

$$-2g^2[N(0)]^2\ln\left(\frac{\epsilon_F}{\max(T,\mu H)}\right)\Bigg\{2\sinh^2\left(\frac{\mu H}{2T}\right)\left(T\frac{\partial\langle S_z^2\rangle_0}{\partial(\mu H)}\right)$$

$$+\left(\frac{\mu H}{T}+\sinh\left(\frac{\mu H}{T}\right)\right)\left(T\frac{\partial\langle S_z\rangle_0}{\partial(\mu H)}\right)\Bigg\}. \tag{23}$$

One notices that for small fields H the second term $\sim g^2I(0)\langle S_z\rangle$ is the largest one. Neglecting for the moment the logarithm term, which is small, we obtain for $H=0$ an instability of the impurity system against a fixed moment $\langle S_z\rangle\neq 0$. With $\partial\langle S_z\rangle_0/\partial(\mu H)=\frac{1}{3}S(S+1)/T$ the transition temperature T_c is given by

$$T_c=-2g^2I(0)\frac{S(S+1)}{3}. \tag{24}$$

Below that temperature a spontaneous symmetry reduction takes place. The impurity spin is polarized in a direction which will be determined by the ubiquitous anisotropies.

It is interesting to determine the associated thermodynamic potential Ω. First of all, it is possible to show that all diagrams with intersecting (or crossing) lines obtained from Eqs. (11) and (13) are of order T/ϵ_F and are therefore small. This holds true for any order in the interaction constant g. Therefore, one may neglect them, and Eq. (14) holds formally for all orders in g. From that equation one may also conclude that the effect of the exchange interaction on the spin energy is threefold: it produces a large shift in the level positions, an additional $\langle S_z\rangle$-dependent shift, and a small shift due to processes of the Kondo type. If these last are neglected, the self-consistency equation for the average value $\langle S_z\rangle$ is of the form

$$\langle S_z\rangle = B\left(\frac{\mu H - 2g^2 I(0)\langle S_z\rangle}{T}\right), \tag{25}$$

where $B(x)$ is the Brillouin function. This equation holds for all values of H and T, except in a narrow temperature interval $|T_c - T| \leqslant T_c^2/\epsilon_F$ near the transition temperature, where corrections of the Kondo type become important. Note that Eq. (24) follows from (25) when $H=0$.

The correction of the thermodynamic potential due to $H_{\rm int}$ is calculated from

$$\frac{\delta\Omega}{\delta g} = \frac{1}{g}\langle H_{\rm int}\rangle. \tag{26}$$

Making use of Eq. (14), we obtain

$$\frac{\delta\Omega}{\delta g} = 2gI(0)\langle S_z\rangle^2 \tag{27}$$

with $\langle S_z\rangle^2$ given by Eq. (25).

In the regime $\mu H \to 0$ we find for the static magnetic moment near the transition temperature

$$\langle S_z\rangle^2 = \frac{5}{3}\left(1 - \frac{T}{T_c}\right)\frac{(S(S+1))^2}{\left(S^2+S+\frac{1}{2}\right)}. \tag{28}$$

Here we have used an expansion of $\langle S_z\rangle_0$ in powers of $(\mu H/T)$. When this is inserted into Eq. (27), we obtain for the change in the thermodynamic potential

$$\Omega - \Omega_0 = -\frac{5}{2T_c}\frac{S(S+1)}{S^2+S+\frac{1}{2}}(T_c - T)^2. \tag{29}$$

This proves that the symmetry-broken solution $\langle S_z\rangle \neq 0$ leads to a lowering of the energy as compared with the symmetry-conserving one.

In conclusion, we have shown that at a temperature much higher than the Kondo temperature the system of a magnetic impurity coupled to conduction electrons becomes unstable against the formation of a polarized impurity-spin state $\langle S_z\rangle \neq 0$. Kondo-type corrections to $\langle S_z\rangle$ are generally small but may become important in the immediate vicinity of the transition temperature. In an isotropic medium the ground state is infinitely

degenerate with respect to the direction of the spontaneous magnetization. However, in a real crystal there is always anisotropy, and the ground state will be only finitely degenerate. An exponentially small transition probability between these different states will lead to the appearance of a new scale, which can be considered as the Kondo temperature.

Yu. N. Ovchinnikov and A. M. Dyugaev wish to acknowledge the Max-Planck-Gesellschaft zur Förderung der Wissenschaften and Max-Planck-Institut für Physik komplexer Systeme for hospitality during the period when this work was done.

The research of Yu. N. Ovchinnikov is supported by the CRDF (Grant RP1-194) and by the contract (N 00173-97-P-3488) with NAVAL Research Laboratory.

The research of A. M. Dyugaev is supported by the INTAS-RFBR (Grant 95-553).

[a)]Permanent address: Landau Institute of Theoretical Physics, Russian Academy of Sciences, 117334 Moscow, Russia

---

[1] J. Kondo, *Solid State Physics, Advances in Research and Applications*, Vol. 23, Academic Press, New York–London (1970).
[2] M. S. Fullenbaum and D. S. Falk, Phys. Rev. **157**, 452 (1967).
[3] A. A. Abrikosov and A. A. Migdal, J. Low Temp. Phys. **3**, 519 (1970).
[4] A. M. Tsvelick and P. B. Wiegmann, Adv. Phys. **32**, 453 (1983).
[5] A. A. Abrikosov, L. P. Gor'kov, and I. E. Dz'yaloshinskiĭ, *Methods of Quantum Field Theory in Statistical Physics*, Prentice-Hall, Englewood Cliffs, N.J. (1963).
[6] A. A. Abrikosov and L. P. Gor'kov, Zh. Eksp. Teor. Fiz. **39**, 1781 (1960) [Sov. Phys. JETP **12**, 1243 (1961)].

Published in English in the original Russian journal. Edited by Steve Torstveit.

Magnetic quantum oscillations in the organic superconductor κ-(BEDT-TTF)$_2$Cu[N(CN)$_2$]Br

H. Weiss
Walther-Meissner-Institut, D-85748 Garching, Germany; High Magnetic Field Laboratory, F-38042, Grenoble Cedex 9, France

M. V. Kartsovnik[a)] and W. Biberacher
Walther-Meissner-Institut, D-85748 Garching, Germany

E. Steep and A. G. M. Jansen
High Magnetic Field Laboratory, F-38042, Grenoble Cedex 9, France

N. D. Kushch
Walther-Meissner-Institut, D-85748 Garching, Germany; Institute of Chemical Physics, Russian Academy of Sciences, 142432 Chernogolovka, Russia

(Submitted 3 July 1997)
Pis'ma Zh. Éksp. Teor. Fiz. **66**, No. 3, 190–194 (10 August 1997)

The interlayer magnetoresistance of the organic superconductor κ-(BEDT-TTF)$_2$Cu[N(CN)$_2$]Br is measured at ambient pressure and under pressures of up to 12.5 kbar. In addition to the slow Shubnikov–de Haas oscillations with a frequency of $\simeq 150$ T observed at $P \geqslant 5$ kbar, rapid oscillations attributed to the magnetic breakdown orbit enveloping an area equal to 100% of the area of the Brillouin zone are found to emerge above $B = 20$ T. The latter oscillations are observed at ambient pressure as well as under pressures of up to 9 kbar.
 [S0021-3640(97)01315-7]

PACS numbers: 74.70.Kn, 73.50.Jt

The organic salts κ-(BEDT-TTF)$_2$X, where BEDT-TTF stands for bis(ethylenedithio)tetrathiafulvalene and X=Cu(NCS)$_2$, Cu[N(CN)$_2$]Cl$_{1-x}$Br$_x$ ($0 \leqslant x \leqslant 1$), and Cu(CN)[N(CN)$_2$] are characterized by a layered crystal structure with the BEDT-TTF molecules arranged in mutually orthogonal dimers and forming conducting layers alternating with insulating layers of the anions X (Refs. 1 and 2). These compounds have been of high interest in recent years due to the wide range of physical properties which they exhibit in spite of very similar crystal structures. For example, κ-(BEDT-TTF)$_2$Cu(NCS)$_2$ is a metal at low temperatures and undergoes a superconducting transition at 9.4 K.[3] At the same time, the salt with X=Cu[N(CN)$_2$]Cl undergoes a metal-to-insulator transition into an antiferromagnetically ordered state which is supposed to be of the Mott type.[4] A moderate pressure ($\geqslant 0.3$ kbar) stabilizes the metallic state, and the compound becomes a superconductor with $T_c = 12.8$ K, the highest among the known organic superconductors.[1] Its close isostructural analog, the salt with X=Cu[N(CN)$_2$]Br can be regarded as the one located nearest to the boundary between the metallic and insulating states: The salt containing hydrogen in the BEDT-TTF molecules, κ-(h_8,BEDT-TTF)$_2$Cu[N(CN)$_2$]Br exhibits metal-like behavior at low tempera-

tures, although with highly pronounced electron correlations (see, e.g., Ref. 5), and undergoes a superconducting transition at $T_c = 11.2$ K,[1] whereas the deuterated salt, κ-(d_8,BEDT-TTF)$_2$Cu[N(CN)$_2$]Br, is suggested to have a charge gap at the Fermi level.[6]

The effect of subtle changes introduced by the substitution of different anions on the electronic ground state of the κ-type salts is not understood so far. The band structure calculations made conventionally in the two-dimensional approximation (i.e., assuming that the electronic bands are formed by only the BEDT-TTF layers) give very similar results for all the three compounds.[1,7,8] These results have been thoroughly proved by numereous studies of the magnetic quantum oscillations in the Cu(NCS)$_2$ salt (see, e.g., Refs. 7 and 9). Recent observations[10] of the Shubnikov–de Haas effect in the metallic state (under pressure) of the κ-(BEDT-TTF)$_2$Cu[N(CN)$_2$]Cl confirm the predicted Fermi surface for this compound. However, neither quantum oscillations nor classical galvanomagnetic effects which could be directly related to the shape of the Fermi surface have been found in the Cu[N(CN)$_2$]Br salt at ambient pressure till now. Very weak Shubnikov–de Haas oscillations have been observed in this compound at $P \approx 9$ kbar.[11,12] The oscillation parameters[11] revealed considerable differences in the Fermi surface with respect to the Fermi surfaces of the Cu(NCS)$_2$ and Cu[N(CN)$_2$]Cl salts, in contradiction with the theoretical predictions. In particular, the frequency of the slow oscillations which could be attributed to the classical hole orbit at the cylindrical part of the Fermi surface was found to be a factor of 4 smaller than in the other two compounds. This result suggests that either the Fermi surface of the Cu[N(CN)$_2$]Br salt deviates strongly from the predicted one[1] already at ambient pressure or it is unusually sensitive to applied pressure.

In order to get further information about the Fermi surface of κ-(BEDT-TTF)$_2$Cu[N(CN)$_2$]Br and its pressure dependence, we have carried out high-field magnetoresistance measurements on this compound. In this paper we present the quantum magnetoresistance oscillations of two different frequencies which are attributed to the Fermi surface cross-sections constituting 100% and $\approx 4\%$ of the corresponding Brillouin zone cross-section area, respectively. The higher frequency oscillations are found down to $P = 0$ kbar, thus providing the first direct evidence for the well defined Fermi surface existing at ambient pressure.

The high quality crystal of κ-(BEDT-TTF)$_2$Cu[N(CN)$_2$]Br used for the experiment was grown electrochemically as described elsewhere.[13] The interlayer (i.e., perpendicular to the highly conducting ac plane of the crystal) resistance was measured down to $T = 0.4$ K by means of the standard ac method with an excitation current of 10 to 100 μA. The contact resistance was less than 10 Ω, while the sample resistance varied from ~ 3 to 35 Ω depending on the pressure applied. A BeCu clamp cell was used to generate quasi-hydrostatic pressure up to 15 kbar at room temperature, which corresponded to ≈ 12.5 kbar at low temperatures. A magnetic field of up to 27 T perpendicular to the ac plane was provided by the hybrid magnet at the High Magnetic Field Laboratory, MPI-CNRS, Grenoble.

The main panel of Fig. 1 represents the high-field trace of the magnetoresistance at ambient pressure and $T = 0.41$ K. Clear oscillations with the frequency of 3790 ± 30 T (see the fast Fourier transformation in inset a of Fig. 1) indicate the electron orbit in k space with an area equal to 100% of the cross-sectional area of the Brillouin zone, as

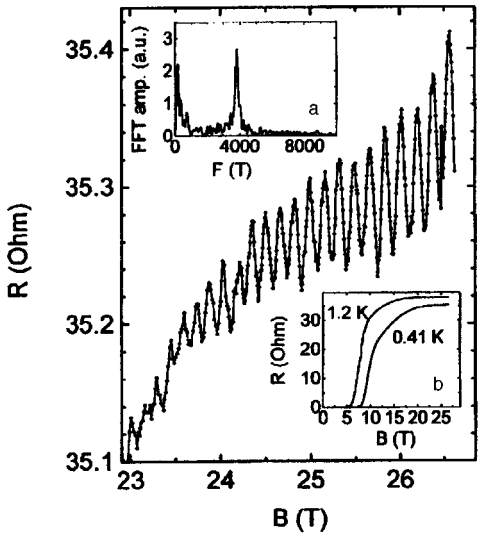

FIG. 1. High magnetic field fragment of the interlayer magnetoresistance at ambient pressure, $T=0.41$ K. Inset a — fast Fourier spectrum of the oscillations. Inset b — field dependence of the interlayer resistance at $T=0.41$ and 1.2 K.

calculated from the room-temperature crystal parameters[1] with allowance for the thermal contraction.[14] This is the first observation of the magnetic quantum oscillations in the present compound at ambient pressure. The cyclotron mass estimated from the temperature dependence of the oscillation amplitude is $(6.4\pm0.5)m_e$, where m_e is the free electron mass. Thus the oscillations are similar to the magnetic breakdown oscillations found earlier[9,10] in the other κ salts, with $X=Cu(NCS)_2$ and $Cu[N(CN)_2]Cl$.

Figure 2 shows the oscillatory magnetoresistance normalized to the background resistance at several pressures. Oscillations of two main frequencies, $F_\alpha \simeq 150$ T and $F_\beta \simeq 3900$ T (hereafter referred to as α and β oscillations), can generally be resolved, in agreement with the previous observation at $P \approx 9$ kbar.[12] The β oscillations correspond to those found at ambient pressure. Their amplitude gradually goes down with increasing pressure, vanishing above 10 kbar. The oscillation frequency changes at a rate $d \ln F_\beta / dP \approx 3.8\times10^{-3}\text{kbar}^{-1}$. This rate is similar to the values obtained for the β oscillations in the salts with $X=Cu(NCS)_2$ (Ref. 15) and $Cu[N(CN)_2]Cl$ (Ref. 10). Since the β frequency is assumed to measure directly the cross-sectional area of the Brillouin zone, its pressure dependence is expected to follow the crystal lattice compressibility. Indeed, the obtained value agrees with the compressibility reported for the κ salts.[8,16]

The α oscillations correspond to situation where the extremal cross section of the Fermi surface occupies $\approx 4\%$ of the area of the Brillouin zone. Their amplitude is somewhat higher than that reported in Ref. 11 and amounts to 1% of the background resistance at around 25 T. The relatively high oscillation amplitude and the resistance ratio, $R(293\text{ K})/R_N(1.5\text{ K}) \approx 50$ and 30 at ambient pressure and at 12.5 kbar, respectively (R_N denotes the normal-state resistance extrapolated from the nonsuperconducting region for

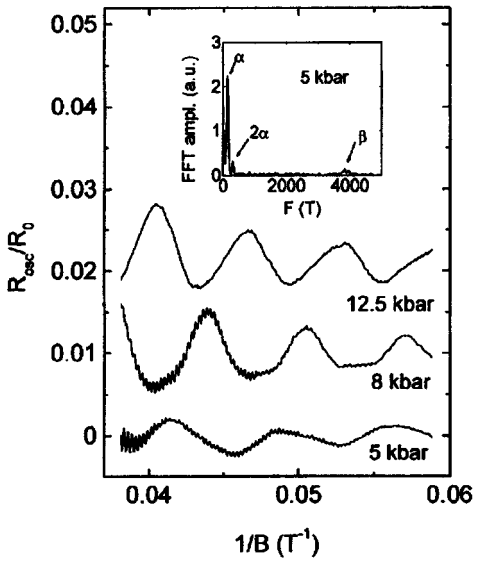

FIG. 2. Oscillatory part of the magnetoresistance normalized to the resistance background at different pressures. The curves at 8 and 12.5 kbar are offset for clarity. Inset: fast Fourier spectrum of the oscillations.

$P=0$ kbar) reflects the good quality of the sample. As the pressure is increased from 5 to 12.5 kbar the frequency F_α gradually grows from 143 to 163 T. As to the oscillation amplitude, it remains nearly unchanged between 8 and 12.5 kbar but becomes significantly smaller at 5 kbar. No α oscillations have been observed at ambient pressure within the magnetic field range investigated.

Turning to the interpretation of the experimental results, we recall that, like in the other κ salts, the Fermi surface of κ-(BEDT-TTF)$_2$Cu[N(CN)$_2$]Br predicted by the band structure calculations[1] is a linear network extended along the $\mathbf{k}_a$ direction and formed by intercoupled cylinders with their axes parallel to the $\mathbf{k}_b$ direction (i.e., perpendicular to the crystallographic ac plane) and cross-sectional areas equal to that of the Brillouin zone. Due to the inversion symmetry characteristic of the crystal structure, the lattice potential is expected to give no gap at the points of intersection between the adjacent cylinders at the Brillouin zone boundary. The observation of only the β oscillations at ambient pressure seems to be consistent with these predictions. Indeed, if the energy gap at the Brillouin zone boundary is negligibly small, only the orbit over the entire Fermi-surface cylinder, with an area equal to the cross-sectional area of the Brillouin zone, should contribute to the oscillations. Such case of the nearly complete magnetic breakdown has been found in the isostructural compound κ-(BEDT-TTF)$_2$I$_3$ (Ref. 17). The relatively small amplitude of the oscillations in comparison with the latter compound may be attributed to the higher Dingle temperature (it is estimated to be 2.5 ± 0.5 K in the present compound against $T_D<1$ K in the other κ salts) and to stronger warping of the Fermi-surface cylinder. The decrease of the amplitude of the β oscillations under pressure and simulteneous enhancement of the α oscillations can be likely explained by structural changes inducing the gap at the Brillouin zone boundary.

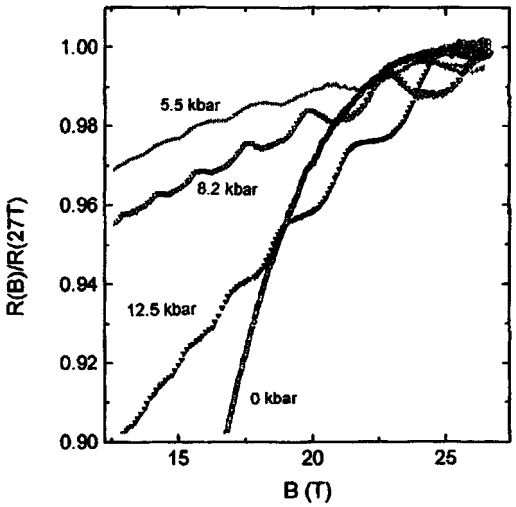

FIG. 3. Magnetoresistance above 13 T at different pressures.

As it was noted earlier,[11] the α oscillations reveal a considerable deviation of the Fermi surface from that predicted theoretically, their frequency being a factor of 4 and the cyclotron mass a factor of 2 smaller than the expected values. The oscillation parameters obtained in our experiment have not shown any sharp transition or unusually strong changes under pressure. Hence we suggest that the specific features characteristic of the Fermi surface at high pressures remain essentially the same at ambient pressure. A possible explanation of the observed discrepancy may consist in structural changes which have been reported by Nogami *et al.*[18] The superlattice reflections found in[18] correspond to doubling of the high temperature lattice along the c direction that should reduce the original Brillouin zone along the $\mathbf{k}_c$ axis and considerably reconstruct the possible electron orbits. In particular, smaller orbits at the folded hole cylinders are likely to be formed. The new orbits may give rise to slow α oscillations. Besides, other closed orbits resulting from multiple intersections of the initial Fermi surface cylinder may be expected. They could give different contributions to the oscillation spectrum depending on the interband gaps and magnetic field strength. In this connection, the prominent peak at $F \approx 2F_\alpha$ (see the inset in Fig. 2) might come from an independent orbit rather than be an anomalously strong second harmonic of the fundamental α frequency. Obviously, if the interband gaps are very small (which could be if the inversion symmetry survives during the structural transition), the main contribution to the oscillatory resistance should come from the β orbit enveloping 100% of the Brillouin zone area. This is probably the case we find at $P = 0$ kbar.

We note that the behavior of the oscillations at low pressures may be considerably affected by the superconduting transition. As is seen from the field dependence of the resistance presented in inset b of Fig. 1, signs of superconductivity survive up to fields of $\simeq 20$ T at ambient pressure. This is even more clearly illustrated by Fig. 3, in which high-field tracks of the resistance normalized to its values at 27 T are shown for different

pressures. For the pressure $P>0$ kbar the resistance shows an almost linear field dependence with a slope that increases with increasing pressure. At the same time the 0 kbar curve shows a very steep initial slope and saturates to the normal behavior at fields not lower than 23 T. A more detailed study is necessary in order to clarify whether it is bulk superconductivity or fluctuations of the order parameter amplitude which determine the resistance above 10 T, but both of these factors should obviously strongly suppress the Shubnikov–de Haas effect.[19] Of course, the slow oscillations which normally start to be visible from 10–12 T are much more affected by the superconductivity than are the β oscillations arising in fields above 22 T. In principle, this may be another reason why the α oscillations are not observed at ambient pressure in the investigated field range.

The work was supported in part by the ''Human Capital and Mobility Program'' of the European Community and by the Russian Fund for Fundamental Research.

[a)]Permanent address: Institute of Solid State Physics, Russian Academy of Sciences, 142432 Chernogolovka, Russia.

[1] J. M. Williams, J. R. Ferraro, R. J. Thorn *et al.*, *Organic Superconductors*, Prentice-Hall, Englewood Cliffs, N.J., 1992.
[2] T. Komatsu, T. Nakamura, N. Matsukawa *et al.*, Solid State Commun. **80**, 843 (1991).
[3] H. Urayama, H. Yamochi, G. Saito *et al.*, Chem. Lett., No. 1, 55 (1988).
[4] K. Miyagawa, A. Kawamoto, Y. Nakazawa, and K. Kanoda, Phys. Rev. Lett. **75**, 1174 (1995).
[5] H. Mayaffre, P. Wzietek, C. Lenoir *et al.*, Europhys. Lett. **28**, 205 (1994); H. Kawamoto, K. Miyagawa, Y. Nakazawa, and K. Kanoda, Phys. Rev. Lett. **74**, 3455 (1995).
[6] Y. Nakazawa and K. Kanoda, Phys. Rev. B **53**, R8875 (1996).
[7] K. Oshima, T. Mori, H. Inokuchi *et al.*, Phys. Rev. B **38**, 938 (1988).
[8] A. J. Schultz, H. H. Wang, J. M. Williams *et al.*, Physica C **234**, 300 (1994).
[9] T. Sasaki, H. Sato, and N. Toyota, Solid State Commun. **76**, 507 (1990); C.-P. Heidmann, H. Müller, W. Biberacher *et al.*, Synth. Met. **41–43**, 2029 (1991).
[10] M. V. Kartsovnik, W. Biberacher, K. Andres, and N. D. Kushch, JETP Lett. **62**, 905 (1995).
[11] M. V. Kartsovnik, G. Yu. Logvenov, H. Ito *et al.*, Phys. Rev. B **52**, R15715 (1995).
[12] M. V. Kartsovnik, G. Yu. Logvenov, W. Biberacher *et al.*, Synth. Met. **86**, 2061 (1997).
[13] L. I. Buravov, N. D. Kushch, V. A. Merzhanov *et al.*, J. Phys. I **2**, 1257 (1992).
[14] M. Kund, H. Müller, W. Biberacher, and K. Andres, Physica B **191**, 274 (1993).
[15] J. Caulfield, W. Lubczynski, F. L. Pratt *et al.*, J. Phys.: Condens. Matter **6**, 2911 (1994).
[16] D. Chasseau, J. Gaultier, M. Rahal *et al.*, Synth. Met. **41–43**, 2039 (1991).
[17] E. Balthes, D. Schweitzer, I. Heinen *et al.*, Z. Phys. B **99**, 163 (1996).
[18] Y. Nogami, J.-P. Pouget, H. Ito *et al.*, Solid State Commun. **89**, 113 (1994).
[19] P. J. van der Wel, J. Caulfield, J. Singleton *et al.*, Physica C **235–240**, 2453 (1994).

Published in English in the original Russian journal. Edited by Steve Torstveit.

Lattice deformation from interaction with electrons heated by an ultrashort laser pulse

L. A. Falkovsky and E. G. Mishchenko
L. D. Landau Institute of Theoretical Physics, Russian Academy of Sciences, 117334 Moscow, Russia

(Submitted 14 July 1997)
Pis'ma Zh. Éksp. Teor. Fiz. **66**, No. 3, 195–199 (10 August 1997)

We propose a model describing the destruction of metals under ultrashort intense laser pulses when heated electrons affect the lattice through the direct electron–phonon interaction. The metal consists of hot electrons and a cool lattice. The lattice deformation is estimated immediately after the laser pulse up to the electron temperature relaxation time. The hot electrons are described with help of the Boltzmann and heat conduction equations. We use an equation of motion for the lattice displacements with the electron force included. Estimates of the lattice deformation show that the ablation regime can be achieved. [S0021-3640(97)01415-1]

PACS numbers: 62.20.Fe, 63.20.Kr

1. It was pointed out in Ref. 1 that an ultrashort UV laser pulse $\sim 10^{-13}$ s produces a nonequilibrium electron gas near a metal surface. Such hot electrons have been observed in experiments on the IR reflection,[2–5] giant electron emission,[6–8] and light radiation[9–11] from metals under subpicosecond laser irradiation. Because the electron specific heat is much less than the lattice one, these pulses raise the electron temperature T_e considerably higher than the lattice temperature T_i. The characteristic cooling time of the electron gas $\tau_e \sim 10^{-12}$ s is determined by the electron–phonon coupling constant.[12] The process of temperature relaxation and the subsequent ablation regime have been studied recently.[13]

We focus here on the other processes which can take place at times much shorter than τ_e, when hot electrons directly affect the lattice expansion through the electron–phonon interaction. This novel effect is caused by the electron gas contribution (depending on T_e) to the elastic constants (sound velocity and optical phonon gap) and by the effective electron force proportional to ∇T_e. This interaction induces the lattice deformation.

The experimental results[14] visualized with the aid of time-resolved x-ray diffraction synchronized with laser pumping can be explained in the framework of the model described below. It was discovered that the laser pumping induces nonstationary increase in lattice parameters of Au(111) and Pt(111) single crystals. The measurement of the shift and intensity variation of Bragg peaks, on the one hand, and observation of the Debye–Waller factor, on the other, allow one to separate the effects of lattice deformation and heating. It was shown that the initial elastic deformation gives way to a subsequent

plastic one. Here we propose a theory of lattice deformation due to direct electron–phonon interaction.

2. We describe the overheated electron gas in terms of the Boltzmann equation. When the lattice temperature T_i is higher than the Debye temperature, the mean free time of the electrons is proportional to $\tau \sim T_i^{-1} \sim 10^{-14}\text{s} \ll \tau_e$. Thus the electron gas is nearly in equilibrium at temperature $T_e \gg T_i$. For our problem, the system obeys the heat conduction equation

$$c(T_e)\frac{\partial T_e}{\partial t} + \nabla \cdot \mathbf{q} = Q - \alpha(T_e - T_i), \tag{1}$$

and the equation for the lattice displacement u_i

$$\rho \frac{\partial^2 u_i}{\partial t^2} - \lambda_{iklm} \frac{\partial^2 u_l}{\partial x_k \partial x_m} = G_i(T_e), \tag{2}$$

where $c(T_e)$ is the electron heat capacity, ρ is the metal density, λ_{iklm} is the tensor of elastic constants, and Q is the density of the laser energy absorbed by the metal:

$$Q(z,t) = I(t)(1-R)\kappa e^{-\kappa z},$$

where R is the reflection coefficient. The function $I(t)$ describes the pulse shape. The last term in Eq. (1) represents the energy flow from nearly equilibrium hot electrons into the lattice.[12] The constant α is determined by the electron–lattice relaxation, $\tau_e \sim \alpha / c(T_e)$. The electron heat flow $\mathbf{q}$ and the driving force $G_i(T_e)$ applied to the lattice[15] are defined by the electronic partition function $f_p(\mathbf{r},t)$:

$$G_i = \frac{\partial}{\partial x_k} \int \frac{2d^3p}{(2\pi)^3} \lambda_{ik}(\mathbf{p}) f_p(\mathbf{r},t), \tag{3}$$

where λ_{ik} is the deformation potential. The effects of the electron interaction (3) on the acoustical phonon spectra (as well as on optical phonons) have been studied in detail in our recent paper.[16] The real part of the force (3) (the corresponding term for optical phonon was written for the first time in Ref. 16) leads to renormalization of the lattice parameters — the sound velocity for acoustical phonons and the optical phonon frequency. The imaginary part results in phonon attenuation due to the electron–phonon interaction. There are two regimes of phonon damping. The first, ballistic one takes place when electrons are nearly collisionless and the attenuation comes from the electrons moving coherently with the phonon. The hydrodynamic regime is realized when the mean free path of the electrons becomes smaller than the phonon wavelength. As a result, the attenuation depends strongly on the electron collision rate.

The electronic distribution function in the linearized form

$$f_p(z,t) = f_0(T_e) + \chi_p(z,t)\frac{\partial f_0}{\partial \varepsilon} \tag{4}$$

obeys the Boltzmann equation

$$\frac{\partial \chi_p}{\partial t}+v_z\frac{\partial \chi_p}{\partial z}+\frac{\chi_p-\overline{\chi_p}}{\tau}=-\lambda_{ik}(\mathbf{p})\frac{\partial u_{ik}}{\partial t}+\frac{\varepsilon_p-\mu}{T_e}\left(\frac{\partial T_e}{\partial t}+v_z\frac{\partial T_e}{\partial z}\right). \tag{5}$$

We write the collision integral in the τ-approximation because the electron temperature is much higher than the Debye temperature, and the electron–phonon collisions have to be elastic. The value averaged over the Fermi surface, $\overline{\chi_p}$, represents the ''in-term'' in the collision integral. Careful consideration shows that this term is unimportant when we are interested in the thermal conductivity but that it renormalizes the electron–phonon deformation potential: $\lambda_{ik}\to\lambda_{ik}-\overline{\lambda_{ik}}$, (see Ref. 17).

We assume in the following that $T_e\ll\varepsilon_F$. This will let us obtain the results in analytical form. For simplicity we suppose that the metal occupies the half space $z>0$ and that the boundary conditions for the above equations have the form

$$\left.\frac{\partial T_e}{\partial z}\right|_{z=0}=0,\quad \left.\frac{\partial u_z}{\partial z}\right|_{z=0}=0. \tag{6}$$

The first condition means that the heat flow through the surface vanishes, while the second one means that no normal stress component is present.

3. For times shorter than the electron–lattice relaxation time τ_e the lattice temperature can be considered as equal to the initial temperature T_0, and the last term in Eq. (1) can be omitted. To solve Eqs. (1)–(5) with boundary conditions (6) we use the even continuation $T_e(z,t)$ and the odd continuation for $u_z(z,t)$ into the half space $z<0$.

Let us consider here the solution of Eqs. (1)–(5) for the most interesting case when the times after laser pulse are much longer than the mean free time of the electrons ($t\gg\tau$) and the mean free path is much less than the skin depth ($\kappa l\ll 1$). Note that the electric field of the laser was omitted in Eq. (5) because it is important only for times of order of mean free time.

The heat flow in Eq. (1) is calculated with the Boltzmann equation (5). The thermal conductivity and the specific heat become proportional to the electron temperature T_e. Equation (1) turns to be linear in T_e^2, and its solution can be obtained easily with the help of a Green's function.

The electron temperature reads

$$T_e^2(z,t)=T_0^2+\int_0^t dt'\int_{-\infty}^{\infty}dz'\,\frac{Q(|z'|,t')}{\beta\sqrt{\pi(t-t')D}}\exp\left(-\frac{(z-z')^2}{4(t-t')D}\right), \tag{7}$$

where the diffusion coefficient $D=\tau\overline{v_z^2}$ and the temperature coefficient of the electronic specific heat $\beta=c(T_e)/T_e$ are introduced. The function (7) is even in z because $Q(z,t)$ was continued into the half space $z<0$ in an even manner. Therefore this solution satisfies the boundary condition (6). For the surface $z=0$ Eq. (7) gives

$$T_e^2(0,t)=T_0^2+\frac{4}{\pi\beta}\int_0^t dt'\,Q(0,\,t-t')e^{\kappa^2Dt'}\,\mathrm{erfc}(\sqrt{\kappa^2Dt'}). \tag{8}$$

Now let us consider the equation for lattice displacements (2) with the force (3). The main contribution to the force G_i comes from the local equilibrium partition function —

the first term in (4), if the condition $t \gg \tau$ is valid. Substituting expression (4) into Eq. (3) and expanding the integral over powers of T_e/ε_F up to the second order, we obtain the force

$$G_i = \Lambda_{ik} \frac{\partial T_e^2}{\partial x_k}, \tag{9}$$

where

$$\Lambda_{ik} = \frac{1}{32\pi} \frac{\partial}{\partial \varepsilon_F} \int \frac{dS}{v} \lambda_{ik}(\mathbf{p}) \sim g\beta,$$

and $g \sim \lambda/\varepsilon_F$ is the dimensionless electron–phonon coupling constant.

To solve the equation of motion of the lattice (Eq. (2)) with the calculated force (9) from hot electrons, we use the continuation described at the beginning of this section. The function u_z acquires a singularity at $z=0$ after the continuation. The singularity contributes a $d\delta(z)/dz$ term to the second derivative d^2u_z/dz^2. One can use the Fourier transform with respect to the spatial coordinate over all space

$$-\rho(\omega^2 - s^2k^2)u_z(k,\omega) = ik\Lambda_{zz}T_e^2(k,\omega) - i\rho s^2 k C(\omega), \tag{10}$$

where $s = \lambda_{zzzz}/\rho$ is the longitudinal sound velocity in the z direction. The last term $C(\omega)$ has to be determined from the boundary condition (6).

The deformation du_z/dz given by the solution of Eq. (2) can be written as

$$\frac{du_z}{dz} = \frac{i\Lambda_{zz}\kappa(1-R)}{\rho\beta} \int \frac{d\omega dk}{(2\pi)^2} \frac{k^2 U(k) I(\omega)}{(\omega + ik^2 D)(\omega^2 - s^2k^2)} (e^{ikz} - e^{i\omega|z|/s}) e^{-i\omega t}, \tag{11}$$

where $U(k) = 2\kappa/(k^2+\kappa^2)$ is the Fourier transform with respect to z of the laser radiation in the metal, and $I(\omega)$ is the Fourier transform of the pulse shape $I(t)$. The second term in the brackets corresponds to the general solution of the homogeneous equation (2) and represents the effect of the surface.

The integrand in (11) contains the poles associated with the diffuson and sound-wave excitations. The sound singularities must be bypassed through the insertion of an infinitesimal imaginary term in ω.

4. The electron temperature (7) immediately after the pulse takes its maximum on the surface

$$T_{\max}^2 \sim \frac{It_0(1-R)}{\beta} \min(\kappa, (Dt_0)^{-1/2}).$$

This result has a simple explanation. For short pulses $\kappa\sqrt{Dt_0} \ll 1$ time dependence of the temperature corresponds to the local laser intensity at the point of observation. In the opposite case, $\kappa\sqrt{Dt_0} \gg 1$, the temperature distribution is determined mainly by the diffusion process.

According to the boundary condition (6), the lattice deformation (11) vanishes at the surface $z=0$. For $z \neq 0$ the second term in (11) represents a deformation wave propagating from the surface into the bulk of the metal. It gives a nonzero contribution only at

sufficiently small depths $z<st\sim10^{-7}$ cm. We see that the maximum deformation takes place at $z\sim10^{-7}\text{cm}\ll\kappa^{-1}$. It is convenient to perform the integral (11) over ω, substituting the Fourier transform $I(\omega)$. We derive the following estimate for the maximum value of lattice deformation:

$$\frac{du_z}{dz}\sim\frac{\Lambda_{zz}\kappa(1-R)}{s\rho\beta}\int_0^t dt' I(t')\int_{-\infty}^{\infty}\frac{dk}{2\pi}U(k)\left(\frac{e^{-isk(t-t')}}{s(s+ikD)}-\frac{e^{-k^2D(t-t')}}{k^2D^2+s^2}\right)$$

$$\sim\Lambda_{zz}T_{\max}^2\kappa^2t^2/\rho. \tag{12}$$

We consider times of the order of the characteristic electron diffusion time $t\ll(\kappa^2D)^{-1}\sim10^{-12}\text{s}\ll(s\kappa)^{-1}$ but less than the period of a sound wave with vavelength $\sim\kappa^{-1}$. Using the estimate $\Lambda/\rho\sim gs^2/\varepsilon_F^2$, we get

$$\frac{du_z}{dz}\sim g\left(\frac{sT_{\max}}{\kappa\tau v^2\varepsilon_F}\right)^2\sim g(1-R)It_0(s/\tau v^2\varepsilon_F)^2/\kappa\beta. \tag{13}$$

Here we put $s/v\sim10^{-2}$, $\kappa\sim10^5$ cm^{-1}, and we arrive at the numerical estimate $du_z/dz\sim10^{-2}g^5(T_e/\varepsilon_F)^2$.

This result agrees with the experiment of Ref. 14, where a deformation as large as $\sim10^{-3}$ was observed. Although our estimate was obtained for $T_e\ll\varepsilon_F$, it is still correct qualitatively up to $T_e\sim\varepsilon_F$. Therefore, an ultrashort intense laser pulse can bring about the destruction and ablation of metals while only the electron component is heated and the lattice stays cool at a considerably lower temperature.

In conclusion we would like to emphasize two points. First, it follows from Eq. (9) that the driving force for the lattice expansion is proportional to $T_e\partial T_e/\partial z$. Because of the high absorption coefficient of metals in the UV region ($\kappa\sim10^5$ cm^{-1}) the temperature gradient reaches $\sim10^9$ K/cm. Note that the extremely high values of this parameter (which is a pecularity of metals) leads to the nonequilibrium expansion of the lattice. Second, the subpicosecond elastic deformation of the lattice, of the order of 10^{-3}–10^{-2}, corresponding to an internal pressure of 10–100 GPa, can provide an effective mechanism for the subsequent laser fracture of metals.

We are grateful to S. I. Anisimov, V. A. Benderskii, and B. Rethfeld for many discussions and comments. The work was supported the by Russian Foundation for Basic Research, Grant No. 97-02-16044. One of the authors (E. M.) also thanks KFA Forschungszentrum, Jülich, Germany, for a Landau Postdoctoral Scholarship.

[1] S. I. Anisimov, A. M. Bonch-Bruevich, M. A. El'yashevich *et al.*, Zh. Tekh. Fiz. **36**, 1273 (1967) [Sov. Phys. Tech. Phys. **11**, 945 (1967)].
[2] I. G. Fugimoto, J. M. Liu, E. P. Ippen *et al.*, Phys. Rev. Lett. **53**, 1837 (1984).
[3] D. M. Riffe, X. Y. Wang, and M. C. Downer, J. Opt. Soc. Am. B **10**, 1424 (1993).
[4] J. P. Girardeau-Montaut and C. Girardeau-Montaut, Phys. Rev. B **51**, 13560 (1995).
[5] S. I. Anisimov, V. A. Benderskii, and G. Farkas, Usp. Fiz. Nauk **122**, 185 (1977) [Sov. Phys. Usp. **20**, 467 (1977)].
[6] A. G. Krivenko, J. Kruger, W. Hautex *et al.*, Benchte Bunsengeselsch. Phys. Chem. **99**, 1489 (1995).
[7] V. A. Benderskii, Russian Electrochem. **33**, 417 (1997).
[8] A. G. Krivenko, J. Kruger, W. Hautex *et al.*, Russian Electrochem. **33**, 426 (1997).
[9] M. B. Agranat, A. A. Benditskii, G. M. Gandel'man *et al.*, JETP Lett. **30**, 167 (1979).
[10] M. B. Agranat, S. I. Anisimov, and B. I. Makshantsev, Appl. Phys. B **47**, 209 (1988).

[11] M. B. Agranat, S. I. Anisimov, and B. I. Makshantsev, Appl. Phys. B **55**, 451 (1992).
[12] M. I. Kaganov, I. M. Lifshits, and L. V. Tanatarov, Zh. Éksp. Teor. Fiz. **31**, 232 (1957) [Sov. Phys. JETP **4**, 173 (1957)].
[13] S. I. Anisimov and B. Rethfeld, Proc. SPIE **3093**, 192 (1997).
[14] P. Rentzepis, *Abstracts of the Second Conference on Modern Trends in Chemical Kinetics*, Novosibirsk, Russia (1995), Vol. 1, p. 142.
[15] V. M. Kontorovich, Usp. Fiz. Nauk **142**, 265 (1984) [Sov. Phys. Usp. **127**, 2134 (1984)].
[16] E. G. Mishchenko and L. A. Falkovsky, Zh. Éksp. Teor. Fiz. **80**, 936 (1995) [JETP **107**, 531 (1995)].
[17] L. A. Falkovsky and E. G. Mishchenko, Phys. Rev. B **51**, 7239 (1995).

Published in English in the original Russian journal. Edited by Steve Torstveit.

Semiclassical theory of the Coulomb anomaly

S. Levitov[a)] and A. V. Shytov[b)]
Massachusetts Institute of Technology, Cambridge, MA 02139, USA;
L. D. Landau Institute of Theoretical Physics Russian Academy of Sciences, 117334 Moscow, Russia

(Submitted 12 May 1997; resubmitted 15 July 1997)
Pis'ma Zh. Éksp. Teor. Fiz. **66**, No. 3, 200–205 (10 August 1997)

An effective action approach for the problem of Coulomb blocking of tunneling is discussed. The method is applied to the strong-coupling problem arising near zero bias, where perturbation theory diverges. We find an instanton for the electrodynamics in imaginary time, and express the anomaly in terms of the exact conductivity of the system $\sigma(\omega,q)$ and the exact interaction. © *1997 American Institute of Physics.* [S0021-3640(97)01515-6]

PACS numbers: 73.23.Hk, 73.40.Gk, 72.15.Qm

Suppression of tunneling conductivity near zero bias (called ''zero-bias anomaly'') is known to be a signature of interaction in a system. The anomaly has been studied in metals and semiconductors since the early 1960s.[1] Initially, the anomaly was attributed to the Kondo effect, but it was realized later that a much more common mechanism is the Coulomb blocking of tunneling. A perturbation theory of this effect was developed by Altshuler, Aronov, and Lee.[2] They show that in a diffusive conductor the blocking of tunneling increases at small bias, leading to a singularity in the tunneling conductivity. The theory has been thoroughly tested experimentally.[3]

In recent years interest has shifted to systems with strong Coulomb effects, such as disordered metals and semiconductors near a metal–insulator transition.[4] It is found that the Coulomb anomaly is sharply enhanced near the transition, providing a test of electron correlations. Another important development is due to studies by Ashoori *et al.* of electron tunneling into a two-dimensional metal in a magnetic field.[5] In this experiment it is found that at certain magnetic field the zero-bias anomaly abruptly increases and transforms to a ''soft Coulomb gap.'' It has been pointed out[6] that this transition is induced by disorder. Eisenstein *et al.* studied systems with higher mobility,[6,7] where tunneling is almost entirely blocked below a certain threshold bias. These findings prompted a lot of theoretical work[7] aimed at relating the tunneling anomaly with microscopic models. Also, the anomaly has been shown to be particularly interesting in the quantum Hall system.[8]

Below we discuss an effective action theory[9] that treats the anomaly as cooperative tunneling. We obtain the tunneling exponent in terms of the action of spreading charge density and express it in terms of the actual conductivity $\sigma(\omega,q)$ of the system. The treatment is nonperturbative and remains accurate both in the weak and strong coupling regimes.

QUALITATIVE DISCUSSION

Tunneling of an electron into a metal involves two steps: traversing the barrier, followed by spreading within the metal. Typically, the traversal time is very short compared to the spreading time. Accordingly, it is legitimate to separate the tunneling into single-electron and many-electron steps and to treat them separately. The first contribution is simply the transmission coefficient of the barrier, constant at small bias. The second contribution is more interesting, since it is a collective effect involving the motion of a large number of electrons in order to accomodate the new electron. At low bias the latter effect completely controls the tunneling rate.

Let us illustrate the effect of charge relaxation on the tunneling rate by using the example of a two-dimensional conducting plane.[10] Charge relaxation in a two-dimensional conductor is a classic electrodynamics problem studied by Maxwell who gave a solution in terms of a moving image charge.[11] In this problem, a point charge e is injected into a conducting sheet with conductivity σ, and one is interested in the time-dependence of the density and potential of spreading charge. Maxwell's solution is that the potential within the sheet is given by that of a point charge e moving along the normal to the plane at a velocity $v=2\pi\sigma$. The size of the charge cloud grows as $r(t)\sim vt$. Let us consider the Coulomb part of the action for the charge:

$$\mathcal{S}(t)\sim\int_{t_0}^{t}\frac{e^2}{r(t')}dt'=\frac{e^2}{2\pi\sigma}\ \ln\left(\frac{t}{t_0}\right). \tag{1}$$

Semiclassically, the action (1) must be added to the under-barrier action. The divergence of (1) at $t\to\infty$ indicates that at large times the action (1) dominates the tunneling rate. We will see that the spreading time diverges at small bias, $t_*=e/\sigma V$. From that, near zero bias the tunneling acquires a suppression factor of $\exp(-(1/\hbar)\mathcal{S}(t_*))$. The estimate (1) showing that the action diverges at small bias means that the semiclassical treatment is meaningful even for a well-conducting metal. However, in the diffusive limit the estimate (1) does not agree with the perturbation theory. We shall see that the reason is that the main part of the action is Ohmic rather than Coulomb, and that after writing the action properly the semiclassical method completely recovers the pertubation theory result.

The relevance of the semiclassical picture can be justified by a more general argument, not involving specific features of 2D relaxation. Let us consider effects caused by one-electron tunneling into a metal. Since the barrier traversal time is much shorter than the relaxation time in the metal, while the electron traverses the barrier other electrons essentially do not move. Thus instantly a large electrostatic potential is formed, due both to the tunneling electron itself and to the screening hole left behind. At small biases eV the increase of the electrostatic energy by an amount much larger than the bias indicates that right after the electron transfer the system is found in a classically forbidden state ''under the Coulomb barrier.'' In order to accomplish tunneling, the charge still has to spread over a large area, so that the potential of the charge fluctuation is reduced below eV. If the conductivity becomes smaller, charge spreading takes a longer time, and thus the action of the cooperative under-barrier motion becomes much greater than $\hbar$.

THE FORM OF THE ACTION

For the electrodynamics problem the action can be written in terms of the charge and current densities $\rho(\mathbf{r},t)$ and $\mathbf{j}(\mathbf{r},t)$. The full action would also contain the electromagnetic potentials, but in the quasistationary electrodynamics ($c\to\infty$) which we shall always assume below, the potentials are ''slaved'' to the charges and can therefore be integrated out. Also, since the contribution to the spreading charge action mainly arises from large space and time scales, we assume that the local deviation from equilibrium is small. Therefore, one can expand the action in powers of $\rho(\mathbf{r},t)$ and $\mathbf{j}(\mathbf{r},t)$ and keep only the quadratic terms. Naturally, the quadratic action must reproduce correctly the classical electrodynamics equations: Ohm's law and the continuity equation for the charge.

In fact, this requirement is entirely sufficient to determine the form of the action. However, it is more instructive to argue in the following way. We are going to use the action to study the dynamics in imaginary time. Therefore, the action is precisely the one that appears in the quantum partition function. The latter action expanded up to quadratic terms in charge and current density must yield the correct Nyquist spectrum of equilibrium current fluctuations:

$$\langle\langle \mathbf{g}^{\alpha}_{\omega,q}\mathbf{g}^{\beta}_{-\omega,-q}\rangle\rangle = \sigma_{\alpha\beta}|\omega| + \sigma_{\alpha\alpha'}D_{\beta\beta'}q_{\alpha'}q_{\beta'}. \tag{2}$$

Here $\mathbf{g}=\mathbf{j}+\hat{D}\nabla\rho$ is the external current and $D_{\alpha\beta}$ is the tensor of diffusion constants, related to the conductivity tensor by the Einstein formula $\hat{\sigma}=e^2\nu\hat{D}$, where $\nu=dn/d\mu$ is the compressibility. Generally, both $\hat{\sigma}$ and $\hat{D}$ are functions of the frequency and momentum. For simplicity, in what follows we will assume zero temperature and isotropic conductivity.

The requirement of matching equilibrium current fluctuations is essentially equivalent to the fluctuation-dissipation theorem. Thus the form of the action is fixed by the response functions of the system. In imaginary time it reads

$$\mathcal{S}=\frac{1}{2}\int\int d^4x_1 d^4x_2\left[\mathbf{g}_1^T\hat{K}_{x_1-x_2}\mathbf{g}_2+\frac{\delta_{12}\rho_1\rho_2}{|\mathbf{r}_1-\mathbf{r}_2|}\right], \tag{3}$$

where $x_{1,2}=(t_{1,2},\mathbf{r}_{1,2})$, and $\delta_{12}=\delta(t_1-t_2)$. The kernel $\hat{K}_{t,\mathbf{r}}$ is related to the current–current correlator

$$(K^{-1}_{\omega,q})_{\alpha\beta}=\langle\langle \mathbf{g}^{\alpha}_{i\omega,q}\mathbf{g}^{\beta}_{-i\omega,-q}\rangle\rangle \tag{4}$$

given by (2), where $\hat{\sigma}$ and $\hat{D}$ are functions of the Matsubara frequency obtained from the real frequency functions by the usual analytical continuation. We take the Coulomb interaction in the second term of the action (3) as nonretarded, since we are going to study systems with relatively low conductivity and hence slow charge relaxation.

INSTANTON

To evaluate the tunneling rate, we construct an instanton, i.e., a ''bounce path'' in imaginary time.[12,13] Among bounce paths symmetric in time, $\rho(\mathbf{r},t)=\rho(\mathbf{r},-t)$, $\mathbf{j}(\mathbf{r},t)=-\mathbf{j}(\mathbf{r},-t)$, we shall find the least-action path, which will give a semiclassical tunneling rate exponent.

In order to get equations of motion from the variational principle one notes that the action (3) contains the charge and current densities as *independent* variables, since Eq. (3) was derived by matching with the equilibrium fluctuations in the *grand canonical ensemble*, where charge is not conserved. Therefore, one must supply the action (3) with the charge continuity constraint: $\dot{\rho}+\nabla\cdot\mathbf{j}=\mathcal{J}(\mathbf{r},t)$, where

$$\mathcal{J}(\mathbf{r},t)=e\,\delta(\mathbf{r})(\,\delta(t+\tau)-\delta(t-\tau)). \tag{5}$$

The charge source $\mathcal{J}(\mathbf{r},t)$ describes an electron injected at $r=0$, $t=-\tau$, and taken back at $t=\tau$, at the same point. It is assumed that tunneling occurs at one point (impurity or a ''hot spot'').

Charge continuity is incorporated in the action by a Lagrange mutiplier:

$$\mathcal{S}_{\text{total}}=\mathcal{S}(\rho,\mathbf{j})+\phi(\mathbf{r},t)(\dot{\rho}+\nabla\mathbf{j}-\mathcal{J}(\mathbf{r},t)), \tag{6}$$

where $\phi(\mathbf{r},t)$ is an independent variable of the problem. For the least action path, the variation of $\mathcal{S}_{\text{total}}$ with respect to infinitesimal changes $\delta\phi$, $\delta\rho$, and $\delta\mathbf{j}$ vanishes. (Note that $\delta\dot{\rho}+\nabla\cdot\delta\mathbf{j}=0$.) After eliminating ϕ we get the standard equations of electrodynamics:

$$\text{(i)}\ \ \dot{\rho}+\nabla\cdot\mathbf{j}=\mathcal{J}(\mathbf{r},t);\quad \text{(ii)}\ \ \mathbf{j}+D\nabla\rho=\hat{\sigma}(\omega,\mathbf{q})\mathbf{E};$$

$$\text{(iii)}\ \ \mathbf{E}(\mathbf{r},t)=-\nabla_{\mathbf{r}}\int dr'\rho(r',t)U(|\mathbf{r}-\mathbf{r}'|). \tag{7}$$

Equations (7) describe evolution in imaginary time, i.e., charge spreading under the Coulomb barrier arising from self-interaction.

Then one must solve Eq. (7) for ρ and $\mathbf{j}$ and compute the action (3). For a spatially homogeneous system, using a Fourier transform gives

$$\rho(\omega,\mathbf{q})=\frac{\mathcal{J}(\omega)}{|\omega|+D\mathbf{q}^2+\sigma\mathbf{q}^2U_q},\quad \mathbf{j}(\omega,\mathbf{q})=-i\hat{K}^{-1}(\omega,\mathbf{q})\mathbf{q}U_q\rho(\omega,\mathbf{q}), \tag{8}$$

where $U_{\mathbf{q}}$ is the Coulomb potential form factor. Then the action (3) becomes

$$\mathcal{S}_0(\tau)=\frac{1}{2}\sum_{\omega,\mathbf{q}}\frac{|\mathcal{J}(\omega)|^2}{|\omega|+Dq^2}\frac{U_q}{|\omega|+Dq^2+\sigma q^2U_q}, \tag{9}$$

which depends on τ through the Fourier component of the charge source: $\mathcal{J}(\omega)=2ie\,\sin\omega\tau$.

ACCOMODATION TIME:

Finally, to obtain the total action of the system we subtract the term $2eV\tau$ from the spreading-charge action $\mathcal{S}_0(\tau)$ in order to account for the work performed by the voltage source: $\mathcal{S}(\tau)=\mathcal{S}_0(\tau)-2eV\tau$. This ensures that energy is conserved. Then one optimizes $\mathcal{S}(\tau)$ in τ:

$$\partial\mathcal{S}_0(\tau)/\partial\tau|_{\tau=\tau_*(V)}=2eV. \tag{10}$$

The optimal time τ_* can be interpreted as the charge accomodation time. By plugging τ_* found from Eq. (10) into the tunneling rate exponent one gets the tunneling conductivity $G(V)=G_0 e^{-\mathcal{S}(\tau_*(V))/\hbar}$. The accuracy of this calculation relies on the assumption that the time τ_* is larger than the barrier traversal time τ_f. This is true whenever there is an anomaly: if τ_* were $\approx\tau_f$, then $\mathcal{S}(\tau_*)\approx\hbar$, and there would be no tunneling suppression.

A more rigorous way to proceed is to write the equal-point Green's function $\widetilde{G}(t)=G_0(t)e^{-S_0(t/2)}$, where $G_0(t)=\nu_0/(t+i0)$ is the equal-point free electron Green's function. The tunneling current can be then written as

$$I=e\mathrm{T}\ \mathrm{Im}\int \widetilde{G}_1(t)\widetilde{G}_2(-t)e^{ieVt}dt, \tag{11}$$

where T is barrier transmission constant, and $G_{1,2}$ are the Green's functions in the leads. The equivalence of Eq. (11) and the above procedure (10) can be established by evaluating the integral (11) by the method of steepest decent.

Using (9) and (11) one can study the tunneling anomaly in different systems. In doing so, while calculating $\tau_*(V)$ and $\mathcal{S}(\tau_*)$ it is essential to check the self-consistency of the assumption that $\tau_*\gg\tau_f$. For example, this assumption will not be fulfilled in a *clean* metal, i.e., in a Fermi liquid without disorder ($D>1$). The reason is that the conductivity of an ideal conductor is $\sigma(\omega)=ine^2/m\omega$. In this case Eq. (9) gives $\mathcal{S}_0(\tau)\approx\hbar$ at any $\tau\gg\tau_f$, and hence $\tau_*\simeq\tau_f$. This indicates the absence of the anomaly in a clean metal, a result familiar from the Fermi-liquid picture. On the contrary, for a one-dimensional metal $\mathcal{S}_0(\tau)\sim\ln\tau/\tau_f$, which leads to the power-law anomaly known from the Luttinger-liquid theory.[14]

COMPARISON WITH PREVIOUS WORK

For a two-dimensional metal with elastic scattering time τ_0 and unscreened Coulomb interaction we set $U_q=2\pi/|q|$ and $\sigma(\omega,q)=\mathrm{const}$ at $|\omega|,v_F|q|\leqslant 1/\tau_0$. Then Eq. (9) gives

$$\mathcal{S}(\tau)=\frac{e^2}{8\pi^2\sigma}\ln\left(\frac{\tau}{\tau_0}\right)\ln(\tau\tau_0\sigma^2(\nu e^2)^2). \tag{12}$$

From Eq. (10), $\tau_*=(e/4\pi^2V\sigma)\ln(\hbar\sigma\nu e/V)$. The theory is self-consistent at long times, $\tau_*\geqslant\tau_0$, i.e., at $eV\leqslant e^2/\sigma\tau_0$. Then the least action is

$$\mathcal{S}(V)=\frac{e^2}{8\pi^2\sigma}\ln\left(\frac{e}{4\pi^2\sigma V\tau_0}\right)\ln\left(\frac{e\tau_0\sigma(\nu e^2)^2}{4\pi^2V}\right). \tag{13}$$

It is interesting to compare this result with the identical double-log dependence derived by Altshuler, Aronov, and Lee[2] for the correction to the tunneling density of states $\delta\nu(\epsilon)$. The calculation[2] assumes that $\delta\nu$ is small, $|\delta\nu|\ll\nu_0$, which is the case only for weak disorder. It was found that $\delta\nu(\epsilon)=-\hbar^{-1}\nu_0\mathcal{S}(eV=\epsilon)$, where $\mathcal{S}(V)$ is given by (13). The main difference is that the double log (13) has to be exponentiated to get the tunneling density of states, while in Ref. 2 the double log appears as a correction to the density of states. Within the domain of perturbation theory the two results agree.

Also, let us mention a connection with the work by Halperin, He, and Platzman[8] dealing with the anomaly in the $\nu = 1/2$ quantum Hall state. The effect considered in this work is a shakeup of low–frequency modes of the system due to the tunneling electron, assuming that the response function is described by the Chern–Simons Fermi-liquid theory.[15] The anomaly was found to have the form:

$$G(V) \sim \exp(-V_0/V), \quad V_0 = 4\pi \frac{e}{\epsilon}\sqrt{\pi n}, \tag{14}$$

where $V \ll V_0$, and n is the density. It is interesting to see how this result can be derived from the effective action. It has been shown[15] that the conductivity of the $\nu = 1/2$ state has strong spatial dispersion: $\sigma(k) = A|k|$, $A = e^2/16\pi\epsilon\sqrt{\pi n}$. If this form is inserted in the action (9), one gets $S(\tau) = \pi\sqrt{2\tau/A}$, which leads to the tunneling rate (14).

SOURCE–DRAIN CORRELATION

For tunneling between source and drain, there are separate contributions to the action due to the relaxation of the electron and hole charges on both sides of the barrier. If the barrier is thin, the positive and negative charges partially screen the field of each other, which makes their spreading correlated. In this case the least action is smaller than the sum of independent contributions of the electrodes, and thus the anomaly is weakened. For $D = 2$, quantitatively, the effect will be that the voltage dependence of the second log in Eq. (13) saturates at $eV \simeq V_0 = \min[\sigma_1, \sigma_2]\hbar/a$, where a is the distance between the electrodes.

This *excitonic* correlation effect can be treated straightforwardly by writing the action (3) for each electrode separately, together with the term describing the interaction across the barrier. Let us consider an example of two parallel planes with different conductivities and diffusion constants, σ_1, σ_2, D_1, and D_2. It is straightforward to generalize the above procedure and to find the instanton. The least action is

$$\mathcal{S}_0(\tau) = \frac{1}{2}\sum_{\omega,q} |J(\omega)|^2 \begin{bmatrix} 1 \\ -1 \end{bmatrix}^{\mathrm{T}} (|\omega| + \mathbf{D}q^2)^{-1}\mathbf{U}(|\omega| + \mathbf{D}q^2 + \mathbf{\Sigma}q^2\mathbf{U})^{-1} \begin{bmatrix} 1 \\ -1 \end{bmatrix}, \tag{15}$$

where we use matrix notation:

$$\mathbf{D} = \begin{pmatrix} \hat{D}_1 & 0 \\ 0 & \hat{D}_2 \end{pmatrix}, \quad \mathbf{\Sigma} = \begin{pmatrix} \hat{\sigma}_1 & 0 \\ 0 & \hat{\sigma}_2 \end{pmatrix}, \quad \mathbf{U} = \begin{pmatrix} U_q & V_q \\ V_q & U_q \end{pmatrix}, \tag{16}$$

$$U_q = \int e^{iqr}\frac{d^2r}{|r|}, \quad V_q = \int \frac{e^{iqr}}{\sqrt{r^2 + a^2}}d^2r.$$

The rows and columns of the matrices (16) correspond to the two planes.

To make it simpler to evaluate $\mathcal{S}_0(\tau)$, let us assume that $e^2\nu_{1,2}a \gg 1$, a condition satisfied in almost all experiments. By carrying out matrix inversion and integration we get

$$\mathcal{S}_0(\tau) = \alpha \ln\left(\frac{\tau}{\tau_0}\right) \quad \text{at} \quad \tau \gg \hbar/eV_0, \tag{17}$$

where

$$\alpha = \frac{e^2}{4\pi^2}\left[\frac{1}{\sigma_1}\ln\frac{4\pi\sigma a}{D_2} + \frac{1}{\sigma_2}\ln\frac{4\pi\sigma a}{D_1}\right], \tag{18}$$

with $\sigma = \sigma_1\sigma_2/(\sigma_1+\sigma_2)$. If the two planes are identical,

$$\alpha = \frac{e^2}{2\pi^2\sigma}\ln 2\pi e^2 \nu a. \tag{19}$$

Thus at $V < V_0$ the $I-V$ curve becomes the power law $I \sim V^{\alpha+1}$. The tunneling suppression in this case is weaker than for the unscreened interaction.

CONCLUSION

The essential feature of the above approach is that it relates the tunneling anomaly with the actual conductivity of the system. This would allow a comparison with experiment in the situations where there is no accepted model for the conductivity. For example, the tunneling current as function of voltage can be taken from experiment and used directly to find $\mathcal{S}(\tau)$ by means of a Legendre transform. Then $\mathcal{S}(\tau)$ can be analyzed by using (9) and (11) to extract the frequency and wave-vector dependence of the conductivity.

To summarize, we have argued that the theory of the Coulomb anomaly in the regime of strong suppression of tunneling is semiclassical. The underlying reason is that the transfer of one electron across the barrier is controlled by the cooperative motion of many other electrons. We treat this motion as classical electrodynamics in imaginary time, for which we construct an effective action and find an instanton path. The instanton action determines tunneling exponent as function of the bias.

[a)]e-mail: levitov@mit.edu
[b)]e-mail: shytov@mit.edu

[1] B. L. Altshuler and A. G. Aronov, in *Electron–Electron Interaction in Disordered Systems*, A. L. Efros and M. Pollak, eds. (North-Holland, 1985); R. C. Dynes and P. A. Lee, Science **223**, 355 (1984).
[2] B. L. Altshuler, A. G. Aronovand P. A. Lee, Phys. Rev. Lett. **44**, 1288 (1980).
[3] R. C. Dynes and J. P. Garno, Phys. Rev. Lett. **46**, 137 (1981); Y. Imry and Z. Ovadyahu, Phys. Rev. Lett. **49**, 841 (1982).
[4] J. M. Valles, R. C. Dynes, and J. P. Garno, Phys. Rev. B **40**, 7590 (1989); Phys. Rev. B **40**, 6680 (1989).
[5] R. C. Ashoori, J. A. Lebens, N. P. Bigelow, and R. H. Silsbee, Phys. Rev. Lett. **64**, 681 (1990); Phys. Rev. B **48**, 4616 (1993).
[6] J. P. Eisenstein, L. N. Pfeiffer, and K. N. West, Phys. Rev. Lett. **69**, 3804 (1992).
[7] S. R. E. Yang and A. H. MacDonald, Phys. Rev. Lett. **70**, 4110 (1993); Y. Hatsugai, P. A. Bares, and X. G. Wen, Phys. Rev. Lett. **71**, 424 (1993); P. Johansson and J. M. Kinaret, Phys. Rev. Lett. **71**, 1435 (1993); A. L. Efros and F. G. Pikus, Phys. Rev. B **48**, 14694 (1993); C. M. Varma, A. I. Larkin, and E. Abrahams, Phys. Rev. B **49**, 13999 (1994); S. R. Renn and B. W. Roberts, Phys. Rev. B **50**, 7626 (1994); I. L. Aleiner, H. U. Baranger, and L. I. Glazman, Phys. Rev. Lett. **74**, 3435 (1995); Phys. Rev. B **50**, 15465 (1994).
[8] S. He, P. M. Platzman, B. I. Halperin, Phys. Rev. Lett. **71**, 777 (1993).
[9] L. S. Levitov and A. V. Shytov, ''Coulomb blocking of tunneling: from zero-bias anomaly to Coulomb gap,'' in *Correlated Fermions and Transport in Mesoscopic Systems*, Les Arcs, Savoie (Editions Frontieres, 1996).
[10] B. Z. Spivak, unpublished (1990).
[11] J. C. Maxwell, *A Treatise on Electricity and Magnetism*, Vol. II, Ch. XII (Oxford: Clarendon Press, 1892), p. 296.

[12] J. S. Langer, Ann. Phys. (N.Y.) **41**, 108 (1967).
[13] S. Coleman, Phys. Rev. D **15**, 2929 (1977).
[14] G. D. Mahan, *Many-Particle Physics* (New York, Plenum Press, 1981), Sec. 4.4.
[15] B. I. Halperin, P. A. Lee, and N. Read, Phys. Rev. B **47**, 7312 (1993).

Published in English in the original Russian journal. Edited by Steve Torstveit.

On the integration of some classes of weakly deformed nonlinear Schrödinger equations

A. I. Zenchuk[a)]

L. D. Landau Institute of Theoretical Physics, Russian Academy of Sciences, 142432 Chernogolovka, Moscow Region, Russia

(Submitted 18 June 1997; resubmitted 26 June 1997)
Pis'ma Zh. Éksp. Teor. Fiz. **66**, No. 3, 206–211 (10 August 1997)

A method is proposed for constructing the solutions of a nonlinear Schrödinger equation with small corrections arising as a result of the introduction of arbitrary functions of the time and coordinates into the operator that dresses the kernel of a local $\overline{\partial}$ problem. © *1997 American Institute of Physics.* [S0021-3640(97)01615-0]

PACS numbers: 03.65.Ge, 11.10.Lm

The nonlinear Schrödinger equation (NSE), which is well-known to be a completely integrable model, has wide applications in physics (for example, nonlinear optics and plasma physics). The assertion that the NSE is completely integrable is, generally speaking, incorrect for arbitrary deformations of the NSE, which are often encountered among equations of mathematical physics. However, there exist classes of deformations which do not destroy the integrability of the NSE. The discovery and study of these classes is an important problem. In Ref. 1, for example, a symmetry approach to the investigation of ''asymptotic integrability'' of the perturbed NSE was used.

Several new classes of such deformations have been found in the present work. This was done with the use of the so-called $\overline{\partial}$ problem,[2–4] which is an implementation of the dressing method[5] in which the investigation of nonlinear systems of equations is reduced by means of dressing operators to the investigation of associated linear systems (which are differential and integrodifferential systems in application to local and nonlocal $\overline{\partial}$ problems, respectively). The construction by the dressing technique of new integrable systems of equations which are deformations of known integrable models was made possible by the use, in dressing the kernel of the $\overline{\partial}$ problem, of operators with arbitrary functions Φ_i of the time and coordinates (i.e., independent variables of nonlinear equations), which engenders a system of nonlinear equations with variable coefficients that depend on the functions Φ_i (Ref. 6). Dressing of this kind describes, for example, the resonance interaction of waves in a nonuniform medium. The functions Φ_i, being arbitrary, can be declared functions of the dependent variables (solutions) of a nonlinear system.

A scheme for constructing weakly deformed integrable models by means of such dressing is presented below. These models differ from the standard integrable ones in that they contain corrections, in the form of an infinite series in powers of a small parameter ε, and arbitrary functions Φ_i. In addition, these equations are exactly integrable with the aid of the $\overline{\partial}$ problem, i.e., they possess a class of exact solutions in the form of analyti-

cally prescribed functions containing a small parameter. This distinguishes them from other types of perturbed equations whose approximate solutions can be written in the form of a power series up to the required order in a small parameter. Just as in Ref. 6, constraints in the form of arbitrary integrodifferential (in the general case) equations (constraint equations) can be imposed on the functions Φ_i and the dependent variables of the nonlinear equations. For example, if the functions Φ_i characterize a weak nonuniformity of the medium, then the constraint equations reflect the influence of a physical quantity, represented by the solution of the nonlinear equation, on the nonuniformity. An important factor is the solvability of these equations with respect to the functions Φ_i. Otherwise the question of constructing the solutions of the nonlinear system of equations with constraints remains open.

The algorithm, examined below for the example of the NSE, for determining weak deformations that do not destroy integrability is also applicable to other completely integrable models which can be handled by the dressing method.

1. We proceed from the local $\overline{\partial}$ problem (in what follows, an overbar on a function denotes complex conjugation)

$$\frac{\partial}{\partial\lambda}\psi(\lambda)=\psi(\lambda)R(x,y;\lambda) \tag{1}$$

with the regular normalization

$$\psi\to\begin{pmatrix}1 & 0\\ 0 & 1\end{pmatrix}+\sum_{j>0}\frac{\psi_j}{\lambda^j},\quad \lambda\to\infty, \tag{2}$$

and a kernel R of the form

$$R(x,y;\lambda)=e^{K(x;\lambda)}R_0(\lambda)e^{-K(x;\lambda)}, \tag{3}$$

where K is the dressing operator

$$K(x;\lambda)=i\left(\lambda x+2\lambda^2 y+\sum_{k=1}^{N_1}\varepsilon^{n_k}\lambda^{k-1}\Phi_k\right)\sigma_3, \tag{4}$$

$\sigma_3=\operatorname{diag}(1,-1)$, N_1 is an integer, Φ_i are arbitrary functions of the parameters x and y, and $\varepsilon\to 0$ is a small parameter.

Since the NSE is handled by the problem (1)–(3) with the dressing operator $K=i\lambda\sigma_3 x+2i\lambda^2\sigma_3 y$, the problem (1)–(4) formulated in this manner describes a weakly deformed NSE.

In what follows we assume that the equation (1) has a unique solution. This assertion is valid at least for kernels of a definite type (see Ref. 2).

We note that the local $\overline{\partial}$ problem handles the same class of nonlinear equations as the local Riemann problem. Therefore the technique proposed in Ref. 7 can be used to construct the solutions of the models described here.

It is obvious that the functions Φ_1, Φ_2, and Φ_3 can be eliminated from the dressing operation by a gauge transformation of the functions $\psi(\lambda)$ and transformations of the independent coordinates x and y. We shall return to this question in Sec. 4. Here we shall examine the dressing operator K of the general form (4).

2. The derivation of the weakly deformed NSE by means of the problem (1)–(4) is based on the construction of operators M_k of the form (see Refs. 2–4)

$$M_k\psi=\sum_{ij} u_{k;ij}D_x^iD_y^j\psi, \quad D_x\psi=\partial_x\psi+\psi\partial_xK, \quad D_y\psi=\partial_y\psi+\psi\partial_yK,$$

which are regular in the complex plane of the parameter λ, such that

$$M_k\psi\to 0 \quad \text{as } \lambda\to\infty.$$

This means that $M_k\psi\equiv 0$ since it has been assumed that the equation (1) has an unique solution.

In our case there exist only two independent operators M_k. They engender an overdetermined linear system of equations for the function ψ:

$$\begin{aligned} &M_1\psi\equiv D_x\psi-U\psi=\partial_x\Psi-U\Psi=0,\\ &M_2\psi\equiv D_y\psi-W\psi=\partial_y\Psi-W\Psi=0, \end{aligned} \tag{5}$$

where $\Psi=\psi\exp(K)$,

$$U=i\lambda\begin{pmatrix}1&0\\0&-1\end{pmatrix}+i\begin{pmatrix}0&q\\r&0\end{pmatrix}+i\sum_{k=1}^{N_1}\varepsilon^{n_k}\partial_x\Phi_kV_k,$$

$$W=2i\lambda^2\begin{pmatrix}1&0\\0&-1\end{pmatrix}+2i\lambda\begin{pmatrix}0&q\\r&0\end{pmatrix}+Q+i\sum_{k=1}^{N_1}\varepsilon^{n_k}\partial_y\Phi_kV_k,$$

$$Q=2i([\psi_2,\sigma_3]-[\psi_1,\sigma_3]\psi_1)=Q_{NS}+Q_\Phi, \quad Q_{NS}=\begin{pmatrix}0&q_x\\-r_x&0\end{pmatrix}-irq\begin{pmatrix}1&0\\0&-1\end{pmatrix},$$

$$\begin{pmatrix}0&q\\r&0\end{pmatrix}=[\psi_1,\sigma_3], \quad V_1=\sigma_3, \quad V_n=\lambda^{n-1}\sigma_3+\sum_{k=0}^{n-2}\lambda^kV_{n,k}, \quad n>1.$$

The coefficients $V_{k,n}$ are related with one another by the formulas

$$V_{n,l}=V_{n-l,0}, \quad V_{2,0}=[\psi_1,\sigma_3], \quad V_{n,0}=[\psi_{n-1},\sigma_3]-\sum_{k=1}^{n-2}V_{n-k,0}\psi_k, \quad n>2. \tag{6}$$

In what follows, we shall use everywhere the reduction

$$r=\overline{q}, \quad \overline{\Phi}_k=\Phi_k \tag{7}$$

(i.e., the functions Φ_k are real).

The deformed NSE follows from the conditions of compatibility of the linear equations (5)

$$U_y-W_x+[U,W]=0. \tag{8}$$

Analyzing this condition, we shall take account of the relations (6). We represent the functions Q_Φ and $V_{k,0}$ as power series in the parameter ε

$$Q_\Phi=\sum_{k\geqslant 1}\varepsilon^k Q_k, \quad V_{n,0}=\sum_{k\geqslant 0}\varepsilon^k V_{n,0,k}$$

and expand the equation (8) in powers of this parameter. Equating to zero the coefficients of all powers of λ, we obtain expressions for the functions Q_k and $V_{n,0,k}$ in terms of the complex function q and the arbitrary functions Φ_j and we also obtain for the function q an equation which has the form of a NSE with a small correction in the form of a power series in the parameter ε:

$$iq_y-q_{xx}-2q^2\overline{q}+\sum_{k\geqslant 1}\varepsilon^k P_k=0. \tag{9}$$

The choice of numbers n_k in Eq. (4) determines Q_k, $V_{n,0,k,}$and P_k as functions of q and Φ_j.

3. We set in the equation (4) $n_k=k$, $k=1,\ldots,4$, and $N_1=4$ and write out the expressions for the first four corrections of Eq. (9):

$$P_1=2i(2q_x\partial_x\Phi_1+q\partial_{xx}\Phi_1-iq\partial_y\Phi_1), \tag{10}$$

$$P_2=-i(2iq_{xx}\partial_x\Phi_2+iq_x\partial_{xx}\Phi_2+q_x\partial_y\Phi_2)+4q(\partial_x\Phi_1)^2, \tag{11}$$

$$\begin{aligned}P_3=&-i(q_{xxx}+4q_xq\overline{q}+2q^2\overline{q}_x)\partial_x\Phi_3-\frac{1}{2}(q_{xx}+2q^2\overline{q})(i\partial_{xx}\Phi_3+\partial_y\Phi_3)\\&-(8iq_x\partial_x\Phi_2\partial_x\Phi_1+4iq\partial_x\Phi_2\partial_{xx}\Phi_1+2iq\partial_{xx}\Phi_2\partial_x\Phi_1+2q\partial_y\Phi_2\partial_x\Phi_1),\end{aligned} \tag{12}$$

$$\begin{aligned}P_4=&-\frac{1}{2}\partial_x(q_{xxx}+6q\overline{q}\overline{q}_x)\partial_x\Phi_4+\frac{1}{4}(q_{xxx}+6q\overline{q}\overline{q}_x)(-\partial_{xx}\Phi_4+i\partial_y\Phi_4)\\&-(6q_{xx}\partial_x\Phi_3\partial_x\Phi_1+2q_x\partial_{xx}\Phi_3\partial_x\Phi_1+6q_x\partial_x\Phi_3\partial_{xx}\Phi_1+4q^2\overline{q}\partial_x\Phi_3\partial_x\Phi_1\\&+q\partial_{xx}\Phi_3\partial_{xx}\Phi_1+2q\partial_x\Phi_3\partial_{xxx}\Phi_1-2iq_x\partial_y\Phi_3\partial_x\Phi_1-iq\partial_y\Phi_3\partial_{xx}\Phi_1\\&+3q_{xx}(\partial_x\Phi_2)^2+3q_x\partial_{xx}\Phi_2\partial_x\Phi_2-iq_x\partial_x\Phi_2\partial_y\Phi_2)-8q\partial_x\Phi_2(\partial_x\Phi_1)^2.\end{aligned} \tag{13}$$

The functions Φ_j in the formulas written out above are arbitrary functions of the parameters x and y. Since the equations (1) are assumed to have a solution, the explicit form of q as a function of Φ_j is known:

$$q=q(\Phi_j). \tag{14}$$

This fact can be used as follows.

We introduce the constraints

$$F_j(q,\overline{q},\Phi_i)=0, \quad j=1,\ldots,N_2, \quad N_2\leqslant N_1, \tag{15}$$

where N_1 is the number of functions Φ_j. Here F_j is an arbitrary operator (in the general case, integrodifferential in x and y) acting on its arguments. If the functions Φ_i characterize the nonuniformity of the medium, then the equations (15) reflect the effect of the

solution q on the degree of nonuniformity. Therefore we have constructed a closed system of equations on the functions Φ_i $(i=1,\ldots,N_2)$ and q that depends parametrically on the functions Φ_i, $i=N_2+1,\ldots,N_1$, and whose solution reduces to solving the equations (15) for the functions Φ_i, $i=1,\ldots,N_2$. The left-hand sides of the equations (15) (taking account of the relation (14)) are arbitrary integrodifferential operators acting on the functions Φ_i.

An important particular case are the equations (15) with $N_2=N_1$, from which the functions Φ_i can be expressed explicitly in terms of q and $\overline{q}$ as:

$$\Phi_j=\Theta_j(q,\overline{q}), \quad j=1,\ldots,N_1, \tag{16}$$

where Θ_j are arbitrary operators. This means that the nonuniformity of the medium is completely determined by the ''perturbation'' q which ''propagates'' in the medium. That is, the equations (16) characterize the nonlinear effects of the interaction of the ''perturbation'' with the medium. Substituting the functions (16) into Eqs. (9)–(13) we obtain a system of equations with constant coefficients for the function q. We shall discuss these equations in greater detail.

The constraint equations (16) determine the structure of the corrections P_k. For example, if equations of the type

$$\Phi_j=D_jI_k, \quad k=1,2,\ldots,$$

where D_i is a linear differential operator in x and y with constant coefficients and I_k are conserved densities of the NSE, are chosen as constraints, then the equation (9) together with the corrections will be invariant under the gauge transformation

$$q\to q\,\exp(i\theta), \quad \mathrm{Im}(\theta)=0. \tag{17}$$

There exist operators D_j such that each correction P_k will be scale-invariant with some scaling weight. A NSE with such corrections appears on passing in the equations of mathematical physics to the limit of smooth envelopes.[2] We recall that the polynomial $P(q,\overline{q},q_x,\overline{q_x},q_{xx},\overline{q_{xx}},\ldots)$ possesses a scaling weight M if it transforms under the scaling transformations $q=s^{\delta_1}u$ and $x=s^{\delta_2}\xi$ (where s and δ_i are real constants) according to the law

$$P(q,\overline{q},q_x,\overline{q_x},q_{xx},\overline{q_{xx}},\ldots)=s^MP(u,\overline{u},u_\xi,\overline{u_\xi},u_{\xi\xi},\overline{u_{\xi\xi}},\ldots).$$

Here we shall not study in detail corrections of any specific type. We shall present several characteristic examples.

The structure of the corrections (10)–(13) of the perturbed NSE (9) that correspond to the simplest constraints is analyzed below. The analysis takes into consideration the different behavior of the corrections under gauge and scaling transformations and the relation between the order of smallness n of the correction P_n $(P_n\sim\varepsilon^n)$ and its scaling weight M_n. We shall characterize the latter relation by the parameter Γ_n:

$$\Gamma_n=M_n-n.$$

This characteristic is meaningful if one is considering Eq. (9) with two or more corrections P_k of different order.

We recall that in a completely integrable model

$$q_y = NS + \sum_{k>3} \varepsilon^{k-2} NS_k, \tag{18}$$

(NS_k are the higher-order symmetries of the NSE) this parameter equals 3 for all corrections: $\Gamma_k = 3$.

We present several examples.

a) $\Phi_1 = q\overline{q}$, $\Phi_k = 0$, $k > 1$.

$P_1 = 4i(q_x^2\overline{q} + 2qq_x\overline{q}_x + q^2\overline{q}_{xx})$

— the correction is scale-invariant and it is invariant under the transformation (17);

b) $\Phi_1 = \partial_x(q\overline{q}) + q\overline{q}$, $\Phi_k = 0$, $k > 1$.

$P_1 = 4i(q_x^2\overline{q} + 2qq_x\overline{q}_x + q^2\overline{q}_{xx} + q_{xx}q_x\overline{q} + q_{xx}\overline{q}_x q + 2q_x^2\overline{q}_x + 3q_x q\overline{q}_{xx} + q^2\overline{q}_{xxx})$,

— scale invariance is destroyed;

c) $\Phi_2 = \partial_x^{-1}(q\overline{q})$, $\Phi_3 = x$, and $\Phi_k = 0$, $k \neq 2, 3$.

$P_2 = 2q(q_{xx}\overline{q} + q_x\overline{q}_x)$, $P_3 = -i(q_{xxx} + 4q_x q\overline{q} + 2q^2\overline{q}_x)$,

— the scaling weight of the correction P_2 is greater than that of the correction P_3: $\Gamma_2 = 3$ and $\Gamma_3 = 1$;

d) $\Phi_1 = q + \overline{q}$, $\Phi_k = 0$, $k > 1$.

$P_1 = 4i(q_x^2 + q_x\overline{q}_x - q^3\overline{q} + q^2\overline{q^2} + q\overline{q}_{xx})$,

— invariance under the transformation (17) is destroyed;

e) $\Phi_3 = x$, $\Phi_4 = \partial_x^{-1}(q\overline{q})$, $\Phi_k = 0$, $k \neq 3, 4$.

$P_3 = -i(q_{xxx} + 4q_x q\overline{q} + 2q^2\overline{q}_x)$,

$$P_4 = -\frac{q}{2}(q_{xxxx}\overline{q} + q_{xxx}\overline{q}_x + 6q_{xx}q\overline{q^2} + 6q_x^2\overline{q^2} + 12q_x q\overline{q}_x\overline{q})$$

— here $\Gamma_3 = 1$ and $\Gamma_4 = 3$.

4. The origin of the corrections considered above can be given a clear interpretation in terms of weak deformations of commuting fluxes. Indeed, the dressing operator

$$K_{NS} = i\left(\lambda\xi + 2\lambda^2\eta + \sum_{k>2} \lambda^k C_{k-2}\tau_{k-2}\right)\sigma_3, \quad C_k = \text{const}, \tag{19}$$

corresponds to a hierarchy of NSEs, where τ_k are the higher-order times of the hierarchy. We write out the equations for the commuting fluxes in the schematic form

$$u_{\theta_1} = u, \quad u_{\theta_2} = u_\xi, \quad u_\eta = NS_3(u) \equiv NS(u), \quad u_{\tau_k} = NS_{3+k}(u), \quad k = 1, 2, \ldots, \tag{20}$$

where $NS_k(u)$ are the order-k symmetries of the NSE:

$$NS_1=u,\quad NS_2=u_\xi,\quad NS_3=u_{\xi\xi}+2u^2\overline{u},\quad NS_4=u_{\xi\xi\xi}+6u\,\overline{u}u_\xi,\ \ldots,$$

Now we apply the infinitesimal transformations

$$u=q\,\exp(-2i\varepsilon^{n_1}\Phi_1),\quad \xi=x+\varepsilon^{n_2}\Phi_2,\quad \eta=y+\frac{\varepsilon^{n_3}}{2}\Phi_3,\quad \tau_k=t_k+\frac{\varepsilon^{n_{k+3}}}{C_k}\Phi_k,$$

$$k=1,2,\ldots, \tag{21}$$

to the equations (20) (here the functions Φ_k depend only on x and y; transformations of the solution q and variable x are equivalent to transformations of the times θ_1 and θ_2), expand in powers of the parameter ε, and eliminate from the third equation of the system (20) the derivatives of the functions q and $\overline{q}$ with respect to the ''higher order times'' t_k. It is obvious that this procedure leads back to the equation (9), since after the transformation (21) the operator K_{NS} will differ from the operator K (see Eq. (4)) only by the polynomial $i\Sigma_{k>2}\lambda^k C_{k-2}t_{k-2}$. The latter fact means that to the operator K_{NS} there are associated the same ''elongated derivatives'' D_x and D_y as for the operator K, which determine the form of the nonlinear equation handled by such a dressing procedure.

In this derivation of the equation (9) all functions Φ_k are equivalent and characterize the deformation of the corresponding variables in the hierarchy of NSEs. This justifies the use in Sec. 1 of the dressing operator K of the general form (4) (see Sec. 1). The general structure of the corrections P_{n_k} is

$$P_{n_k}=2\left(\frac{-i}{2}\right)^{k-1}((NS_k(q))(i\partial_{xx}\Phi_k+\partial_y\Phi_k)+2i\partial_x(NS_k(q))\partial_x\Phi_k)+F_{n_k}, \tag{22}$$

where the functions F_{n_k} depend on Φ_j, NS_j $(j\neq k)$ and on their derivatives with respect to x and y.

We note that the solutions constructed in this manner for the equation (9) depend parametrically on t_k, $k=1,2,\ldots$.

The REDUCE package of computer codes for analytical calculations was used to obtain a number of formulas.

I thank S. V. Manakov for helpful discussions. This work was supported by the Russian Fund for Fundamental Research (Grant No. 94-01-00899-a).

[a)]e-mail: zenchuk@itp.ac.ru

[1] I. Kodama and A. V. Mikhailov, in *Algebraic Aspects of Integrability*, edited by I. M. Gelfand and A. Fokas, Birkhauser, 1996.
[2] V. E. Zakharov and S. V. Manakov, Funktsion. Analiz Ego Pril. **19**(2), 11 (1985).
[3] L. V. Bogdanov and S. V. Manakov, J. Phys. A: Math. Gen. **21**, L537, (1988).
[4] A. I. Zenchuk and S. V. Manakov, Teor. Mat. Fiz. **105** (3), 371 (1995).
[5] V. E. Zakharov and A. B. Shabat, Funktsion. Analiz Ego Pril. **8**(3), 43 (1974).
[6] A. Degasperis, S. V. Manakov, and A. I. Zenchuk, *Multidimensional Soliton Equations in Inhomogeneous Media*, to be published.
[7] V. E. Zakharov and A. B. Shabat, Funktsion. Analiz Ego Pril. **13**(3), 13 (1979).

Translated by M. E. Alferieff